R. & M. No. 3032
(18,205)
A.R.C. Technical Report

MINISTRY OF SUPPLY

AERONAUTICAL RESEARCH COUNCIL
REPORTS AND MEMORANDA

The Effects of Taper on the Supervelocities on Three-Dimensional Wings at Zero Incidence

By

K. W. NEWBY

LONDON: HER MAJESTY'S STATIONERY OFFICE
1957
PRICE £1 1s 0d

The Effects of Taper on the Supervelocities on Three-Dimensional Wings at Zero Incidence

By

K. W. NEWBY

COMMUNICATED BY THE DIRECTOR GENERAL OF SCIENTIFIC RESEARCH (AIR), MINISTRY OF SUPPLY

Reports and Memoranda No. 3032*

June, 1955

Summary.—Relationships have been derived for expressing the velocities on three-dimensional tapered wings at zero incidence in terms of the velocities on untapered infinite swept wings. The theoretical investigation of the effects of taper is confined to simple wings having aerofoil sections formed by cubic or parabolic arcs ; some experimental evidence is given to show that the results of this investigation can probably be applied quantitatively to wings having conventional aerofoil sections.

The results given in this report show that plan-form and thickness taper have a marked effect on the velocities near the centre of a wing, but that these effects decrease with increase of sweepback.

A calculation method is outlined in section 4.2.6 of the text for applying the results obtained for wings having parabolic-arc aerofoil sections, to wings having arbitrary section shapes.

1. *Introduction.*—For aerodynamic and structural reasons, thickness and plan-form taper have become important parameters in the design of wings for high-speed aircraft. It is known that in general, a combination of thickness and plan-form taper (such as occurs on a delta wing having constant thickness/chord ratio throughout the span), results in a decrease in the velocities over the inboard parts of the wing, and an increase over the outboard parts, as compared with an untapered wing of the same thickness/chord ratio. Little is known, however, of the separate contributions of plan-form and thickness taper, and how these contributions are affected by sweepback.

The present report, which is based upon an analysis of calculations made in 1949-50 for wings having simple plan-form and aerofoil-section shapes, provides a qualititative indication of the effects of plan-form taper, thickness taper, aspect ratio, and aerofoil-section shape on the flow past three-dimensional wings at zero incidence. Throughout this paper the terms ' plan-form taper ' and ' thickness taper ' have their true meaning, *viz.*,

Plan-form taper means that the wing chord varies across the span ; it does not imply a corresponding variation of wing thickness

Thickness taper refers to the spanwise variation of the absolute thickness, and not to the spanwise variation of thickness/chord ratio.

In general it is not possible to obtain an exact solution for the flow past a wing of arbitrary plan-form, spanwise thickness distribution and section shape ; several papers (*e.g.*, Refs. 1, 2 and 3) have dealt with the flow past untapered, swept and unswept wings, having thin symmetrical parabolic-arc aerofoil sections, by the use of linearised theory. These papers have shown that within the limitations of the linearised theory, it is possible to express the velocity at the centre-line of an infinite swept wing, and also the streamwise velocity on an infinite sheared wing by general equations applicable to any aerofoil-section shape, *i.e.*, (using the notation of Ref. 4) :

*R.A.E. Report Aero. 2544, received 6th February, 1956.

$$\frac{V_x(x)}{V_0} = 1 + \left\{ S^{(1)}(x) - S^{(2)}(x)\, f(\varphi) \right\} \cos\varphi \qquad \ldots \quad \ldots \quad \ldots \quad \ldots \quad \ldots \qquad (1)$$

at the centre-line of an infinite swept wing, and :

$$\frac{V_x(x)}{V_0} = 1 + S^{(1)}(x) \cos\varphi \qquad \ldots \quad \ldots \quad \ldots \quad \ldots \quad \ldots \quad \ldots \quad \ldots \qquad (2)$$

on an infinite sheared wing, where

V_0 is the free-stream velocity,

V_x is the chordwise velocity on the wing chord plane,

$S^{(1)}(x)$ is the chordwise supervelocity ratio as derived by linearised theory for the corresponding unswept two-dimensional wing (*see* Ref. 4),

$S^{(2)}(x)$ is the slope of the aerofoil section at position x,

$$f(\varphi) = \frac{1}{\pi} \ln \left(\frac{1 + \sin\varphi}{1 - \sin\varphi} \right),$$

φ is the angle of sweepback of the wing.

Except for a region close to the centre-line of the wing (within about one half-chord length), the flow past an infinite swept wing is the same as that past an infinite sheared wing; furthermore it is seen from equation (1) that the expression for the velocity at the centre of an infinite swept wing contains the term $1 + S^{(1)}(x) \cos\varphi$, which represents the velocity on the infinite sheared wing of the same sweep (equation (2)). The remaining term in equation (1), viz., $S^{(2)}(x)\, f(\varphi) \cos\varphi$, is generally known as the ' kink ' term, since it expresses the effect of the discontinuity or kink in the plan-form at the centre-line, on the velocities at the centre of the wing.

It has been suggested in Ref. 4 that the velocities over the part of the wing which lies between the centre-line and the region where the flow is the same as that over an infinite sheared wing, can also be expressed in terms of the infinite sheared wing supervelocity and the ' kink ' term, by introducing a ' kink '-term reduction factor K_2 into equation (2), *i.e.*:

$$\frac{V_x}{V_0} = 1 + \left\{ S^{(1)}(x) - K_2\, S^{(2)}(x)\, f(\varphi) \right\} \cos\varphi \,. \qquad \ldots \quad \ldots \quad \ldots \quad \ldots \qquad (3)$$

The factor K_2, which is the ratio of the ' kink ' term at any spanwise position to the value at the centre-line, decreases with spanwise distance from the centre-line ; a curve for the spanwise variation of K_2 is given in Ref. 4 (Fig. 12) for an infinite swept wing.

Equation (3) does not give the complete answer for the flow past an infinite swept wing, however, since it implies that the velocity at the maximum thickness position, where $S^{(2)}(x)$ is zero, is independent of spanwise position. That this is not so, is apparent from the results of Refs. 1 to 4. If at any spanwise position, the increase of the supervelocity at the maximum-thickness position, as a fraction of that on the corresponding infinite sheared wing is denoted by K_1, *i.e.*,

$$1 + K_1 = \frac{\text{supervelocity at maximum-thickness position of infinite swept wing}}{\text{supervelocity at maximum-thickness position of infinite sheared wing}},$$

then it has been shown in Ref. 5 that over a large portion of the chord :

$$\frac{V_x}{V_0} = 1 + \left\{ (1 + K_1) S^{(1)}(x) - K_2 S^{(2)}(x)\, f(\varphi) \right\} \cos\varphi \qquad \ldots \quad \ldots \quad \ldots \qquad (4)$$

gives almost exactly the velocity at any point of the infinite swept wing.

One of the chief limitations of the linearised theory is that it can only give the supervelocities in the chord plane, and not on the surface of the aerofoil. For small thickness/chord ratios, this does not constitute a serious limitation, provided the aerofoil section is not round-nosed. For moderate and large thickness/chord ratios, however, the results given by linearised theory differ considerably from the true values for the supervelocity at the surface. In the case of infinite unswept wings of elliptic aerofoil section, the true velocities at the surface can be obtained from those calculated using linearised theory by multiplying by the factor :

$$\left\{\frac{1}{1 + (S^{(2)}(x))^2}\right\}^{1/2} \quad . \quad . \quad . \quad . \quad . \quad . \quad . \quad . \quad . \quad (5)$$

It is shown in Ref. 6 that the application of this correction factor to the velocities obtained from linearised theory for a symmetrical Joukowsky aerofoil section, gives results which are in close agreement with those obtained from the exact solution.

Küchemann and Weber have applied this correction term to the case of the swept wing in Ref. 4, in order to bring the theoretical results into closer agreement with experiment for fairly thick, round-nosed aerofoil sections. The use of this correction term does, however, destroy the simple concept that the velocity at the centre of an infinite swept wing is equal to that on the corresponding infinite sheared wing, plus a ' kink ' term, since in Ref. 4, it is shown that at the centre-line, the pressure coefficient at the surface is :

$$C_p(x, z) = \frac{-2\cos\varphi\{S^{(1)}(x) - S^{(2)}(x)\,f(\varphi)\} - \{S^{(1)}(x) - (S^{(2)}(x))\,f(\varphi)\}^2\cos^2\varphi + (S^{(2)}(x))^2}{1 + (S^{(2)}(x))^2} \quad (6)$$

for an infinite swept wing.

Simply removing the ' kink ' terms $(S^{(2)}(x))\,f(\varphi)$ from equation (6) gives for the pressure coefficient at the surface of an infinite sheared wing :

$$C_p(x, z) = \frac{-2\cos\varphi\,S^{(1)}(x) - (S^{(1)}(x))^2\cos^2\varphi + (S^{(2)}(x))^2}{1 + (S^{(2)}(x))^2}, \quad . \quad . \quad . \quad (7)$$

whereas in Ref. 4, it is shown that for an infinite sheared wing, the correct expression for C_p is :

$$C_p(x, z) = \frac{-2\cos\varphi\,S^{(1)}(x) - (S^{(1)}(x))^2 + (S^{(2)}(x))^2}{\left\{1 + \frac{(S^{(2)}(x))^2}{\cos^2\varphi}\right\}} \quad . \quad . \quad . \quad . \quad (8)$$

Thus for thick wings it is no longer possible to apply an interpolation factor K_2 for the spanwise variation of the ' kink ' term just outboard of the centre-line. For this reason, the results obtained in this report using linearised theory have not been corrected to allow for the difference between the supervelocity at the chord plane, and that on the surface of the aerofoil. This should not, however, affect the validity of the results near the maximum-thickness position where the slope of the aerofoil section is small, since the correction terms $1 + (S^{(2)}(x))^2$ and $1 + \{(S^{(2)}(x))^2\}/\cos^2\varphi$ approximate to unity when $S^{(2)}(x)$ is small ; an approximation to the thickness correction could, if desired, be introduced when applying the results of this report to a specific case by increasing the calculated velocities by the appropriate factors :

$$\frac{1}{1 + (S^{(2)}(x))^2} \text{ or } \frac{1}{1 + \frac{(S^{(2)}(x))^2}{\cos^2\varphi}}.$$

No account has been taken in the present report of any spanwise component of the velocity, since in general it is expected to be small compared with the streamwise velocity, and at the centre-line, it is zero (by symmetry).

For the present purpose, it is important to note that the two terms in equation (4) derived by linearised theory, relate only to untapered wings of infinite aspect ratio, and therefore take no account of the effects of finite aspect ratio, plan-form taper or thickness taper. The effects of finite aspect ratio on the velocities at the centre of swept and unswept, untapered wings, have been considered in Ref. 3, where it is shown that an aspect-ratio correction term can be added to the expression for the velocity at the centre of an infinite swept wing, *i.e.*:

$$\frac{V_x}{V_0} = 1 + \left\{ S^{(1)}(x) - S^{(2)}(x)\, f(\varphi) - \frac{\Psi \cos^2 \varphi}{4A^2} (3 \sin^2 \varphi - 1) + \ldots \right\} \cos \varphi \,, \tag{9}$$

where Ψ is the area coefficient of the aerofoil section,

$$\text{i.e., } \Psi = \frac{\text{area of profile}}{\text{area of circumscribing rectangle}} \,.$$

As a basis for analysis in this report, it has been assumed that equations (4) and (9) can be applied to wings tapered in plan-form, by regarding φ as the local geometric angle of sweep, and hence the effects of thickness taper and plan-form taper on the various factors in these equations determined.

The results obtained have been considered in three main parts :

(*a*) the effects of thickness taper and aerofoil section shape for rectangular wings

(*b*) the effects of plan-form taper, thickness taper and aerofoil-section shape for wings having zero sweep on the maximum-thickness line

(*c*) the effects of plan-form taper, thickness taper and aerofoil-section shape for swept wings.

The only results at present available for tapered wings are given in Ref. 7. These are, however, restricted in scope and refer only to wings having constant thickness/chord ratio throughout the span ; hence they do not give any indication of the separate effects of plan-form and thickness taper, nor do they show the effects of sweepback. Equations are derived in Ref. 7 for the velocities on swept, tapered wings, having constant thickness/chord ratio throughout the span, but the computational work involved in deriving numerical results is prohibitive without the aid of electronic computation methods.

In the present report, consideration of the effects of taper is restricted to results obtained for a few simple wings. Since there is little hope of being able to solve the general problem (including higher order terms) for wings of any aerofoil-section shape, only linear-order terms are considered, and these only for a special class of aerofoil section. This, however, is eminently suitable for the present purpose, since the general trends of the effects of the various parameters can be found without getting involved in the usual exceedingly tedious numerical calculations. In particular it has been found that special functions for the spanwise variation of thickness can be devised which lead to a considerable simplification of the analysis.

The results obtained for these special cases, give qualititative answers for the general aerofoil shape, and have been expressed in terms of the supervelocities obtained by linearised theory for the infinite unswept wing and for the ' kink ' term. Hence they can be applied as correction terms in the relationship discussed earlier for finite and infinite swept wings. The weakest point in this procedure is the applicability of the results to aerofoil sections of conventional round-nosed shape. However, the order of the velocity changes, as well as the general trends of the effects of

sweepback and taper, should be reasonably well represented. In one simple case considered in this report, the quantitative agreement between the results predicted by these simple methods, and the experimental results, is very good.

The main practical advantage of this procedure, is that the additional computational work necessary to allow for the effects of taper in calculating the velocity distribution over a given wing is insignificant. A further advantage is that by using sheared wing and ' kink ' terms as measuring units, it is possible to present the results in an orderly manner, considering each of the many parameters in turn ; this makes it possible to follow the general trends more easily.

It should be noted that the results obtained in this report refer only to zero Mach number. They can, however, be applied at high Mach number, provided the aspect ratio of the analogous wing is not too small (i.e., $A_M = A_{M=0}\sqrt{(1 - M^2)}$. The application of the results to wings at $M = 1$ has not been considered.

A short programme of tests[8] has been planned to obtain experimental velocity distributions on a series of tapered wings. The results obtained will be compared with those predicted by linearised theory to check whether the velocity changes due to taper and sweepback are of the same order as those given in the present report. Knowing the general trends of these effects from the theoretical results, it should be possible from these few experimental results to make any quantitative changes to the results given in this report, which might appear to be necessary to give closer agreement with experiment.

2. *Wings Considered.*—All the wings considered in this report have been derived from four simple basic wings, by the method of superposition. Results have, however, been abstracted from Ref. 7 to check some of the results obtained and also for the spanwise variation of the supervelocity at the maximum thickness of a wing having constant thickness/chord ratio throughout the span.

The first of the basic wings is rectangular in plan-form, and has a linear variation of thickness/chord ratio from (t_0/c_0) at the centre-line to $\mu(t_0/c_0)$ at the tips. The aerofoil section chosen for this wing is formed by arcs of cubics, to enable the maximum-thickness position $(x = k)$ of the section to be readily altered. When the maximum thickness is at the mid-chord point $(k = 0)$, this section reduces to a symmetrical parabolic-arc section, and thus gives a direct comparison with the results available for two-dimensional wings having this section shape.

By changing the factor μ, this rectangular wing can be varied from a fully ' tapered in thickness ' wing to an untapered wing, of any aspect ratio. This property has been used to derive wings having various spanwise thickness distributions. For instance, wing (1) of this report (Fig. 1) has been formed by adding to this basic wing, two outer panels of constant thickness ; these panels were obtained by subtracting an untapered wing of span ψs and constant thickness/chord ratio $\mu(t_0/c_0)$ from a similar wing of span s. The equation for the supervelocity at any point of this wing has been derived in the text.

The second basic wing (wing 2, Fig. 1) has been chosen because of the simple manner in which it can be represented by sources and sinks in a uniform stream. As is well known, the infinite swept wing with parabolic-arc aerofoil section can be represented by a source distribution which is uniform in strength parallel to the maximum-thickness line, and which varies linearly in the streamwise direction. The second basic wing has been obtained by removing those sources and sinks representing an infinite swept-back wing, which lie outside the tapered plan-form of the required wing. The resulting wing has again a symmetrical parabolic-arc aerofoil section, the thickness/chord ratio of which decreases linearly from (t_0/c_0) at the centre-line to zero at the tips.

Although it has not been possible to vary the aerofoil section of this wing in the same way as for the rectangular wing discussed above (since this would destroy the essential simplicity of the wing), some indication of the effects of change of aerofoil-section shape has been obtained by forming wings having aerofoil sections of different parabolic arcs ahead of, and behind the maximum-thickness line. This has been achieved by superimposing the front half of a wing of aspect ratio $Ac_0/(c_0 - 2k)$ and centre-line thickness/chord ratio $\{c_0/(c_0 - 2k)\}(t_0/c_0)$ on to the rear half of a similar wing of aspect ratio $Ac_0/(c_0 + 2k)$ and centre-line thickness/chord ratio $\{c_0/(c_0 + 2k)\}(t_0/c_0)$,

where c_0 is the root chord of the required wing

A is the aspect ratio of the required wing

$$k = \frac{\text{distance of maximum-thickness ahead of mid-chord point}}{\text{half centre-line chord}}$$

(t_0/c_0) is the centre-line thickness/chord ratio of the required wing,

both parts of the wing having the same sweep on the maximum-thickness line.

The third basic wing (wing 3, Fig. 1) is again swept, and tapered in plan-form. The aerofoil section is symmetrical parabolic arc, and the thickness/chord ratio varies inversely as the local chord across the span. Thus the absolute thickness on any percentage-chord line is constant across the span. This wing was chosen because, apart from the variable sweep of the constant-percentage-chord lines, it is directly comparable with an untapered swept wing of finite aspect ratio, and therefore provides an indication of the effects of plan-form taper.

The fourth basic wing (wing 4, Fig. 1) has again been chosen because of the simple way in which it can be represented by sources in a uniform stream, and because, by suitably superimposing a particular form of this wing (i.e., $N = 2$ in equation (IV.1)) on to wing (3) to give wing (5), and then superimposing wing (5) on to wing (2), a wing (wing 6) is obtained which has almost constant thickness/chord ratio over the inboard 50 per cent of the semi-span. Thus it has been possible to extend, in a very simple manner, the results obtained by laborious calculation in Ref. 7 for the centre-line of a tapered wing having constant thickness/chord ratio throughout the span.

Wing (4) is tapered in plan-form, and has zero sweep on the mid-chord line. The section shape is symmetrical parabolic arc throughout, and the thickness/chord ratio varies as $(1 + N\eta)(1 - \eta)$ across the span, where :

$$\eta = \frac{\text{spanwise distance from centre-line}}{\text{semi-span}},$$

N is a factor, varying from -1 to $+\infty$, which defines the spanwise thickness distribution for this type of wing.

3. *Rectangular Wings Tapered in Thickness.*—As pointed out in the introduction, the expressions for the velocities at the centre of an infinite swept wing and on an infinite sheared wing, as obtained by linearised theory, contain a term for the velocity on the corresponding unswept two-dimensional wing. The first section of this report is therefore restricted to the determination of the effects of aspect ratio and spanwise taper of absolute thickness on the velocities on rectangular wings. Thus the effects of plan-form taper and sweepback are eliminated from the problem.

The supervelocity v_x at a point (x, y) of a rectangular wing which is tapered in thickness from t_0 at the centre-line to μt_0 at the tips, is derived in Appendix I by replacing the wing by unswept source lines of varying strength along the span $q(x, y) = -2V_0[\{\partial z(x, y)\}/\partial x]$ and by obtaining the contribution of the source-line element from an integration across the span, and subsequently the total supervelocity from an integration along the chord. Such splitting up of the double

integral into two single integrals is evidently permissible in the present case, and for the special thickness distribution $z(x, y)$ chosen, the integrations yield explicit relations which have been derived in Appendix I.

3.1. *Equation for Wing with Parabolic-Arc Aerofoil Section, and Linear Spanwise Thickness Taper over the Central Part of the Span (Wing 1).*—The simple case of the equation for the supervelocity v_x at any point (x, y) of a rectangular wing which has a symmetrical parabolic-arc aerofoil section and a linear spanwise variation of thickness/chord ratio from (t_0/c_0) at the centre-line to $\mu(t_0/c_0)$ at a spanwise position ψs (where s is the wing semi-span), and a constant thickness outboard of ψs, is derived as an example. The equations for wings having more complex variations of thickness can be derived following the same procedure, though it will be shown later that many of the results for such wings can be obtained by superposition of results for this simple wing.

Substituting ηs for y and ψs for s in equation (I.9) of Appendix I, where s is the semi-span of the complete wing, and ψs is the semi-span of the tapered part of the wing, the contribution of the inboard tapered panels of the wing to the supervelocity v_x at the point (x, η) is given by :

$$\begin{aligned}\frac{\pi v_x(x,\eta)}{4V_0(t_0/c_0)} &= \frac{(1-\mu)}{8\psi s}(1+x)(K_1+K_2-2K_3)\\
&+\frac{(1-\mu)}{8\psi s}(1-x)(K_4+K_5-2K_6)\\
&+\frac{s}{4}(\psi-\eta)\left\{1-\frac{(\psi+\eta)}{2\psi}(1-\mu)\right\}\ln\frac{K_4+(1+x)}{K_1-(1-x)}\\
&+\frac{s}{4}(\psi+\eta)\left\{1-\frac{(\psi-\eta)}{2\psi}(1-\mu)\right\}\ln\frac{K_5+(1+x)}{K_2-(1-x)}\\
&+\frac{x}{4}\left\{1-\frac{\eta}{\psi}(1-\mu)\right\}\ln\left\{\frac{K_4+s(\psi-\eta)}{K_1+s(\psi-\eta)}\right\}\left\{\frac{K_6+\eta s}{K_3+\eta s}\right\}\\
&+\frac{x}{4}\left\{1+\frac{\eta}{\psi}(1-\mu)\right\}\ln\left\{\frac{K_5+s(\psi+\eta)}{K_2+s(\psi+\eta)}\right\}\left\{\frac{K_6-\eta s}{K_3-\eta s}\right\}\\
&-\frac{\eta^2 s}{4\psi}(1-\mu)\ln\frac{K_6+(1+x)}{K_3-(1-x)}-x\ln\left(\frac{1+x}{1-x}\right), \quad .. \quad .. \quad .. \qquad (10)\end{aligned}$$

where
$$\begin{aligned}K_1^2 &= (1-x)^2+s^2(\psi-\eta)^2\\
K_2^2 &= (1-x)^2+s^2(\psi+\eta)^2\\
K_3^2 &= (1-x)^2+\eta^2 s^2\\
K_4^2 &= (1+x)^2+s^2(\psi-\eta)^2\\
K_5^2 &= (1+x)^2+s^2(\psi+\eta)^2\\
K_6^2 &= (1+x)^2+\eta^2 s^2.\end{aligned}$$

The contribution to v_x due to the outer untapered panels of the wing can be obtained as the difference between the contributions of two wings of constant thickness/chord ratio $\mu(t_0/c_0)$ and having semi-spans of s and ψs respectively. This can be derived from equation (I.10) of Appendix I which gives the supervelocity distribution on a finite rectangular wing of thickness/chord ratio t_0/c_0.

Thus, using the same notation as for equation (10), the supervelocity v_x induced at the point (x, η) by the outer panels of the wing is :

$$\frac{\pi v_x(x,\eta)}{4V_0(t_0/c_0)} = \frac{\mu s}{4}\left\{(1-\eta)\ln\frac{K_9+(1+x)}{K_7-(1-x)} + (1+\eta)\ln\frac{K_{10}+(1+x)}{K_8-(1-x)}\right\}$$

$$-\frac{\mu s}{4}\left\{(\psi-\eta)\ln\frac{K_4+(1+x)}{K_1-(1-x)} + (\psi+\eta)\ln\frac{K_5+(1+x)}{K_2-(1-x)}\right\}$$

$$+\frac{\mu x}{4}\ln\left\{\frac{K_1+s(\psi-\eta)}{K_4+s(\psi-\eta)}\right\}\left\{\frac{K_2+s(\psi+\eta)}{K_5+s(\psi+\eta)}\right\}\left\{\frac{K_9+s(1-\eta)}{K_7+s(1-\eta)}\right\}\left\{\frac{K_{10}+s(1+\eta)}{K_8+s(1-\eta)}\right\} \quad (11)$$

where
$$K_7^2 = (1-x)^2 + s^2(1-\eta)^2$$
$$K_8^2 = (1-x)^2 + s^2(1+\eta)^2$$
$$K_9^2 = (1+x)^2 + s^2(1-\eta)^2$$
$$K_{10}^2 = (1+x)^2 + s^2(1+\eta)^2.$$

Combining equations (10) and (11) gives the supervelocity v_x at (x, η) due to the whole of the wing as :

$$\frac{\pi v_x(x,\eta)}{4V_0(t_0/c_0)} = \frac{(1-\mu)}{8\psi s}\left\{(1+x)(K_1+K_2-2K_3) + (1-x)(K_4+K_5-2K_6)\right\}$$

$$+\frac{s}{4}(1-\mu)\left\{(\psi-\eta)^2\ln\frac{K_4+(1+x)}{K_1-(1-x)} + (\psi+\eta)^2\ln\frac{K_5+(1+x)}{K_2-(1-x)}\right\}$$

$$+\frac{\mu s}{4}\left\{(1-\eta)\ln\frac{K_9+(1+x)}{K_7-(1-x)} + 1+\eta)\ln\frac{K_{10}+(1+x)}{K_8-(1-x)}\right\}$$

$$+\frac{x(1-\mu)}{4\psi}\left\{(\psi-\eta)\ln\frac{K_4+s(\psi-\eta)}{K_1+s(\psi-\eta)} + (\psi+\eta)\ln\frac{K_5+s(\psi+\eta)}{K_2+s(\psi+\eta)}\right\}$$

$$+\frac{x}{4}\left[\left\{1-\frac{\eta}{\psi}(1-\mu)\right\}\ln\frac{K_6+\eta s}{K_3+\eta s} + \left\{1+\frac{\eta}{\psi}(1-\mu)\right\}\ln\frac{K_6-\eta s}{K_3-\eta s}\right]$$

$$+\frac{\mu x}{4}\ln\left\{\frac{K_9+s(1-\eta)}{K_7+s(1-\eta)}\right\}\left\{\frac{K_{10}+s(1+\eta)}{K_8+s(1+\eta)}\right\}$$

$$-\frac{\eta^2 s(1-\mu)}{4\psi}\ln\frac{K_6+(1+x)}{K_3-(1-x)} - x\ln\frac{1+x}{1-x}. \quad .. \quad .. \quad .. \quad (12)$$

3.2. *The Shape of the Chordwise Supervelocity Distribution on Rectangular Wings.*—A number of chordwise supervelocity (v_x) distributions have been calculated at various spanwise positions on rectangular wings having symmetrical parabolic-arc aerofoil sections, both for wings of constant spanwise thickness, and for wings tapered in thickness over part, or the whole, of the span. Some of these results are presented in Figs. 2a to 4a. Results for constant-thickness wings are not given, since the v_x distributions for a wing of aspect ratio 2 can be found in Ref. 3.

All the results calculated, show that for rectangular wings of symmetrical parabolic-arc aerofoil section, the supervelocity distributions are similar in shape to the corresponding two-dimensional distribution (Figs. 2b to 4b), but with the supervelocities at all points of the chord reduced in approximately the same ratio (τ). Hence if the two dimensional v_x distribution and the supervelocity at one point on the chord are known, the complete chordwise v_x distribution can be determined to a close degree of approximation by multiplication with a factor τ. Thus the problem reduces to determining the factor τ as a function of the thickness taper.

The supervelocity distribution at the centre-line of a rectangular wing tapered in thickness, and having a symmetrical aerofoil section formed by arcs of cubics (*see* Appendix I) with maximum-thickness position at one-third chord (Fig. 5), shows that change of aerofoil-section shape (at least for these simple sections) does not affect the manner in which the velocities are reduced relative to the two-dimensional values.

This does not necessarily mean that wings having more conventional aerofoil sections will behave in the same way. Whether this is so, will be determined from the experimental programme of Ref. 8 for wings having RAE 101 aerofoil-section shape.

3.3. *Variation of the Supervelocity at the Maximum-Thickness Position of the Centre-line Chord, with Aspect Ratio and Spanwise Extent of Thickness Taper.*—Since the supervelocity at one point of the chord is required to obtain the relationship between the actual and the two-dimensional v_x distributions, it seems reasonable to consider the effects of aspect ratio, etc., on the supervelocity $v_x(k)$ at the maximum-thickness position of the centre-line chord.

Fig. 6a shows the variation of $v_x(k)$ with aspect ratio for several values of k, and it is seen that reduction of aspect ratio causes a decrease of $v_x(k)$ for all values of k. Forward movement of the maximum-thickness position (*i.e.*, increase of k) causes an increase of $v_x(k)$ for both the finite and the infinite aspect ratio wings (Fig. 6a). For a given aspect ratio, however, the reduction of $v_x(k)$ relative to the corresponding two-dimensional value is almost independent of maximum-thickness position (Fig. 6b). This will not be true for very small aspect ratios, since according to the linearised theory, $v_x(k) = 0$ for zero aspect ratio. Furthermore, it may be found that for conventional round-nosed sections, the reduction of $v_x(k)$ due to aspect ratio and thickness taper may be different from that obtained for these simple sections. Results given recently in Ref. 11 for a rectangular wing tapered in thickness, and having a 10 per cent thick RAE 101 aerofoil section do, however, show that in this case agreement with the results obtained for these simple sections is very good.

It seems reasonable to restrict further discussion of the effects of thickness taper on the supervelocity at the maximum-thickness position of the centre-line chord, to the simple case of a wing with symmetrical parabolic-arc aerofoil section.

Figs. 7, 8 and 9 show the effects of aspect ratio A, spanwise extent of thickness taper ψs, and spanwise rate of thickness taper on the supervelocity $v_x(o)$. In these figures, s' is the spanwise distance from the centre-line at which upper and lower surface generators for the inboard tapered part of the wing, intersect the wing chord plane ; thus s' and t_0 (the centre-line thickness) define the spanwise rate of thickness taper.

The main conclusions to be drawn from these results are :

(*a*) The supervelocity at the centre of a rectangular wing decreases as the rate of spanwise thickness taper over the central part of the span is increased.

(*b*) For a given rate of spanwise thickness taper over the central part of the wing, and a given thickness of the outer wing panels, aspect ratio has little effect on $v_x(o)$, except when both the aspect ratio and the spanwise extent of taper are small (Fig. 7b). This is also shown by the similarity between the curves for $s'/c_0 = 2{\cdot}0$ of Figs. 8b and 9b.

(*c*) For all aspect ratios, the rate of decrease of $v_x(o)$ with decrease of ψ, is greatest when ψ is small.

(*d*) For a given rate of spanwise thickness taper over the central part of the span, $v_x(o)$ decreases with increase in the spanwise extent of the taper. This is caused by the reduced effect of the outer panels of the wing. For wings having only a small amount of thickness taper over the central part of the span, little reduction of $v_x(o)$ occurs for $\psi > 0{\cdot}2$ (Figs. 8a and 9a ; $s' > 2{\cdot}0c_0$).

3.4. *Spanwise Variation of the Supervelocity at the Maximum-Thickness Position.*—Fig. 10a shows the spanwise variation of $v_x(\bar{k})$, the supervelocity at the maximum-thickness position, for rectangular wings having a linear spanwise variation of thickness/chord ratio from t_0/c_0 at the centre-line to zero at the tips. $v_x(\bar{k})$ does not decrease linearly across the span as would be the case if $v_x(\bar{k})$ was dependent only on the local thickness/chord ratio. At about $0{\cdot}65$ semi-span $v_x(\bar{k})$ is almost independent of aspect ratio, the supervelocity being the same as that on an unswept two-dimensional wing of the local thickness/chord ratio.

Inboard of $\eta = 0{\cdot}65$, $v_x(\bar{k})$ is smaller than the corresponding two-dimensional value, and decreases with reduction of aspect ratio because of the larger effect of thickness taper. Outboard of $\eta = 0{\cdot}65$, $v_x(\bar{k})$ is greater than the corresponding two-dimensional value, and increases with reduction of aspect ratio.

The reduction of $v_x(\bar{k})$ below the corresponding two-dimensional value is plotted in Fig. 10b. As at the centre-line, the reduction of $v_x(\bar{k})$ due to thickness taper is, for a given plan-form and thickness distribution, almost independent of maximum-thickness position. The tests of Ref. 8 are to be extended to provide (by means of ' creeper ' static tubes) results over the outer part of the span for wings of RAE 101 section shape, to determine whether the results of Fig. 10b can also be applied to conventional round-nosed aerofoil sections.

Further investigation of the effects of spanwise thickness taper is restricted to the simple case of a wing with biconvex parabolic-arc aerofoil section. Figs. 11 and 12 illustrate the effects of spanwise extent of taper and the relative thickness of the outer panels on the spanwise variation of $v_x(o)$ for a wing of aspect ratio 4.

In Fig. 11, the rate of thickness taper over the inboard panels is maintained constant and the spanwise extent of the taper (ψ) varied, with a corresponding variation in the thickness/chord ratio of the outer panels. The effect of spanwise extent of taper on the supervelocities near the centre-line is negligible for $\psi > 0{\cdot}25$, as shown earlier (Figs. 7 and 8). For smaller values of ψ the velocities near the centre of the wing are increased due to the proximity of the outer panels. At the thickness crank the supervelocities are increased, the effect fading out about $0{\cdot}1s$ either side of the change in thickness taper. From Fig. 11b, which shows the reduction of $v_x(o)$ relative to the corresponding two-dimensional value, it is seen that the increase of $v_x(o)$ at the thickness crank is almost independent of the spanwise position of the crank.

Changing the spanwise rate of thickness taper over the inner part of the wing, while keeping the thickness of the outboard panels constant (Fig. 12), has a large effect on the supervelocities near the centre of the wing (inboard of about $\eta = 0{\cdot}1$) because of the variation in the thickness taper of the central panels. The increase of supervelocity at the thickness crank relative to the corresponding two-dimensional value is not independent of the spanwise position of the crank in this case, but is large for small values of ψ, becoming less marked with increase of ψ. Furthermore the spanwise extent of the wing influenced by the effects of the thickness crank increases with reduction of ψ.

From the results of Figs. 11 and 12, it is concluded that the relative increase of $v_x(o)$ at the crank in the thickness distribution is chiefly a function of the change of rate of thickness taper across the crank.

It should be noted that this increase of $v_x(o)$ at the thickness crank is due only to the change in thickness taper. In many practical cases, a change of thickness taper is associated with a change of plan-form taper or plan-form sweep, which will have a further effect on the supervelocities in the crank[9].

As a further illustration of the effects of thickness distribution, the results of Fig. 13 have been obtained by superimposing the wings, results for which are given in Figs. 11 and 12.

Comparison of curve A (Fig. 13) with the curve $\psi = 0{\cdot}25$, $\mu = 0{\cdot}75$ of Fig. 11, shows that decreasing the change of thickness taper at $\psi = 0{\cdot}25$ has caused a reduction in the supervelocity at both the centre-line and at the thickness crank ; at the crank, the supervelocity is almost equal to the corresponding two-dimensional value. At the outboard crank, the supervelocities are nearly the same as those shown in the curve $\psi = 0{\cdot}75$, $\mu = 0{\cdot}5$ of Fig. 12, since these two wings are similar near the crank.

Curve B of Fig. 13, shows that for a given spanwise extent of taper, and a given tip thickness, a considerable gain can be obtained over the inboard part of the wing by tapering in two stages, as compared with the curve $\psi = 0{\cdot}5$, $\mu = 0{\cdot}5$ of Figs. 11 and 12. The supervelocities are reduced near the centre-line because of the larger rate of taper over the centre part of the wing, and over the intermediate part of the wing because of the reduced thickness/chord ratio. At the inboard crank of wing B (Fig. 13), the supervelocity exceeds the corresponding two-dimensional value by about the same amount as the supervelocity at the crank of the wing of Fig. 12 ($\psi = 0{\cdot}5$, $\mu = 0{\cdot}5$) ; the changes in the rate of thickness taper across the two cranks are approximately the same. At the outer crank of wing B (Fig. 13), the excess supervelocity is considerably less than for the wing of Fig. 12, having only one thickness crank.

Wing C of Fig. 13 does not compare directly with any of the other wings considered, but has been included to show the wide variety of wing thickness distributions which can be obtained by the method of superposition. On this wing the supervelocities at the maximum-thickness position are approximately equal to or less than the corresponding two-dimensional values.

From the above discussion, it seems probable that if the thickness distribution across the cranks was faired to give a smooth variation across the span, some reduction of the supervelocity at the cranks could be obtained even though the thickness/chord ratio would have to be slightly increased locally ; this fairing out would certainly give better flow conditions on actual wings.

3.5. *Brief Summary of Main Results for Rectangular Wings.*—It has been shown that for rectangular wings having the simple aerofoil sections considered, the chordwise supervelocity distribution at any part of the span is related to the two-dimensional supervelocity distribution by a factor τ which is approximately constant across the chord. Furthermore, the reduction of the supervelocity at the maximum-thickness position relative to the corresponding two-dimensional value is, within the limitations of linearised theory, independent of aerofoil-section shape for the range of section shapes considered.

4. *Wings Tapered in Plan-form and Thickness.*—In the previous section the effects of thickness taper on the velocities on unswept rectangular wings were considered. In the present section, the effects of thickness taper on the velocities on unswept and swept wings tapered in plan-form are dealt with, and, by comparing wings having the same spanwise thickness taper, the effects of plan-form taper derived.

All the wings considered in this section have symmetrical parabolic-arc aerofoil sections. They are :

Wing (2) (Fig. 1).—A tapered wing having a linear spanwise variation of thickness/chord ratio from t_0/c_0 at the centre-line to zero at the tips.

The supervelocity v_x at a point (x, η) of this wing is derived in Appendix II by replacing the wing by swept source lines parallel to the maximum-thickness line, of constant strength across the span. In order to avoid singularities within the plan-form of the wing, use has been made of the fact that the source distribution required to represent this wing is the same as that for the portion of an infinite swept-back wing which lies within the wing (2) plan-form. Thus the velocity at any point of wing (2) has been derived as the difference between the velocity at that point due to a complete infinite swept-back wing, and the velocity due to that part of the infinite wing which lies outside the plan-form of wing (2).

Wing (3) (Fig. 1).—A tapered wing having a constant absolute thickness along constant percentage chord-lines throughout the span, *i.e.*, the thickness/chord ratio increases towards the tips in inverse proportion to the local chord.

The supervelocity v_x at the centre-line of this wing is derived in Appendix III by replacing the wing by swept source filaments along constant percentage chord-lines, the chordwise width of the filaments varying across the span in the same proportion as the chord, and the source strength increasing across the span inversely as the chord. In order to investigate the effects of plan-form taper the wing is cropped to give a non-zero taper ratio, and the velocity due to the fully tapered wing derived as the limit as the taper ratio (λ) approaches zero (*see* Appendix III).

Wings 4, 5 and 6 (Fig. 1).—Wing (4) is an unswept tapered wing, the thickness/chord ratio of which varies as $(1 + N\eta)(1 - \eta)$† across the span.

This wing is represented by source filaments parallel to the maximum-thickness line, the strength of which vary linearly across the span, *i.e.*, as $(1 + N\eta)$. For $N = 0$, this wing is the same as wing (2), $\varphi_0 = 0$ deg.

The value of N of most interest in this report is 2, since superimposing this wing on to wing (3) gives a wing (wing (5) of Fig. 1) which, when in turn superimposed on wing (2), produces wing (6). Wing (6) has almost constant thickness/chord ratio over the inboard half of the semi-span, and can be used to determine in a simple manner the approximate centre-line supervelocities for the wing of Ref. 7.

4.1. *Unswept Wings.*—4.1.1. *The shape of the chordwise supervelocity distribution at any spanwise position.*—Since unswept tapered wings are in fact swept along constant percentage chord lines at all but one chordwise position, it seems logical to consider them on the basis of known results for untapered swept wings. Some confirmation that this approach to the problem is reasonable, is provided by the results obtained in Appendix III. These show that the supervelocity at any point on the centre-line of a wing tapered in plan-form, but of constant thickness throughout the span, is exactly the same as that at the corresponding point of an infinite swept wing, having the same sweep as the constant percentage chord-line passing through that point.

Three types of supervelocity distribution can therefore be defined for comparison with the results obtained for wings tapered in plan-form, *viz.*:

(*a*) *'Pseudo-infinite sheared wing' distribution.*—This is defined as the supervelocity distribution for an infinite unswept wing of the same section shape, multiplied by the cosine of the local geometric sweep angle (φ) of the tapered wing (*i.e.*, sweep of constant percentage chord-line).

Therefore
$$\frac{v_x(x)}{V_0} = S^{(1)}(x) \cos \varphi, \quad \ldots \quad \ldots \quad \ldots \quad \ldots \quad \ldots \quad \ldots \quad \ldots \quad \ldots \quad (13)$$

where $v_x(x)$ is the chordwise supervelocity at chordwise position x, V_0 is the free-stream velocity, and $S^{(1)}(x)$ is a known function of (x) depending only on the aerofoil section shape $z(x)$ (*see* Ref. 4).

† $\eta = \frac{\text{spanwise distance from centre-line}}{\text{semi-span}}$

N is an arbitrary coefficient varying between -1 and $+\infty$ for wings having positive thickness throughout the span.

(*b*) *' Pseudo-infinite wing centre ' distribution.*—This is the same as for the centre of an infinite swept wing, with the constant sweep of the untapered wing replaced by the local geometric sweep (φ) of the tapered wing, *i.e.*:

$$\frac{v_x}{V_0} = \left\{ S^{(1)}(x) - S^{(2)}(x) f(\varphi) \right\} \cos \varphi, \qquad (14)$$

where $S^{(2)}(x)$ is a known function of (x) depending on aerofoil section shape[4].

(*c*) *' Pseudo-infinite wing tip ' distribution.*—The supervelocity distribution at the downstream tip of a semi-infinite wing is, according to linearised theory, the same as that at the centre of an infinite swept-forward wing having the same angle of sweep, but with the supervelocities reduced by one half. Thus substituting the local angle of sweep (φ) of the tapered wing, for the wing sweep of the untapered wing, the pseudo-infinite wing tip distribution is given by :

$$\frac{v_x}{V_0} = \tfrac{1}{2}\{ S^{(1)}(x) + S^{(2)}(x) f(\varphi) \} \cos \varphi \, . \qquad (15)$$

These pseudo-infinite wing distributions are shown for an unswept tapered wing of aspect ratio 3 in Fig. 14b, in the form $v_x(x)/v_x(k)$ (where $v_x(k)$ is the supervelocity at the maximum-thickness position). In this figure they are compared with calculated distributions of $v_x(x)/v_x(k)$ for various spanwise positions of wing (2), the actual supervelocity distributions for this wing being given in Fig. 14a.

For $\eta \simeq 0{\cdot}2$, the shape of the v_x distribution for wing (2) (Fig. 14b) is in close agreement with that for the pseudo-infinite sheared wing. At the centre-line, and near the tip ($\eta = 0{\cdot}8$), the v_x distributions are similar in shape to the pseudo-infinite wing ' centre ' and ' tip ' distributions, though here the agreement is not so good.

A similar comparison for the same type of wing of higher aspect ratio (Fig. 15a) shows much closer agreement between the shapes of the actual and pseudo-infinite wing distributions. In this case, the spanwise position at which the wing supervelocity distribution is similar in shape to that of the pseudo-infinite sheared wing, is further outboard (i.e., $\eta \simeq 0{\cdot}3$ instead of $\eta = 0{\cdot}2$ as for the $A = 3$ wing).

For both aspect ratios, the shape of the supervelocity distribution agrees with the pseudo-infinite sheared wing distribution at only one spanwise position, indicating that the ' centre ' and ' tip ' effects spread over the whole wing surface.

Results given in Ref. 7 for an aspect-ratio 6·67 wing having constant thickness/chord ratio throughout the span (reproduced in Fig. 15b), show that for this wing, the ' centre ' effect is negligible outboard of 0·2 semi-span, and that at $\eta = 0{\cdot}7$, the furthest outboard position for which results are given, the distortion of the supervelocity distribution due to the tip effect is quite small.

The comparison shown in Fig. 15 between wing (2) and the wing of Ref. 7 (both of aspect ratio 6·67), is not necessarily the correct one, however, since presenting the results in the form $v_x(x)/v_x(k)$ implies that both the ' two-dimensional ' and the ' kink ' components of the v_x distributions are related to the local thickness/chord ratio, and hence the spanwise thickness taper. Examination of the curves for $\eta = 0$ (Figs. 15a and 15b) shows that though the two wings have different rates of spanwise thickness taper at their centres (the spanwise thickness taper at the centre of wing (2) is double that at the centre of the wing of Ref. 7), the centre-line supervelocity distributions are almost identical.

This is very important, since it shows that (at least for $A \simeq 6{\cdot}67$) the ' kink ' term is independent of spanwise thickness taper. The expression for the supervelocity at the centre-line of a tapered wing having constant spanwise thickness, derived in Appendix III, shows that the ' kink ' term is also independent of spanwise variation of thickness/chord ratio. From this it follows that for a wing having the same aerofoil-section shape throughout the span, changes in spanwise rate of thickness taper do not introduce local ' kink ' effects, provided there is no change in plan-form sweep. There is of course a general increase or decrease in the supervelocities at, and near, the thickness crank as shown in section 3.4.

In Fig. 16, the results for wing (2), $A = 6{\cdot}67$, have been replotted to show the shape of the local chordwise supervelocity distribution compared with the pseudo-infinite sheared wing distribution for the local thickness/chord ratio. The ' tip effect ' is now seen to be of the same order as for the wing of Ref. 7.

The spanwise variation of the local ' kink ' effect, as a fraction (K_2) of the full centre-line value, has been plotted in Fig. 17a for both wing (2), $A = 6{\cdot}67$, and the wing of Ref. 7. These values of K_2 are not quite exact, since there is a small variation across the chord (within the accuracy of the computed results). This variation is due (in part) to ignoring the small $K_1 S^{(1)}(x) \cos\varphi$ term in equation (4). The results are sufficiently accurate, however, to show that the spanwise variation of K_2 is independent of the spanwise distribution of thickness.

Fig. 17b shows the effect of aspect ratio on the spanwise variation of K_2 for wing (2). The two major factors apparent in this figure are :

(*a*) the spanwise position at which K_2 is zero moves inboard with reduction of aspect ratio ($\eta = 0{\cdot}29$ for $A = 6{\cdot}67$; $\eta = 0{\cdot}17$ for $A = 3$)

(*b*) the ' kink ' effect near the centre of the $A = 3$ wing, is considerably less than the theoretical value for the pseudo-infinite wing distribution. It will be shown later that for a wing having a constant rate of spanwise thickness taper throughout the span, K_2 is unity at the centre-line ; if an allowance is made for the effects of finite aspect ratio on the pseudo-infinite centre distribution, the value of K_2 for wing (2) is also approximately unity even for aspect ratios as low as $A = 1$.

Thus it appears reasonable to assume that for $A = 3$, the spanwise variation of K_2 is as shown in Fig. 17b, with $K_2 = 1$ at the centre-line.

In Fig. 17c, values of K_2 for tapered wings of aspect ratio 3 and $6{\cdot}67$ are compared with the spanwise variation of K_2 for an infinite swept wing given in Ref. 4 (*see* section 3·4 of Ref. 4). For $A = 6{\cdot}67$, K_2 decreases more gradually away from the centre-line than for the infinite swept wing, though K_2 is zero at $y/c_0 = 0{\cdot}5$ for both wings. Thus though thickness taper does not materially affect the spanwise variation of K_2, plan-form taper does. Reducing the aspect ratio from $6{\cdot}67$ to 3, causes a considerable increase in the spanwise rate of decay of K_2, and reduces the spanwise distance from the centre at which K_2 is zero.

From these results it is clear that the effects of plan-form taper and aspect ratio on the spanwise variation of the ' kink '-term factor K_2, need further investigation, particularly for small amounts of plan-form taper. It is proposed, when time permits, to determine these effects using wing (3) of this report, which is untapered in thickness.

The results of Fig. 17 do, however, give a useful indication of the approximate spanwise variation of K_2 for wings having moderate and large amounts of plan-form taper.

Before discussing the centre-line supervelocity distribution in greater detail, one interesting result which applies only to unswept wings tapered in plan-form and thickness is worthy of mention. It enables one to derive very quickly the approximate supervelocity distribution over the whole wing, provided the aspect ratio is not too small ($A \leqslant 3$).

The method is illustrated for wing (2) in Figs. 18 and 19a, where it is shown that over a large portion of the chord, the actual reduction of the supervelocity (v_x) relative to the corresponding infinite unswept wing value, is almost independent of the chordwise position. Thus it is only necessary to know the two-dimensional supervelocity distribution for the appropriate thickness/chord ratio, and the actual supervelocity at one chordwise position in order to determine the approximate supervelocity over the whole wing.

A similar process has been applied to the results for the wing of Ref. 7 ($A = 6{\cdot}67$) in Fig. 19b. Again it is seen that over most of the span, the same method can be used ; at the centre-line a better approximation to the shape of the v_x distribution would, as shown earlier, be obtained from the pseudo-infinite wing centre distribution in this case.

4.1.2. *The shape of the centre-line supervelocity distribution.*—No results for very small aspect-ratio tapered wings have so far been considered. It was shown in Figs. 14b and 15a that the agreement between the actual centre-line supervelocity distribution for wing (2) and the pseudo-infinite wing centre distribution, deteriorated with decrease of aspect ratio. Unfortunately, the centre-line v_x distribution for a tapered wing having constant thickness/chord ratio throughout the span, is only given for $A = 6{\cdot}67$ in Ref. 7, so that it is not known whether this deterioration also applies to a wing of this type. Results have, however, been derived in this report, by suitably superimposing wings 2, 3 and 4 ($N = 2$), for the centre-line supervelocity distribution of a wing having approximately constant thickness/chord ratio over the inboard 50 per cent of the span. The variation of thickness/chord ratio over the outer parts of the wing should not have a material effect on the centre-line v_x distribution, except perhaps for very small aspect ratios.

The centre-line supervelocity distributions for wings 2, 3 and 6 are shown in Figs. 20 to 22 for $A = 1$, 3 and 5. These results show the very marked effect of spanwise thickness taper near the centre-line on the centre-line supervelocities (wing (3) has constant thickness throughout the span ; wing (6) has effectively constant thickness/chord ratio throughout the span, and wing (2) has a linear spanwise decrease of thickness/chord ratio to zero at the tips).

In addition to the actual supervelocity distributions, the shapes of the supervelocity distributions are presented in Figs. 20 to 22 in terms of $v_x(x)/v_x(k)$, where $v_x(k)$ is the supervelocity at the maximum-thickness position.

For all aspect ratios, the shape of the supervelocity distribution for wing (6) is almost identical with that for wing (3), which is the same as the pseudo-infinite wing centre distribution. The centre-line v_x distribution for wing (2), is however, relatively flatter than those for wings (3) and (6), particularly for $A = 1$. A curve for the supervelocity at the corresponding point of a finite untapered wing having the same span/centre-line chord ratio, and the same sweep as the local geometric sweep of the tapered wing (in future called the pseudo-finite wing centre distribution), is included in Fig. 20 : it is seen that the shape of this curve is similar to that for the v_x distribution at the centre-line of wing (2). This suggests that the less peaky supervelocity distribution at the centre of wing (2), as compared with that for wing (6), may be due to a more pronounced low-aspect–ratio effect, caused by the greater spanwise thickness taper. For larger aspect ratios ($A > 3$), the differences in shape between the centre-line v_x distributions for wings (2), (3) and (6) are small.

4.1.3. *Effect of aerofoil-section shape on the supervelocity at the centre-line maximum-thickness position.*—For wings tapered in plan-form and thickness/chord ratio (wing 2) it is not possible as in the case of rectangular wings, to change the aerofoil-section shape by substituting cubic-arc sections for parabolic-arc sections, without destroying the essential simplicity of the source distribution required to represent this wing. An aerofoil section which has its maximum thickness at a point other than the mid-chord position can, however, be formed from parabolic arcs which are different ahead of, and behind the maximum-thickness line. The portion of such a wing which lies ahead of the maximum-thickness line (assuming the maximum-thickness line to

remain unswept), is identical with the front half of wing (2) of the appropriate aspect ratio and centre-line thickness/chord ratio. Similarly the portion of this wing aft of the maximum-thickness line, is identical with the rear half of wing (2) of a different aspect ratio and thickness/chord ratio. The appropriate effective aspect ratios and thickness/chord ratios of the front and rear parts of this wing are determined (*see* Introduction) from the conditions that :

(a) the spans of the front and rear parts of the wing must be equal

(b) the maximum thicknesses of the front and rear parts of the wing must be equal

(c) the maximum thickness must be appropriate to the required thickness/chord ratio.

The contributions of both parts of the wing to the supervelocity at the maximum-thickness position can be readily determined for an unswept wing from the results for wing (2), since from considerations of symmetry the front and rear halves of wing (2) must contribute equally to $v_x(k)$ at the maximum-thickness position.

The results given in Fig. 23 show that, as for rectangular wings, the reduction of the supervelocity at the centre-line maximum-thickness position due to decrease of aspect ratio is almost independent of the position of the aerofoil-section maximum thickness. Results for other spanwise positions are discussed later (section 4.1.5.).

4.1.4. *Effect of aspect ratio, plan-form taper, and thickness taper on the supervelocity at the centre-line maximum-thickness position.*—It has been shown in section 4.1.1 that the supervelocity distribution at the centre-line of an unswept wing tapered in plan-form and thickness is similar in shape to either the pseudo-infinite or pseudo-finite wing centre distribution depending on aspect ratio. Thus the actual centre-line distribution can be obtained by multiplying the supervelocities at all chordwise positions, as defined by these pseudo-centre distributions, by a constant factor τ. Since the reduction of the supervelocity at the centre-line maximum-thickness position due to decrease of aspect ratio is independent of the chordwise position of the maximum thickness, it seems eminently suitable to define τ as the ratio :

$$\frac{\text{actual supervelocity at centre-line maximum thickness}}{\text{pseudo wing supervelocity at centre-line maximum thickness}}$$

as for the case of the rectangular wing.

Having thus defined the centre-line supervelocity distribution, it is necessary to consider the effects of plan-form and thickness taper on the actual supervelocity at the maximum-thickness position of the centre-line chord. Only the case of the symmetrical parabolic-arc aerofoil section is considered, since it has been shown that for both rectangular and tapered plan-form wings, the reduction of $v_x(k)$ at the maximum-thickness position, due to aspect ratio, is independent of maximum-thickness position.

The results are first presented in Fig. 24a with aspect ratio (A) as the independent variable, since this is the parameter having the greatest aerodynamic significance in plan-form design. For wings tapered in plan-form, four curves are given, *i.e.*:

Wing (3)—constant absolute thickness throughout the span

Wing (6)—constant thickness/chord ratio over the inboard 50 per cent of the span

Wing of Ref. 7—constant thickness/chord ratio throughout the span

Wing (2)—linear spanwise decrease of thickness/chord ratio to zero at the tips.

It is interesting to note the very close agreement between the results for wing (6), and those given in Ref. 7. This shows that the assumption that the small difference in tip thickness between these two wings is not sufficient to materially affect the centre-line supervelocities.

In addition to the curves for tapered wings, two curves are given for wings of rectangular plan-form :

Wing (1), $\psi = 1$, $\mu = 1$—constant thickness throughout the span

Wing (1), $\psi = 1$, $\mu = 0$—linear spanwise decrease of thickness to zero at the tips.

For a given aspect ratio and type of spanwise thickness distribution, it is immediately apparent that, in general, plan-form taper has only a small effect on the supervelocity $v_x(k)$ at the maximum-thickness position of the centre-line chord (except in the case of wings having constant spanwise thickness and $A < 2$). As would be expected from the earlier discussion, increase of spanwise thickness taper near the centre-line causes a reduction in $v_x(k)$.

For a given aspect ratio, however, rectangular and tapered wings have different spans, and Fig. 24a does not give a true indication of the effects of plan-form and thickness taper. The results of Fig. 24a have been replotted against the ratio :

$$\frac{s}{c_0} = \frac{\text{semispan}}{\text{centre-linechord}}$$

in Fig. 24b. Comparing the results for wing (6) and wing (1), $\psi = 1$, $\mu = 0$, it is now seen that for $s/c_0 > 1{\cdot}5$, plan-form taper has little effect on the supervelocity $v_x(k)$, at the centre-line maximum-thickness position. For smaller values of s/c_0, plan-form taper causes an increase in the value of $v_x(k)$, thus counteracting the beneficial effects of thickness taper. When s/c_0 is very small (*i.e.*, $s/c_0 \simeq 0{\cdot}25$), the value of $v_x(k)$ for wing (6) is almost as large as that for wing (1), $\psi = 1$, $\mu = 1$, and the value of $v_x(k)$ for wing (2) is approximately equal to that for wing (1), $\psi = 1$, $\mu = 0$. Thus in these cases, the reduction in $v_x(k)$ due to the thickness taper has been almost completely balanced by the increase in $v_x(k)$ due to plan-form taper.

Fig. 25a shows the increase in $v(k_x)$ caused by plan-form taper. Comparison of the results for wing (1), $\psi = 1$, $\mu = 0$ with those for wing (3), $\lambda = 0$ (*i.e.*, a fully tapered wing having constant spanwise thickness), gives the effect of plan-form taper for a wing untapered in thickness. A similar comparison between the results for wing (1), $\psi = 1$, $\mu = 0$, and wing (6), gives the effect of plan-form taper for a wing having a linear spanwise variation of thickness. It is seen that for $s/c_0 > 0{\cdot}5$, spanwise thickness taper has only a small effect on the increase of $v_x(k)$ due to plan-form taper.

Hence, a further curve has been given in Fig. 25a to show the effect of tapering a wing so that the taper ratio λ (tip chord/centre-line chord) is $0{\cdot}5$. This curve was obtained by comparing the supervelocities given by equation (III.10) of Appendix III for $\lambda = 0{\cdot}5$, with those for wing (1), $\psi = 1$, $\mu = 1$. The increase of $v_x(k)$ due to plan-form taper does not increase quite linearly with decrease of taper ratio, but these two curves are sufficient to enable a fairly accurate estimate of the effect of λ to be made (intermediate values can be obtained quite easily from equations (III.10) and (III.11) of Appendix III).

A similar procedure has been adopted in Fig. 25b to illustrate the effects of thickness taper. In this case, comparison of the results for $\mu = 0$ and $\mu = 1$ for wing (1), $\psi = 1$, gives the reduction in $v_x(k)$ due to thickness taper for a rectangular wing, and comparison between wings (3) and (6), the corresponding value for wings tapered in plan-form. The close agreement between the two curves for $\Delta v_x(k)$ so obtained, shows that the effects of thickness taper are virtually independent of plan-form taper. It is concluded from the results of Figs. 25a and 25b that the effects of plan-form and thickness taper are almost independent of each other.

Since the results presented in Figs. 25a and 25b give the increase of $v_x(k)$ due to plan-form taper, and the reduction of $v_x(k)$ due to thickness taper, relative to the corresponding finite untapered wing, the reduction in $v_x(k)$ due to decrease of aspect ratio ($A = 2s/c_0$ for an untapered wing) is shown in Fig. 25c. Results for two values of (k) have been calculated ($k = 0$ and $k = 0{\cdot}33$, representing maximum-thickness positions at $0{\cdot}5$ and $0{\cdot}33$ chord). As for rectangular and tapered wings, tapered in thickness, maximum-thickness position has little effect on the reduction of $v_x(k)$ relative to the two-dimensional value.

In Fig. 25d, the reduction of $v_x(k)$ relative to the unswept two-dimensional value has been plotted for wings (2) and (6), and for wing (1), $\psi = 1$, $\mu = 0$, against the ratio s'/c_0 (s' is the spanwise distance from the centre-line at which a tangent to the maximum-thickness line, at the centre of the wing, cuts the wing chord plane). Thus for a given value of s'/c_0 all three wings have the same spanwise rate of thickness taper at the centre-line. They have, however, different amounts of plan-form taper, λ being 1, $0{\cdot}5$ and 0 for wings (1), (2) and (6) respectively.

The main point of interest in this figure, is the small difference in $\Delta v_x(k)$ between wings (2) and (6). From Figs. 25a and 25b, the value of $\Delta v_x(k)$ for wing (2) would be expected to be approximately the mean of the values for wings (1) and (6), but the continual reduction in thickness taper away from the centre-line reduces the value of $\Delta v_x(k)$ in the same way as shown earlier for rectangular wings, when ψ was small. This characteristic of wing (2) has been used later in this report to determine the approximate supervelocity at the centre-line maximum-thickness position for a swept tapered wing having constant thickness/chord ratio throughout the span.

4.1.5. *Spanwise variation of the supervelocity at the maximum-thickness position.*—The spanwise variation of the supervelocity at the maximum-thickness position is shown for wing (2) in Fig. 26a. It is seen that reduction of aspect ratio results in a decrease in the supervelocities over the inboard part of the wing, and an increase in those over the outer part. At about mid–semi-span, aspect ratio has little effect on the supervelocities at the maximum-thickness position.

One result has been calculated for a wing having an aerofoil section formed by parabolic arcs, but having its maximum-thickness position ($x = k$) at $0{\cdot}38$ of the half chord length ahead of the mid-chord point. As in the case of the rectangular wing, this forward movement of the maximum-thickness position results in an increase of the supervelocities across the whole span, but again does not significantly alter the reduction of the supervelocity relative to the two-dimensional value for the local thickness/chord ratio (Fig. 26b). It is of interest to note that from Fig. 26b, the point at which the supervelocity is the same as the local two-dimensional value, moves outboard with decrease of aspect ratio, whereas, as was seen earlier, the spanwise position at which the supervelocity distribution is similar in shape to the pseudo-infinite wing distribution, moves inboard.

Results have also been derived from Ref. 7 to show the effect of moving the maximum-thickness position forward to $0{\cdot}33$ chord on the spanwise variation of the supervelocity at the maximum thickness of a constant thickness/chord ratio wing. These are presented in Fig. 27 for an aspect ratio of $3{\cdot}33$. Again, forward movement of the maximum-thickness position results in an increase in the supervelocities across the whole wing, but as shown in Fig. 27b, it does not alter significantly the reduction of the supervelocities relative to the two-dimensional value for the local thickness/chord ratio. Results for the spanwise variation of the supervelocity at the maximum thickness for tapered wings, having constant thickness/chord ratio throughout the span, can be found for other aspect ratios in Ref. 7.

4.1.6. *Effect of plan-form and thickness taper on the spanwise variation of the supervelocity at the maximum thickness.*—In Fig. 28, a comparison is made between the spanwise variations in the reduction of supervelocity due to taper for wings having different plan-form and thickness tapers. In each comparison, the rate of thickness taper at the centre-line has been kept constant

(i.e., s'/c_0 = constant), since it has been shown earlier that the ratio s'/c_0 is the chief parameter defining the reduction of v_x at the centre-line.

Comparison of the results for wings having rectangular and tapered plan-forms and linear spanwise variation of absolute thickness (*i.e.*, wing (1), $\psi = 1$, $\mu = 0$, and the wing of Ref. 7) shows that the effect of plan-form taper, which was found to be present at the centre-line, rapidly diminishes, and outboard of $\eta \simeq 0{\cdot}1$, the reduction of v_x at any spanwise position is virtually independent of plan-form. For values of $s'/c_0 > 2{\cdot}0$, plan-form taper has little effect on the supervelocity at the maximum thickness even at the centre-line. Thus spanwise distribution of thickness/chord ratio is not an important parameter in determining the reduction of the supervelocity due to taper.

Comparing the results for the two wings tapered in plan-form (*i.e.*, wing (2) having linear spanwise variation of thickness/chord ratio, and the wing of Ref. 7 having linear spanwise variation of absolute thickness) shows that the reduction of v_x due to taper is in agreement only at the centre-line. The absolute spanwise distance from the centre-line at which the reduction of the supervelocity relative to the local two-dimensional value becomes zero, is however approximately the same for the two wings, since the span of wing (2) is twice that of the wing of Ref. 7. Replotting the results against $\eta' = y/s'$ to allow for the difference in span of the two wings does not however bring the results into very close agreement.

Since the results for wings having linear spanwise variation of absolute thickness do not indicate any marked effect due to changes in thickness/chord ratio (wing (1) and wing of Ref. 7), it seems probable that the differences are due to the different surface slopes at a given spanwise distance from the centre-line. In Fig. 29, the results of Fig. 28 have been multiplied by a factor $t_0(1 - \eta)/t\eta$ to allow for the difference in surface slopes, and then plotted against η': the factor $t_0(1 - \eta)/t\eta$ does not affect the results for wings having a linear spanwise variation of absolute thickness, but brings the results for wing (2) into much closer agreement with those for wing (1) and for the wing of Ref. 7. It is seen that the results for all three types of wing are now in fairly close agreement, except near the centre-line, where the effects of plan-form taper are apparent. From these results, it is concluded that the effects of plan-form taper on the reduction of the supervelocity relative to the corresponding two-dimensional value due to thickness taper are small, except close to the centre-line of the wing. It should be possible, therefore, from the results given in this report to determine the supervelocity reduction at any spanwise position relative to the local two-dimensional value, for a wing of any spanwise thickness distribution. The reduction of v_x at the centre-line can be determined from the separate effects of plan-form and thickness taper (Fig. 25) and the spanwise variation of Δv_x from results for a wing having the same spanwise variation of absolute thickness. For wings having sharp changes of thickness distribution, this equivalent wing should be derived as suggested in section 3.1 from the equations given in Appendix I, while for wings having non-linear but continuous spanwise thickness distributions, the results for wing (2) (Appendix II) and the wing of Ref. 7 should be used.

As an example of the way in which the method of superposition can be used to derive wings having other than parabolic spanwise thickness distributions, results have been given in Fig. 30a for an aspect ratio 6·67 wing, tapered in plan-form, and having different linear spanwise variations of thickness/chord ratio. These results were obtained by superimposing the results for wing (2) ($A = 6{\cdot}67$) on those for the wing of Ref. 7 ; in Fig. 30, μ is the ratio of the thickness/chord ratio at the tip, to that at the centre-line. The main effect of increasing the thickness/chord ratio at the tip, is to increase the supervelocities over the outer part of the wing. A smaller increase of v_x also occurs at the centre of the wing due to the reduction in the rate of thickness taper at the centre-line, even though the thickness/chord ratio is unchanged.

The results of Fig. 30a have been replotted to show the reduction of the supervelocity relative to the two-dimensional value for the local thickness/chord ratio, in Fig. 30b. It is apparent that

most of the change in v_x of the outer parts of the wing is due to the alteration in thickness/chord ratio, but over the inboard parts (*i.e.*, for $\eta < 0{\cdot}1$) a genuine change of v_x due to change in thickness taper is apparent.

4.1.7. *Effect of spanwise thickness distribution on the isobar pattern for a tapered wing.*—Fig. 31 demonstrates the effect of spanwise thickness distribution on the isobar pattern for an unswept tapered wing of aspect ratio 6·67. For $\mu = 1$ (*i.e.*, constant thickness/chord ratio throughout the span), a band of high supervelocities, exceeding 90 per cent of the two-dimensional value for the aerofoil section, spreads over almost the whole span. The isobars which form the boundary of this high supervelocity region are almost unswept except in a region close to the centre-line. If it is assumed that the critical Mach number at any spanwise section of a wing is dependent on the component of the local Mach number normal to the isobars (or isobaric surfaces), then the flow over the whole span of this wing will be supercritical at a free-stream Mach number a little above the two-dimensional $M_{\text{crit.}}$ for the aerofoil section.

Introducing spanwise taper of thickness/chord ratio (*i.e.*, reducing μ) causes a large reduction of the supervelocities over the outer parts of the wing, due to the decrease in the local thickness/chord ratio, and a smaller reduction of the supervelocities near the centre of the wing due to the greater amount of thickness taper. The net result of these changes is a reduction of the maximum supervelocity on the wing, and an inboard movement of its location. Coupled with this, is a reduction of the spanwise extent of the high supervelocity regions, and a general increase in isobar sweep near the maximum-thickness line of the wing. Both the reduction of the supervelocities, and the increase of the isobar sweep should produce an improvement in the critical Mach number of the wing. The larger isobar sweep should also tend to restrict the chordwise expansion of the supersonic flow regions when they form.

One practical difficulty introduced by spanwise taper of thickness/chord ratio is the loss of volume within the wing (for $\mu = 0$, the wing volume is only three quarters of the volume for $\mu = 1{\cdot}0$). Because of the beneficial effects of thickness taper, however, the maximum supervelocity on the wing is only 0·82 of the centre-line-section two-dimensional value when $\mu = 0$, whereas for $\mu = 1$, the supervelocity is at least 3 per cent higher than the two-dimensional value outboard of $\eta = 0{\cdot}8$. Thus the thickness/chord ratios throughout the span of the $\mu = 0$ wing can be increased by over 25 per cent without the maximum supervelocity exceeding the supervelocity at $\eta = 0{\cdot}8$ on the $\mu = 1$ wing. This brings the volume of the $\mu = 0$ wing up to 94 per cent of the volume of the $\mu = 1$ wing, and provides greater structural and storage depth near the centre of the wing without any loss of critical Mach number. With the thin wings at present in use on aircraft, this increase in depth could lead to a significant saving in structure weight, and the elimination of many small excrescences made necessary by the impossibility of complete internal stowage of equipment within the wings.

4.1.8. *Brief summary of results for unswept wings.*—For rectangular or tapered unswept wings having zero or linear spanwise variation of thickness, the shape of the chordwise supervelocity distribution at any spanwise position is similar to the pseudo-infinite sheared wing distribution for the local thickness/chord ratio, with a proportion K_2 of the full centre-line ' kink ' effect added. The centre-line ' kink ' term, and the spanwise variation of the factor K_2, are virtually independent of the spanwise thickness distribution, but are dependent on plan-form taper.

The actual supervelocity distributions are related to these pseudo infinite distributions by a factor τ, which is almost constant across the chord at any spanwise position. Thus, using the notation of equation (4),

$$\frac{V_x(x,\eta)}{V_0} = 1 + \frac{v_x(x,\eta)}{V_0}$$

$$= 1 + \tau\{(1 + K_1(x,\eta))S^{(1)}(x,\eta) - K_2\, S^{(2)}(x,0)\, f(\varphi)\}\cos\varphi. \quad \ldots \quad \ldots \quad (16)$$

The factor K_1 has been included in equation (16) to make it more general, even though no allowance has been made in the analysis of the results for unswept wings. K_1 is zero at the maximum-thickness line, and at the centre-line of the wing, and can be ignored except for wings of very small aspect ratio.

If the spanwise thickness taper is large near the centre of the wing, and is restricted to a small spanwise extent, the results for wing (2) suggest that an allowance should be made for the effect of finite aspect ratio on the shape of the pseudo untapered wing supervelocity distribution (*see* Ref. 3).

The value of τ in equation (16) can be expressed in terms of the reduction of the supervelocity $v_x(k)$ at the maximum-thickness position, relative to the corresponding two-dimensional value. Within the limitations of the linearised theory, and the range of sections considered, this decrease of $v_x(k)$ is independent of aerofoil-section shape.

For an unswept wing, at $x = k$, $\varphi_k = 0$, $K_1 = 0$ and $f(\varphi)_k = 0$.

Therefore from equation (16) :

$$\tau = \frac{1}{V_0}\frac{v_x(k, \eta)}{S^{(1)}(k, \eta)}$$

$$= 1 - \frac{\Delta v_x(k, \eta)}{V_0 S^{(1)}(k, \eta)} \qquad \ldots \ldots \ldots \ldots \ldots \ldots \ldots \qquad (17)$$

where $V_0 S^{(1)}(k, \eta)$ is the supervelocity at the maximum thickness position of the corresponding two-dimensional wing (*see* Ref. 4), and $\Delta v_x(k, \eta)$ is the reduction of $v_x(k, \eta)$ relative to the two-dimensional value.

At the centre-line, $\Delta v_x(k, o)$ is obtained for the appropriate span, plan-form taper and thickness taper from Fig. 25, but outboard of $\eta = 0 \cdot 1$, where $\Delta v_x(k, \eta)$ is independent of plan-form taper, it should be derived for a wing having the same spanwise thickness distribution. In general, wings have linear spanwise distributions of thickness, whether the rate of thickness taper is the same throughout the span or not, and hence the expressions derived in Appendix I are most useful in determining $\Delta v_x(k)$. For wings having non-linear spanwise distributions of thickness, the expressions derived in Appendices II and IV provide a wide range of distributions as a guide.

4.2. *Swept Wings.*—Only two types of tapered swept wing are considered in this section, *i.e.*:

Wing (2)—having a linear spanwise variation of thickness/chord ratio from (t_0/c_0) at the centre-line to zero at the tips

Wing (3)—having constant thickness throughout the span. Two values of taper ratio have been used for this wing to show the effect of taper ratio on the supervelocity at the centre-line maximum-thickness position.

4.2.1. *Shape of the chordwise supervelocity distribution.*—It is not necessary to discuss in great detail the chordwise supervelocity distributions for swept wings, since the conclusions derived for unswept wings should apply equally well to swept wings (unswept tapered wings are themselves swept at all but the maximum-thickness position). In order to check these conclusions, a few comparable results are shown for swept wings in Figs. 32 to 35.

Fig. 32a shows the supervelocities at various chordwise and spanwise positions of a 60 deg swept wing of aspect ratio 3 (wing (2)) as calculated from equation (II.17) of Appendix II (indicated by symbols in Fig. 32a). These are compared with chordwise supervelocity distributions calculated from the expression used for unswept wings (*see* equation 16) :

$$\frac{V_x(x, \eta)}{V_0} = \left\{(1 + K_1(x, \eta))S^{(1)}(x, \eta) - K_2 S^{(2)}(x, o) f(\varphi)\right\} \cos \varphi \ , \qquad \ldots \qquad \ldots \qquad (18)$$

φ being the local angle of sweepback.

Values of K_1 for infinite swept wings of the appropriate sweep angle φ (*see* Fig. 46) have been used. The values of K_2 were determined by comparing the results given by equation (18) for $K_2 = 0$, with those given by equation (II.17) of Appendix II. At the centre-line, a value of unity has been assumed for K_2 in calculating the results of Fig. 32a, though the value necessary to give agreement between the supervelocities calculated using equations (18) and (II.17) of Appendix II is approximately $0{\cdot}6$.

It is seen from Fig. 32a that the agreement between the supervelocities derived from the two equations is good, except at the centre-line, where the effects of finite span distort the shape of the supervelocity distribution, as in the case of the unswept wing. The spanwise variation of the ' kink '-term reduction factor K_2, derived as explained above, is compared with the corresponding values for an unswept wing of aspect ratio 3 in Fig. 32b. It is apparent that sweepback has little effect on the spanwise variation of K_2, and hence the results given in Fig. 17 (and reproduced in Fig. 48b) can be used for tapered wings of any sweep, to supplement the interpolation curve derived in Ref. 4 for infinite swept wings.

Fig. 32b shows that K_2 has approximately the same value at the centre-line (not unity) for both the swept and unswept wing. This suggests that, as for the unswept wing, a better approximation to the shape of the centre-line supervelocity distribution might be obtained by using the pseudo finite wing centre distribution. Figs. 33 to 35 show comparisons between the centre-line supervelocity distributions for wing (2), and the corresponding pseudo infinite and pseudo finite centre distributions (wing (3) has the same centre-line supervelocity distribution as the pseudo-infinite wing). In view of the small aspect ratio of the wings considered, the agreement between the shape of the supervelocity distributions at the centre of wing (2) and those for the corresponding pseudo finite wings, is reasonbly good. These results show that the supervelocities at the centre of wing (2), behave in a similar manner, irrespective of wing sweepback.

No calculated supervelocity distributions are available for swept, tapered wings having constant thickness/chord ratio throughout the span, but on the basis of the comparison between the swept and unswept centre distributions for wing (2), it seems reasonable to assume that the shape of the centre-line supervelocity distribution for such a wing would be the same as that for the centre-line of the pseudo-infinite swept wing. This assumption is supported by results given in Ref. 4 for a delta wing having RAE 104 section shape throughout the span, which show that even with this entirely different type of aerofoil section, the measured pressure distribution at the centre of the wing is similar in shape to that for the pseudo-infinite wing.

Estimated centre-line supervelocity distributions are shown in Figs. 33 to 35 for swept wings having constant thickness/chord ratio parabolic-arc aerofoil sections throughout the span. The value of $v_x(k)$ at the maximum thickness position has been estimated from the results for wing (2), taking the same sweepback and the same spanwise rate of thickness taper as for the constant thickness/chord ratio wings. It is seen that for the $A = 1$ delta wing, the large amount of thickness taper near the centre of wing (2) relative to that at the centre of the wing with constant thickness/chord ratio throughout the span, has a marked effect, not only on the level of the supervelocities, but also on the position of the maximum supervelocity. This shows that the sweep of the peak suction line near the centre of wing (2) is greater than that for the constant (t/c) wing, since the shape of the supervelocity distribution further outboard should be similar for the two wings. This should have an important effect on the comparison of the critical Mach numbers for the two wings, in addition to the direct effects of difference in thickness/chord ratio.

A few examples of centre-line supervelocity distributions are given in Figs. 36 and 37 for wing (2) to illustrate the qualitative effects of sweepback and aspect ratio. The main points of interest are :

(*a*) For a given aspect ratio, the supervelocities at the centre-line of a tapered wing do not decrease as rapidly with sweepback as in the case of untapered wings of moderate or large aspect

ratio. The maximum supervelocity is, in fact, almost independent of sweepback (Fig. 36) for angles of sweep less than 45 deg. The peak supervelocity is, however, considerably less than that on an infinite swept wing having the same sweep on the maximum-thickness line.

(*b*) Reduction of aspect ratio causes a decrease of the supervelocities at the centre of a tapered wing (whereas for an untapered wing, if the angle of sweepback is greater than about 35 deg. decrease of aspect ratio causes an initial increase in the supervelocities). This effect is partly due to the increase of thickness taper at the centre-line with reduction of aspect ratio, and partly to the change of the local geometric sweep of the wing. The reduction of sweep aft of the maximum thickness reduces the local centre or ' kink ' effect.

(*c*) Reduction of aspect ratio causes a forward movement of the peak supervelocity position. This is largely caused by the change in the local angle of sweepback, and the consequent chordwise variation of the finite aspect-ratio and ' kink ' effects for this type of wing.

(d) For a wing tapered in thickness/chord ratio and plan-form, the forward movement of the peak supervelocity position is roughly proportional to the decrease in the maximum supervelocity.

4.2.2. *Effect of plan-form and thickness taper on the supervelocity at the centre-line maximum-thickness position.*—The variation of the supervelocity $v_x(k)$ at the centre-line maximum-thickness position of wing (3), with span/centre-line chord ratio, is shown in Fig. 38a for three values of taper ratio (i.e., $\lambda = 0$, $0{\cdot}5$ and 1).

As shown earlier, increase of plan-form taper increases the value of $v_x(k)$ relative to the corresponding untapered wing value, for unswept wings of fairly small aspect ratio. This effect becomes less marked with increase of sweep, and for $\varphi \simeq 50$ deg, plan-form taper has little effect on the value of $v_x(k)$. For sweep angles greater than 50 deg, increase of plan-form taper reduces the value of $v_x(k)$ slightly.

Fig. 39a shows the increase of $v_x(k)$ for sweep angles between 0 deg and 70 deg for two values of taper ratio ($\lambda = 0$ and $\lambda = 0{\cdot}5$).

Only one set of results is available for swept wings tapered in thickness, *i.e.*, results for wing (2). These are compared in Fig. 38b with $v_x(k)$ values for wing (3) of the same plan-form. As in the case of plan-form taper, the effect of thickness taper on $v_x(k)$ decreases with increase of sweepback, and for $\varphi = 70$ deg, thickness taper has no effect for $s/c_0 > 0{\cdot}75$.

The variation of the reduction of $v_x(k)$ due to thickness taper with sweepback is shown in Fig. 39b. These values have been plotted against the ratio s'/c_0 (s' is the spanwise distance from the centre-line at which a tangent to the maximum-thickness line at the centre of the wing cuts the wing chord plane), since it has been shown that for an unswept wing, the supervelocity $v_x(k)$ at the centre of wing (2) is almost equal to that at the centre of wing (6) (constant thickness/chord ratio throughout the span) for the same rate of thickness taper at the centre-line. This must still be approximately true for swept wings, since superimposing wing (3) on to wing (2) gives a crude approximation to a constant thickness/chord ratio wing near the centre, and the values of $v_x(k)$ for such a wing, obtained from the results of Fig. 38b, are in fairly close agreement with these for wing (2) at the same value of s'/c_0.

As the increase of $v_x(k)$ due to plan-form taper shown in Fig. 39a is given relative to the value for the corresponding untapered, finite aspect-ratio wing, the reduction of $v_x(k)$ due to decrease of aspect ratio has been given in Fig. 39c. These results apply to a wing having a parabolic-arc aerofoil section, but as shown in Ref. 3, the first order correction term for the effect of finite aspect ratio depends on the ratio :

$$\frac{\text{area of aerofoil profile}}{\text{area of circumscribing rectangle}} \quad (\textit{see} \text{ equation (9)}).$$

This ratio is reasonably independent of aero-foil-section shape, varying between about $0{\cdot}65$ and $0{\cdot}75$, and hence it would be expected that the results obtained for a parabolic-arc section, would apply fairly well to other aerofoil sections, except for very small aspect ratios, when higher order correction terms must be included.

Hence the supervelocity at the centre-line maximum-thickness position of a wing can be obtained using the results given in Figs. 39a, 39b and 39c, provided the corresponding infinite-swept wing value is known.

4.2.3. *Spanwise variation of the supervelocity at the maximum-thickness position.*—Theoretical results for the spanwise variation of the supervelocity at the maximum-thickness position are given in Fig. 40 for wing (2). These are the only theoretical results available for swept, tapered wings.

The effect of sweepback on the spanwise variation of v_x for a constant aspect ratio ($A = 3$) is shown in Fig. 40a, where it is seen that increase of sweepback causes a reduction of v_x at all spanwise positions. The reduction of the supervelocities due to sweep, is greatest at the centre and tips, the smallest change occurring at about $\eta = 0{\cdot}2$. Comparative spanwise distributions have been given for infinite aspect-ratio swept-back, and sheared wings, of the local thickness/chord ratio. The curves for the infinite swept wings show a similar trend to those for the finite aspect-ratio swept wing, and indicate that the effects of taper (particularly near the centre-line) decrease with increase of sweep.

In Fig. 40b, a similar comparison is made for wings of 45-deg sweepback, to show the effect of changing the aspect ratio. Again the curves for the finite and infinite aspect-ratio swept wings show similar trends. The change in the infinite aspect-ratio wing curves is due to the fact that a given spanwise distance from the centre-line (in terms of the centre-line chord), represents a different value of η for each of the three wings, and hence, a change in the local thickness/chord ratio which has been allowed for in the results. The general effects of reducing the aspect ratio for the 45-deg wing are similar to those found for the unswept wing (*see* Fig. 26a), *i.e.*, a decrease of the supervelocities near the centre, due to an increase in the spanwise thickness taper, and a small increase near the tips. The spanwise position at which aspect ratio has little effect on the supervelocity is, however, further inboard for the swept wing (i.e., $\eta \simeq 0{\cdot}3$) than for the unswept wing ($\eta \simeq 0{\cdot}5$).

The results for wing (2) shown in Fig. 40 have been replotted in Fig. 41, after deducting the increase of supervelocity due to the centre effect for the corresponding untapered, infinite swept-back wing of the local thickness/chord ratio. This increase of v_x which is the difference, between the supervelocity on an infinite swept wing and that on an infinite sheared wing, of the local thickness/chord ratio, and having the same sweepback as the maximum-thickness line :

$$v_x(k)_{A=\infty,\text{ swept wing}} \quad - v_x(k)_{A=\infty,\text{ sheared wing}}$$

can be expressed as :

$$K_1 v_x(k)_{A=\infty \text{ sheared wing}}$$

or

$$V_0 K_1 S^{(1)}(k) \cos \varphi_k ,$$

$V_0 S^{(1)}(k)$ being the supervelocity $v_x(k)$ on the corresponding unswept two-dimensional wing.

The resulting spanwise variation of the supervelocity at the maximum-thickness position, $v_x(k) - V_0 K_1 S^{(1)}(k) \cos \varphi_k$, is termed the ' quasi-sheared–wing spanwise supervelocity distribution ' in this report.

The quasi-sheared–wing spanwise supervelocity distributions shown in Fig. 41a indicate that for a given aspect ratio, the supervelocity decreases with increase of sweepback by an amount which is almost independent of spanwise position. In fact, the maximum variation in the reduction of $\Delta v_x(k)/V_0$ from the value at the centre-line, nowhere exceeds $0{\cdot}05$ for unit centre-line thickness/chord ratio.

The results of Fig. 41b confirm that this result is not confined to one aspect ratio, but applies equally well to smaller and larger aspect ratios, at least for $\varphi = 45$ deg. Indeed it is clear that for infinite swept wings, deducting the increase of supervelocity $(K_1 v_x(k)_{A=\infty, \text{sheared wing}}$ due to the centre effect, from the actual supervelocity, will give the supervelocity on the infinite sheared wing. The reduction of the supervelocity due to sweep is therefore completely independent of spanwise position for an infinite swept wing, and is equal to $V_0(1 - \cos \varphi_k)\, S^{(1)}(k)$.

Thus for swept wings having symmetrical parabolic-arc aerofoil sections, and a linear spanwise variation of thickness/chord ratio, the spanwise variation of $v_x(k)$ at the maximum-thickness line can be obtained to a close degree of approximation from the results for the corresponding unswept wing if the reduction of v_x at the centre-line, and the appropriate values of K_1 are known.

4.2.4. *Effect of aerofoil-section shape, and spanwise thickness distribution on the spanwise variation of the supervelocity at the maximum-thickness position.*—Theoretical results are not available for swept tapered wings having parabolic-arc aerofoil sections, and constant spanwise thickness/chord ratio, to determine whether spanwise thickness distribution has any effect on the conclusions drawn in the previous section. Experimental results are however available for an aspect-ratio–3 delta wing having a 10 per cent thick NACA 0010 aerofoil section throughout the span, which were obtained in the Royal Aircraft Establishment 10 ft × 7 ft High-Speed Tunnel at a Mach number $M = 0{\cdot}5$. The results for higher Mach numbers indicate that the variation of the pressure coefficients for this wing with Mach number are small below $M = 0{\cdot}5$.

The method used for determining the spanwise variation of the pressure coefficients for this wing is given in Table 1, and discussed in section 6. Briefly, it has been assumed that the conclusions drawn in the previous section for wing (2) are applicable to wings having other aerofoil-section shapes and other spanwise thickness distributions. From the results for unswept tapered wings, it is known that for the simple aerofoil-section shapes considered, section shape has little effect on the reduction of the supervelocity due to taper relative to the corresponding untapered wing value. The results of Ref. 7 have therefore been used to determine from the two-dimensional supervelocity the spanwise variation of v_x at the maximum thickness for an unswept tapered wing having NACA 0010 aerofoil section throughout the span. The reduction of v_x at the centre-line has been obtained from Fig. 39, for the appropriate sweep angle and span/centre-line chord ratio, and the quasi-sheared–wing spanwise distribution of v_x obtained by applying this reduction of v_x at all spanwise stations. Finally, the additional supervelocity due to the centre effect, $K_1 v_{x\,A=\infty, \text{sheared wing}}$, has been added to the quasi-sheared–wing spanwise distribution of v_x, to give the estimated spanwise variation of v_x (values of K_1 for a parabolic-arc aerofoil section have been used). These estimated supervelocities have been converted into pressure coefficients at zero Mach number, using the formula :

$$C_p = 1 - \left(1 + \frac{v_x}{V_0}\right)^2$$

(where V_0 is the free-stream velocity)

and are presented in Fig. 42a together with experimental values obtained at $M = 0{\cdot}5$.

It is seen that over the outer part of the span, the agreement between the experimental and the estimated values is extremely good, and even near the centre of the wing, the agreement is reasonably good. Some of the discrepancy between the estimated and the experimental results inboard of $\eta = 0{\cdot}3$ may be due to the use of K_1 factors calculated for the parabolic-arc section. Haines[5], in unpublished work has shown that section shape does influence both the level and spanwise distribution of K_1 slightly.

These results indicate that change of aerofoil-section shape and spanwise thickness distribution do not have a marked effect on the conclusions derived earlier from the results for wing (2). The same method has therefore been applied to derive an approximate spanwise distribution of v_x (Fig. 42b) for a 45-deg swept tapered wing having a parabolic-arc aerofoil section of constant thickness/chord ratio throughout the span. This result will be useful for checking against other results for this type of wing when they become available (*see* Ref. 7).

4.2.5. *Effect of sweepback on the shape of the isobar pattern for wing* (2).—Isobar patterns have been plotted in Fig. 43 for wing (2), aspect ratio 3, to show the effect of changing the sweepback from 0 deg to 60 deg. The chief effect of sweepback (apart from reducing the supervelocities at any spanwise position), is to distort the isobars near the centre and tips of the wing, in much the same manner as for an untapered wing (*e.g.*, Refs. 1, 2, 3). It is shown, however, that the centre or ' kink ' effect, which causes the backward movement of the peak supervelocity near the centre of the wing, extends over only a very limited portion of the span (about 17 per cent of the centre-line chord length from the centre), whereas, for untapered wings, the centre effect spreads over about three times this distance. It is interesting to note that near the centre of the swept wing, the isobars in the high supervelocity region aft of the maximum-thickness position (e.g., $(\pi v_x)/\{4V_0(t_0/c_0)\} = 0{\cdot}5$) are almost unswept, as far outboard as $\eta = 0{\cdot}2$. On the unswept wing, however, the isobars in this region are (except very close to the centre-line) fairly highly swept. This small isobar sweep (which also occurs on untapered swept wings having parabolic-arc aerofoil sections) would probably reduce considerably the increase in critical Mach number normally associated with sweepback. It would not be profitable, however, to discuss these isobar patterns in greater detail, since they refer only to one particular case, and it has been found that for untapered wings, aerofoil-section shape has a considerable effect on the detailed picture (*i.e.*, comparison of Fig. 23 of Ref. 3 and Fig. 21 of Ref. 4). These results showed that changing the aerofoil section from symmetrical parabolic-arc to a round-nosed section, caused a relative increase in the supervelocities near the tips, and completely changed the shape of the isobar loops. It is unlikely that change of section shape would have such a marked effect on the results for wing (2), but the isobar loops might become more elongated, with a greater sweep on the isobars aft of the maximum thickness.

Change of spanwise thickness distribution has already been discussed for the case of the unswept wing (Fig. 31), and it is probable that similar effects will occur in the case of the swept wing.

4.2.6. *Brief summary of results for swept wings.*—It has been shown that the expression for the supervelocity at any point of an infinite aspect-ratio swept wing :

$$\frac{v_x(x,\eta)}{V_0} = \frac{V_x(x,\eta)}{V_0} - 1 = \{(1 + K_1)S^{(1)}(x) - K_2S^{(2)}(x)\,f(\varphi)\}\cos\varphi \qquad .. \qquad (19)$$

(*see* equation (4)), can be used to find the shape of the supervelocity distribution at any spanwise position of a finite aspect-ratio swept tapered wing, if φ is taken to be the local angle of sweep.

The value of K_1 is dependent on the local angle of sweep, and hence for a tapered wing, is replaced by $K_1(x)$. The value of K_2 is independent of sweep, and varies only with spanwise position and plan-form taper.

The actual supervelocity distributions are related to this pseudo infinite wing distribution by a factor τ which is almost independent of chordwise position. Thus, in general terms, the supervelocity $v_x(x, \eta)$ can be expressed as :

$$\frac{v_x(x,\eta)}{V_0} = \tau[\{1 + K_1(x,\eta)\}S^{(1)}(x,\eta) - K_2S^{(2)}(x,o)\,f(\varphi)]\cos\varphi\,, \qquad .. \qquad .. \qquad (20)$$

where $v_x(x, \eta)$ is the chordwise supervelocity at the point (x, η),

V_0 is the free-stream velocity,

$V_0 S^{(1)}(x, \eta)$ represents the supervelocity at the corresponding chordwise position of an unswept two-dimensional wing of the same aerofoil section (*see* Ref. 4),

$S^{(2)}(x, o)$ represents the slope of the aerofoil section at the point (x, o) on the centre-line of the wing (*see* Ref. 4),

φ is the local angle of sweepback,

$$f(\varphi) = \frac{1}{\pi} \ln\left(\frac{1 + \sin\varphi}{1 - \sin\varphi}\right) \text{ (see Fig. 45)},$$

$$1 + K_1 = \frac{\text{supervelocity at maximum thickness of infinite swept wing}}{\text{supervelocity at maximum thickness of infinite sheared wing}}$$

for the local angle of sweep (*see* Fig. 46a),

K_2 is the centre-line ' kink '-term reduction factor (*see* Fig. 46b).

Since τ is almost constant across the chord, its value can be related to the reduction of the supervelocity at the maximum-thickness position. At the maximum-thickness position, $S^{(2)}(x, o)$ is zero, and hence, from equation (20) :

$$\tau = \frac{v_x(k, \eta)}{V_0\{1 + K_1(k, \eta)\} S^{(1)}(k, \eta) \cos\varphi_k} \quad \ldots \quad \ldots \quad \ldots \quad \ldots \quad \ldots \quad (21)$$

The supervelocity $v_x(k, \eta)$ for a swept wing can be expressed as :

$$\frac{v_x(k, \eta)}{V_0} = \frac{\{v_x(k, \eta)\}_{\varphi=0}}{V_0} - \frac{\Delta v_x(k, o)_\varphi}{V_0} + K_1(k, \eta)\, S^{(1)}(k, \eta) \cos\varphi_k, \quad \ldots \quad \ldots \quad (22)$$

where $\{v_x(k, \eta)\}_{\varphi=0}$ is the supervelocity at the corresponding position of an unswept wing having the same plan-form taper, and the same spanwise distribution of thickness

$\Delta v_x(k, o)_\varphi$ is the reduction of $v_x(k, o)$ due to sweepback, relative to the corresponding unswept wing, *i.e.*,

$$\frac{\Delta v_x(k, o)_\varphi}{V_0} = \frac{\{v_x(k, o)\}_{\varphi=0}}{V_0} - \frac{v_x(k, o)}{V_0}.$$

At the centre-line, $v_x(k, \eta)_{\varphi=0} = v_x(k, o)_{\varphi=0}$, can be determined from the unswept two-dimensional supervelocity for the centre-line section shape, and the results given in Figs. 25a, 25b and 25c, *i.e.*,

$$\frac{\{v_x(k, o)\}_{\varphi=0}}{V_0} = S^{(1)}(k, o) - \frac{\{\Delta v_x(k, o)_s\}_{\varphi=0}}{V_0} + \frac{\{\Delta v_x(k, o)_\lambda\}_{\varphi=0}}{V_0} - \frac{\{\Delta v_x(k, o)_t\}_{\varphi=0}}{V_0} \quad \ldots \quad (23)$$

where $\{\Delta v_x(k, o)_s\}_{\varphi=0}$ is the reduction of $v_x(k, o)$ due to finite aspect ratio (Fig. 25c)

$\{\Delta v_x(k, o)_\lambda\}_{\varphi=0}$ is the increase of $v_x(k, o)$ due to plan-form taper (Fig. 25a)

$\{\Delta v_x(k, o)_t\}_{\varphi=0}$ is the reduction of $v_x(k, o)$ due to thickness taper.

Outboard of about $\eta = 0{\cdot}1$, plan-form taper has little effect on the reduction of $v_x(k, \eta)$ relative to the corresponding two-dimensional value $V_0 S^{(1)}(k, \eta)$ and $v_x(k, \eta)_{\varphi=0}$ can be expressed as :

$$\frac{\{v_x(k, \eta)\}_{\varphi=0}}{V_0} = S^{(1)}(k, \eta) - \frac{\{\Delta v_x(k, \eta)\}_{\varphi=0}}{V_0}, \quad \ldots \quad \ldots \quad \ldots \quad \ldots \quad \ldots \quad \ldots \quad (24)$$

$\frac{\{\Delta v_x(k, \eta)\}_{\varphi=0}}{V_0}$ being obtained from (for instance) Figs. 10b, 11b, 12b, 26b, 27b, 28 and 30b for a wing having the same spanwise distribution of thickness. For wings not covered by the above figures, the expressions given in Appendices I to IV should be used to derive the appropriate value of $\frac{\{\Delta v_x(k, \eta)\}_{\varphi=0}}{V_0}$.

$v_x(k, o)$ can similarly be expressed as :

$$\frac{v_x(k, o)}{V_0} = S^{(1)}(k, o) \cos \varphi_k - \frac{\Delta v_x(k, o)_s}{V_0} + \frac{\Delta v_x(k, o)_\lambda}{V_0} - \frac{\Delta v_x(k, o)_t}{V_0} \quad \ldots \quad (25)$$

$$\text{Hence } \frac{\Delta v_x(k, o)}{V_0} = S^{(1)}(k, o)\{1 - \cos \varphi_k\} - \left[\frac{\{\Delta v_x(k, o)_s\}_{\varphi=0}}{V_0} - \frac{\Delta v_x(k, o)_s}{V_0}\right]$$

$$+ \left[\frac{\{\Delta v_x(k, o)_\lambda\}_{\varphi=0}}{V_0} - \frac{\Delta v_x(k, o)_\lambda}{V_0}\right]$$

$$- \left[\frac{\{\Delta v_x(k, o)_t\}_{\varphi=0}}{V_0} - \frac{\Delta v_x(k, o)_t}{V_0}\right] \quad \ldots \quad (26)$$

$$= S^{(1)}(k, o)\{1 - \cos \varphi_k\} - \frac{\Delta v_x(k, o)_{s, \varphi}}{V_0}$$

$$+ \frac{\Delta v_x(k, o)_{\lambda, \varphi}}{V_0} - \frac{\Delta v_x(k, o)_{t, \varphi}}{V_0}, \quad \ldots \quad (27)$$

where $\Delta v_x(k, o)_{s, \varphi} = \{\Delta v_x(k, o)_s\}_{\varphi=0} - \Delta v_x(k, o)_s$, etc.

Values of $\frac{\Delta v_x(k, o)_{s, \varphi}}{V_0}$, etc., are given in Fig. 47.

Thus $v_x(k, \eta)$ can be determined from equations (22), (23), (24) and (27), and the value of τ obtained. $\{v_x(x, \eta)\}/V_0$ can then be calculated from equation (20).

It should be noted that if there is a change in the spanwise rate of thickness taper close to the centre-line (*i.e.*, wing (2)) the supervelocities at the centre-line may not be in very good agreement with equation (20). In this case, an allowance for the effect of finite aspect ratio on the shape of the pseudo infinite wing centre distribution should be made (*see* Figs. 20, 33, 34 and 35), and a similar procedure to that used above, adopted.

An approximate correction for the effect of finite thickness can be applied to the velocities derived from equation (20), if desired, by multiplying $V_x(x, o)$ at the centre-line, by the factor :

$$\left[\frac{1}{1 + \{S^{(2)}(x, o)\}^2}\right]^{1/2}.$$

Further outboard, where the flow approximates more closely to sheared wing conditions, the factor :

$$\left[\frac{1}{1 + \left\{\frac{S^2(x, \eta)}{\cos \varphi}\right\}^2}\right]^{1/2}$$

should be used.

5. *Effect of Aerofoil-Section Shape and Thickness on the Conclusions Derived from Linearised Theory.*—In order to check whether aerofoil-section shape, and finite thickness, cause any radical changes in the effects of plan-form and thickness taper as deduced by linearised theory, the results obtained in this report have been used to estimate the supervelocities on a simple delta wing for which experimental pressure distributions are available. This wing has an aspect ratio of 3·08 (i.e., $s/c_0 = s'/c_0 = 0{\cdot}77$) and NACA 0010 aerofoil section throughout the span.

The calculation of the pressure distributions for this wing is set out in Table 1. The two-dimensional supervelocity distribution $S^{(1)}(x)$ for the NACA 0010 section is abstracted from Ref. 10, but had this information not been available, it could have been calculated by the method given in Ref. 4.

The chordwise pressure distributions obtained in Table 1 are plotted in Fig. 44; these are shown for the pressure coefficient calculated from the supervelocity on the chord plane, and also for the approximate supervelocity at the surface, obtained by applying a thickness correction term $(1/[1 + \{S^{(2)}(x, \eta)\}^2])^{1/2}$. The calculations of Ref. 4 suggest that this correction term is only applicable at the centre-line of the wing, but it is found that applying the infinite-sheared-wing correction term $(1/[1 + \{s^{(2)}(x, \eta)/\cos\varphi\}^2])^{1/2}$ gives values of $-C_p$ which are much too small compared with the experimental results. It may be that this is due to ignoring the spanwise component of velocity induced by the wing, or possibly to the fact that the centre and tip effects are present over practically the whole surface of the wing. More experimental results are needed to show whether this type of thickness correction term can be applied in general to wings having conventional section shapes.

In general there is very good agreement between the estimated pressure coefficients (with an allowance for the effects of thickness) and the experimental results, showing that, at least for this particular wing, the pressure distribution at any spanwise position can be estimated with reasonable accuracy using the results obtained for the wings considered in this report. The greatest discrepancies between the estimated and experimental results occur over the inboard part of the span, particularly at $\eta = 0{\cdot}165$. This may be due to the use of K_1 factors obtained for wings with parabolic-arc aerofoil section, since it has been shown by Haines[5] that aerofoil section has an effect† on the value of K_1. The difficulty of obtaining reliable experimental results near the centre of a wing should not, however, be overlooked. The experimental pressure coefficients shown in Fig. 44 were obtained from tests in the R.A.E. 10 ft × 7 ft High-Speed Tunnel, results for the four outboard sections being taken from tests on a half-model, and the centre-line results from tests on a twin-sting–supported complete model. The pressure-plotting station, $\eta = 0{\cdot}165$, was also represented on the sting model for comparison with the half-model tests. All the results are given for $M = 0{\cdot}5$, since the accuracy of the tests was greater at this Mach number than at lower values of M, and the tests indicated that there was little variation of C_p with Mach number below $M = 0{\cdot}5$.

It is seen that for $\eta = 0{\cdot}165$, there is a considerable discrepancy between the results obtained from the half-model and the sting model. There are two main reasons why this difference might exist:

(*a*) In the half-model tests, the presence of the tunnel-floor boundary layer might alter the effective spanwise position of the pressure-plotting station, and affect the boundary-layer conditions, particularly towards the rear of the wing.

(*b*) In the sting-model tests, the twin support stings were close to the pressure-plotting station at $\eta = 0{\cdot}165$, and extended forward outside the wing contour to about 20 per cent chord ahead of the trailing edge.

†*See* Ref. 12.

It is clear from the above discussion that reliable experimental pressure-plotting data are required for comparison with the estimated results, before the full limitations of the method suggested in this report are known. This is partly catered for in the programme of test[8] initiated in 1952, which will provide pressure distributions at low speed on seven swept and unswept wings having RAE 101 section shape, and different amounts of plan-form and thickness taper. Meanwhile, the results presented in Fig. 44 give some indication that finite thickness and change of section shape do not invalidate the conclusions derived by means of linearised theory for wings having simple cubic or parabolic-arc aerofoil-section shapes.

6. *Conclusions.*—The results considered in this report show that for wings having thin, symmetrical cubic or parabolic-arc aerofoil sections :

(*a*) the velocities on straight tapered or untapered wings can be expressed in terms of :

(i) the velocities on the corresponding unswept two-dimensional wing

(ii) the centre or ' kink ' effect of the corresponding infinite swept wing

(*b*) the increase or decrease of the supervelocity on a straight tapered, or untapered wing relative to the velocity on the corresponding infinite sheared wing is independent of aerofoil-section shape (for cubic and parabolic-arc aerofoil sections)

(*c*) spanwise variation of absolute thickness has a marked effect on the velocities near the centre of a wing, the velocities being reduced with increase of spanwise thickness taper near the centre-line

(*d*) the effect of thickness taper decreases with increase of sweepback

(*e*) plan-form taper has a marked effect on the velocities near the centre of a wing, but little effect (apart from any change in local thickness/chord ratio) on the velocities outboard of about 0·1 semi-span

(*f*) the effects of plan-form taper decrease with increase of sweepback

(*g*) a relative increase of velocity generally occurs at a position where the rate of spanwise thickness taper is reduced discontinuously. This increase of velocity is mainly dependent on the change in the rate of thickness taper across the discontinuity.

Although the above conclusions have been derived from results for wings having parabolic or cubic-arc aerofoil sections, there is some evidence that they apply equally well to wings having conventional aerofoil-section shapes. A method for calculating the pressure distribution over a wing having a conventional aerofoil section, using the results for the parabolic-arc aerofoil section, is outlined in the text.

7. *Further Work Required.*—The results given in this report provide a qualititative (and probably a quantitative) indication of the main effects of plan-form and thickness taper on the velocities on swept and unswept wings. Experimental results are required to provide more information on the effects of aerofoil-section thickness and shape.

Consideration should also be given to the effect of varying the aerofoil-section shape across the span, or part of the span, since many high-speed aircraft have wings of this form to reduce the effects of the discontinuities at the root and tips of the wing. The results of Appendix III can be adapted to provide some information on this point for aerofoil sections formed by parabolic arcs, and it is hoped to publish these results shortly.

NOTATION

x, y, z	Rectangular co-ordinates ; x-axis coincident with centre-line chord ; y-axis spanwise
s	Semi-span
c_0	Centre-line chord
A	Aspect ratio
φ	Geometric sweepback of constant percentage chord-line
φ_l	Leading-edge sweepback
φ_t	Trailing-edge sweepback
φ_0	Mid-chord-line sweepback
φ_k	Maximum-thickness–line sweepback
k	Value of x at maximum-thickness position on centre-line chord
λc_0	Tip chord
t_0/c_0	Thickness/chord ratio at wing centre-line
$\mu(t_0/c_0)$	Thickness/chord ratio at wing tip
c_η	Local chord length
η	y/s
(t_η/c_η)	Local thickness/chord ratio
ψ	$(1 - \mu)s'/s$
s'	Spanwise distance at which tangent to maximum-thickness line at centre of wing cuts wing-chord plane
η'	y/s'
N	Factor which determines spanwise thickness distribution of wing (4) (*see* Appendix IV)
v_x	Chordwise supervelocity component
$\Delta v_x(k, o)_s$	Reduction of supervelocity at centre-line maximum-thickness position due to finite aspect ratio
$\Delta v_x(k, o)_\lambda$	Increase of supervelocity at centre-line maximum-thickness position due to plan-form taper
$\Delta v_x(k, o)_t$	Decrease of supervelocity at centre-line maximum-thickness position due to thickness taper
$\Delta v_x(k, o)_{s,\varphi}$	Reduction of $\Delta v_x(k, o)_s$ due to sweepback
$\Delta v_x(k, o)_{\lambda,\varphi}$	Reduction of $\Delta v_x(k,o)_\lambda$ due to sweepback
$\Delta v_x(k, o)_{t,\varphi}$	Reduction of $\Delta v_x(k, o)_t$ due to sweepback
V_0	Free-stream velocity
$V_0\, S^{(1)}(x)$	Supervelocity for two-dimensional wing (*see* Ref. 4)
$S^{(2)}(x)$	Slope of aerofoil-section contour (*see* Ref. 4)
$K_1 = \left(\frac{\text{supervelocity at maximum-thickness of infinite swept wing}}{\text{supervelocity at maximum-thickness of infinite sheared wing}} - 1\right)$	(*see* Fig. 46)
K_2	' Kink '-term reduction factor (*see* Fig. 46)
$f(\varphi) = \frac{1}{\pi}\ln\left(\frac{1 + \sin\varphi}{1 - \sin\varphi}\right)$	
τ	Supervelocity reduction factor

REFERENCES

No.	Author	Title, etc.
1	D. Küchemann	Wing junction, fuselage and nacelles for swept-back wings at high Mach number. Included in R. & M. 2908. August, 1947.
2	S. Neumark	Velocity distribution on straight and swept-back wings of small thickness and infinite aspect ratio at zero incidence. R. & M. 2713. May, 1947.
3	S. Neumark and J. Collingbourne ..	Velocity distribution on untapered sheared and swept-back wings of small thickness and finite aspect ratio at zero incidence. R. & M. 2717. March, 1949.
4	D. Küchemann and J. Weber ..	The subsonic flow past swept wings at zero lift without and with body. R. & M. 2908. March, 1953.
5	A. B. Haines	Some notes on the pressure distribution at an arbitrary section of an untapered swept wing at zero incidence and sub-critical Mach numbers. R.A.E. (Unpublished.)
6	J. Weber	The calculation of the pressure distribution over the surface of two-dimensional and swept wings with symmetrical aerofoil sections. R. & M. 2918. July, 1953.
7	S. Neumark and J. Collingbourne ..	Velocity distribution on thin tapered wings with fore and aft symmetry and spanwise constant thickness ratio at zero incidence. R. & M. 2858. June, 1951.
8	K. W. Newby	Proposed test programme in the No. 2, 11½-ft Tunnel to determine the effects of taper on the flow near the centre of wings. R.A.E. (Unpublished.)
9	G. G. Brebner	The calculation of the loading and pressure distribution on cranked wings. R. & M. 2947. January, 1953.
10	J. H. Abbott and A. E. von Doenhoff	*Theory of Wing Sections.* McGraw-Hill Book Co. Inc. 1949.
11	J. Weber	The calculation of the pressure distribution on thick wings of small aspect ratio at zero lift in subsonic flow. R. & M. 2993. Sept. 1954.
12	A. B. Haines	Wing-section design for swept-back wings at transonic speeds. Paper presented at the IXth International Congress of Applied Mechanics. Brussels. 1956.

APPENDIX I

Derivation of the Supervelocity at any Point on the Chord Plane of a Rectangular Wing Having a Symmetrical Cubic-Arc Aerofoil Section and a Linear Spanwise Variation of Thickness/Chord Ratio

In Fig. 48 the origin is taken at the midpoint of the centre-line chord, the leading and trailing edges being at $x = 1$ and $x = -1$ respectively ; y is taken positive to the right, the semi-span being s.

The equation to the surface of the right-hand half of the wing is :

$$z' = \frac{t_0}{c_0}\left\{1 - \frac{y'}{s}(1-\mu)\right\}\frac{(1-3k^2)}{(1-k^2)^2}(1-x'^2)\left(\frac{1+2kx}{1-3k^2}\right), \quad .. \quad .. \quad \text{(I.1)}$$

where z' = half-thickness at (x', y')

$\frac{t_0}{c_0}$ = centre-line thickness/chord ratio

$\frac{\mu t_0}{c_0}$ = tip thickness/chord ratio

k = x-co-ordinate of maximum-thickness line ($-(1/3) \leqslant k \leqslant (1/3)$).

The corresponding source strength per unit area required to represent this wing is :

$$q' = -2V_0 \frac{\partial z'}{\partial x'}$$

$$= 4V_0 \frac{t_0}{c_0} \left\{1 - \frac{y'}{s}(1-\mu)\right\} \frac{(x'-k)(1+3kx')}{(1-k^2)^2}, \qquad \text{(I.2)}$$

where V_0 is the free-stream velocity.

Representing the wing by a series of source-sink filaments parallel to the y-axis, the elemental chordwise velocity δv_x induced at the point (x, y) by a source element at the point (x', y') is :

$$\delta v_x = -\frac{q'\,dx'\,dy'}{4\pi R^2} \frac{(x-x')}{R}, \qquad \text{(I.3)}$$

where $R^2 = (x-x')^2 + (y-y')^2$.

Then the elemental velocity due to the right-hand half of the source filament is :

$$dv_x = \frac{V_0 t_0 (x'-k)(1+3kx')(x-x')\,dx'}{c_0 \pi (1-k^2)^2} \int_0^s \frac{\left\{1 - \frac{y'}{s}(1-\mu)\right\} dy'}{\{(x-x')^2 + (y-y')^2\}^{3/2}}. \qquad \text{(I.4)}$$

Integrating (I.4) and rearranging terms gives the velocity due to a single source line as :

$$(1-k^2)^2 \frac{\pi\, dv_x}{V_0(t_0/c_0)} =$$

$$(x'-k)(1+3kx')\,dx' \left(\left[\frac{(y-s)}{(x-x')} \left\{1 - \frac{y}{s}(1-\mu)\right\} - \frac{(1-\mu)}{s}(x-x') \right] \frac{1}{\{(x-x')^2 + (y-s)^2\}^{1/2}} \right.$$

$$\left. - \left[\frac{y}{(x-x')} \left\{1 - \frac{y}{s}(1-\mu)\right\} - \frac{(1-\mu)}{s}(x-x') \right] \frac{1}{\{(x-x')^2 + y^2\}^{1/2}} \right). \qquad \text{(I.5)}$$

Substituting $x' = x - (x - x')$ and rearranging terms, the velocity v_x induced at the point (x, y) by the right-hand half of the wing is given by :

$$(1-k^2)^2\frac{\pi\,dv_x}{V_0(t_0/c_0)}=\left\{3k\mu(y-s)-\frac{(x-k)(1+3kx)(1-\mu)}{s}\right\}\int_{-1}^{+1}\frac{(x-x')\,dx'}{\{(x-x')^2+(y-s)^2\}^{1/2}}$$

$$-\mu(1+6kx-3k^2)(y-s)\int_{-1}^{+1}\frac{dx'}{\{(x-x')^2+(y-s)^2\}^{1/2}}$$

$$+(x-k)(1+3kx)(y-s)\left\{1-\frac{y}{s}(1-\mu)\right\}\int_{-1}^{+1}\frac{dx'}{(x-x')\{(x-x')^2+(y-s)^2\}^{1/2}}$$

$$+\frac{(1-\mu)}{s}(1+6kx-3k^2)\int_{-1}^{+1}\{(x-x')^2+(y-s)^2\}^{1/2}\,dx'$$

$$-\frac{3k}{s}(1-\mu)\int_{-1}^{+1}(x-x')\{(x-x')^2+(y-s)^2\}^{1/2}\,dx'$$

$$-\left\{3ky-\frac{(x-k)(1+3kx)(1-\mu)}{s}\right\}\int_{-1}^{+1}\frac{(x-x')\,dx'}{\{(x-x')^2+y^2\}^{1/2}}$$

$$+y(1+6kx-3k^2)\int_{-1}^{+1}\frac{dx'}{\{(x-x')^2+y^2\}^{1/2}}$$

$$-y(x-k)(1+3kx)\left\{1-\frac{y}{s}(1-\mu)\right\}\int_{-1}^{+1}\frac{dx'}{(x-x')\{(x-x')^2+y^2\}^{1/2}}$$

$$-\left(\frac{1-\mu}{s}\right)(1+6kx-3k^2)\int_{-1}^{+1}\{(x-x')^2+y^2\}^{1/2}$$

$$+\frac{3k}{s}(1-\mu)\int_{-1}^{+1}(x-x')\{(x-x')^2+y^2\}^{1/2}. \quad .. \quad .. \quad .. \quad .. \quad (I.6)$$

These integrals are all of standard form and present no difficulties provided care is taken in obtaining the correct principal values for the third and eighth terms.

Then :

$$(1-k^2)^2\frac{\pi v_x}{V_0(t_0/c_0)}=$$

$$\left\{3k\mu(s-y)+\frac{(x-k)(1+3kx)(1-\mu)}{s}\right\}[\{(x-1)^2+(y-s)^2\}^{1/2}-\{(x+1)^2+(y-s)^2\}^{1/2}]$$

$$+\left\{3ky-\frac{(x-k)(1+3kx)(1-\mu)}{s}\right\}[\{(x-1)^2+y^2\}^{1/2}-\{(x+1)^2+y^2\}^{1/2}]$$

$$-\frac{(1-\mu)}{2s}(1+6kx-3k^2)\,[(x-1)\{(x-1)^2+(y-s)^2\}^{1/2}-(x+1)\{(x+1)^2+(y-s)^2\}^{1/2}]$$

$$+\left(\frac{1-\mu}{2s}\right)(1+6kx-3k^2)\,[(x-1)\{(x-1)^2+y^2\}^{1/2}-(x+1)\{(x+1)^2+y^2\}^{1/2}]$$

$$+\frac{k}{s}(1-\mu)[\{(x-1)^2+(y-s)^2\}^{3/2}-\{(x+1)^2+(y-s)^2\}^{3/2}]$$

$$-\frac{k}{s}(1-\mu)\,[\{(x-1)^2+y^2\}^{3/2}-\{(x+1)^2+y^2\}^{3/2}]$$

$$+(y-s)(1+6kx-3k^2)\left\{1-\frac{(s+y)}{2s}(1-\mu)\right\}\ln\frac{\{(x-1)^2+(y-s)^2\}^{1/2}+(x-1)}{\{(x+1)^2+(y-s)^2\}^{1/2}+(x+1)}$$

$$-y(1+6kx-3k^2)\left\{1-\frac{y}{2s}(1-\mu)\right\}\ln\frac{\{(x-1)^2+y^2\}^{1/2}+(x-1)}{\{(x+1)^2+y^2\}^{1/2}+(x+1)}$$

$$-(x-k)(1+3kx)\left\{1-\frac{y}{s}(1-\mu)\right\}\ln\left[\frac{\{(x-1)^2+(y-s)^2\}^{1/2}+(s-y)}{\{(x+1)^2+(y-s)^2\}^{1/2}+(s-y)}\right]$$

$$\left[\frac{\{(x-1)^2+y^2\}^{1/2}+y}{\{(x+1)^2+y^2\}^{1/2}+y}\right]$$

$$-2(x-k)(1+3kx)\left\{1-\frac{y}{s}(1-\mu)\right\}\ln\left(\frac{1+x}{1-x}\right). \qquad \text{(I.7)}$$

The contribution to the velocity v_x at (x, y) due to the left-hand half of the wing is the same as the contribution of the right-hand half of the wing to the velocity at the point $(x, -y)$. Then changing the sign of y in equation (I.7) and adding the result to equation (I.7) gives the velocity v_x at the point (x, y) due to the whole wing :

$$(1-k^2)^2\frac{\pi v_x}{4V_0(t_0/c_0)}=$$

$$\left[\frac{(1-\mu)}{8s}(1+x)(1+2kx-3k)^2+\frac{k}{4}(s-y)\left\{1+2\mu-(1-\mu)\frac{y}{s}\right\}\right]\{(1-x)^2+(s-y)^2\}^{1/2}$$

$$+\left[\frac{(1-\mu)}{8s}(1+x)(1+2kx-3k^2)+\frac{k}{4}(s+y)\left\{1+2\mu+(1-\mu)\frac{y}{s}\right\}\right]\{(1-x)^2+(s+y)^2\}^{1/2}$$

$$-\left(\frac{1-\mu}{4s}\right)\left\{(1+x)(1+2kx-3k^2)+2ky^2\right\}\{(1-x)^2+y^2\}^{1/2}$$

$$+\left[\frac{(1-\mu)}{8s}(1-x)(1+2kx-3k^2)-\frac{k}{4}(s-y)\left\{1+2\mu-(1-\mu)\frac{y}{s}\right\}\right]\{(1+x)^2+(s-y)^2\}^{1/2}$$

$$+\left[\frac{(1-\mu)}{8s}(1-x)(1+2kx-3k^2)-\frac{k}{4}(s+y)\left\{1+2\mu+(1-\mu)\frac{y}{s}\right\}\right]\{(1+x)^2+(s+y)^2\}^{1/2}$$

$$-\left(\frac{1-\mu}{4s}\right)\left\{(1-x)(1+2kx-3k^2)-2ky^2\right\}\{(1+x)^2+y^2\}^{1/2}$$

$$-\frac{(s-y)}{4}(1+6kx-3k^2)\left\{1-\frac{(s+y)}{2s}(1-\mu)\right\}\ln\frac{\{(1-x)^2+(s-y)^2\}^{1/2}-(1-x)}{\{(1+x)^2+(s-y)^2\}^{1/2}+(1+x)}$$

$$-\frac{(s+y)}{4}(1+6kx-3k^2)\left\{1-\frac{(s-y)}{2s}(1-\mu)\right\}\ln\frac{\{(1-x)^2+(s+y)^2\}^{1/2}-(1-x)}{\{(1+x)^2+(s+y)^2\}^{1/2}+(1+x)}$$

$$+\frac{y^2}{4s}(1-\mu)(1+6kx-3k^2)\ln\frac{\{(1-x)^2+y^2\}^{1/2}-(1-x)}{\{(1+x^2)+y^2\}^{1/2}+(1+x)}$$

$$-\frac{(x-k)}{4}(1+3kx)\left\{1-\frac{y}{s}(1-\mu)\right\}\ln\left[\frac{\{(1-x)^2+(s-y)^2\}^{1/2}+(s-y)}{\{(1+x)^2+(s-y)^2\}^{1/2}+(s-y)}\right]$$

$$\times\left[\frac{\{(1-x)^2+y^2\}^{1/2}+y}{\{(1+x)^2+y^2\}^{1/2}+y}\right]$$

$$-\frac{(x-k)}{4}(1+3kx)\left\{1+\frac{y}{s}(1-\mu)\right\}\ln\left[\frac{\{(1-x)^2+(s+y)^2\}^{1/2}+(s+y)}{\{(1+x)^2+(s+y)^2\}^{1/2}+(s+y)}\right]$$

$$\times\left[\frac{\{(1-x)^2+y^2\}^{1/2}-y}{\{(1+x)^2+y^2\}^{1/2}-y}\right]$$

$$-(x-k)(1+3kx)\ln\left(\frac{1+x}{1-x}\right). \quad .. \quad .. \quad .. \quad .. \quad .. \quad .. \quad .. \quad .. \quad \text{(I.8)}$$

The particular case of a rectangular wing tapered in thickness, and having a symmetrical parabolic-arc aerofoil section is obtained from equation (I.8) by putting $k = 0$:

$$\frac{\pi v_x}{4V_0(t_0/c_0)} =$$

$$\left(\frac{1-\mu}{8s}\right)(1+x)\left[\{(1-x)^2+(s-y)^2\}^{1/2}+\{(1-x)^2+(s+y)^2\}^{1/2}-2\{(1-x)^2+y^2\}^{1/2}\right]$$

$$+\left(\frac{1-\mu}{8s}\right)(1-x)\left[\{(1+x)^2+(s-y)^2\}^{1/2}+\{(1+x)^2+(s+y)^2\}^{1/2}-2\{(1+x)^2+y^2\}^{1/2}\right]$$

$$-\frac{(s-y)}{4}\left\{1-\frac{(s+y)}{2s}(1-\mu)\right\}\ln\frac{\{(1-x)^2+(s-y)^2\}^{1/2}-(1-x)}{\{(1+x)^2+(s-y)^2\}^{1/2}+(1+x)}$$

$$-\frac{(s+y)}{4}\left\{1-\frac{(s-y)}{2s}(1-\mu)\right\}\ln\frac{\{(1-x)^2+(s+y)^2\}^{1/2}-(1-x)}{\{(1+x)^2+(s+y)^2\}^{1/2}+(1+x)}$$

$$+\frac{y^2}{4s}(1-\mu)\ln\frac{\{(1-x)^2+y^2\}^{1/2}-(1-x)}{\{(1+x)^2+y^2\}^{1/2}+(1+x)}-$$

$$-\frac{x}{4}\left\{1-\frac{y}{s}(1-\mu)\right\}\ln\left[\frac{\{(1-x)^2+(s-y)^2\}^{1/2}+(s-y)}{\{(1+x)^2+(s-y)^2\}^{1/2}+(s-y)}\right]\left[\frac{\{(1-x)^2+y^2\}^{1/2}+y}{\{(1+x)^2+y^2\}^{1/2}+y}\right]$$

$$-\frac{x}{4}\left\{1+\frac{y}{s}(1-\mu)\right\}\ln\left[\frac{\{(1-x)^2+(s+y)^2\}^{1/2}+(s+y)}{\{(1+x)^2+(s+y)^2\}^{1/2}+(s+y)}\right]\left[\frac{\{(1-x)^2+y^2\}^{1/2}-y}{\{(1+x)^2+y^2\}^{1/2}-y}\right]$$

$$-x\ln\left(\frac{1+x}{1-x}\right). \qquad \text{(I.9)}$$

The equation for the supervelocity distribution on a finite rectangular wing of parabolic-arc aerofoil section and constant thickness/chord ratio can now be found from (I.9) by putting $\mu = 1$:

$$\begin{aligned}\frac{\pi v_x}{4V_0(t_0/c_0)} &= \frac{(s-y)}{4}\ln\frac{\{(1+x)^2+(s-y)^2\}^{1/2}+(1+x)}{\{(1-x)^2+(s-y)^2\}^{1/2}-(1-x)}\\ &+\frac{(s+y)}{4}\ln\frac{\{(1+x)^2+(s+y)^2\}^{1/2}+(1+x)}{\{(1-x)^2+(s+y)^2\}^{1/2}-(1-x)}\\ &+\frac{x}{4}\ln\frac{\{(1+x)^2+(s-y)^2\}^{1/2}+(s-y)}{\{(1-x)^2+(s-y)^2\}^{1/2}+(s-y)}\\ &+\frac{x}{4}\ln\frac{\{(1+x)^2+(s+y)^2\}^{1/2}+(s+y)}{\{(1-x)^2+(s+y)^2\}^{1/2}+(s+y)}\\ &-\frac{x}{2}\ln\left(\frac{1+x}{1-x}\right), \qquad \text{(I.10)}\end{aligned}$$

which is the formula given in Ref. 3, equation (4.13).

APPENDIX II

Derivation of the Supervelocity at any Point of the Chord Plane of a Tapered, Swept-back Wing, Having a Symmetrical Biconvex Parabolic-Arc Aerofoil Section, and a Linear Spanwise Distribution of Thickness/chord Ratio (Wing 2)

In Fig. 48, the origin is taken to be at the mid-point of the centre-line chord, the leading and trailing edges of the centre-line chord being at $x = +1$, and $x = -1$ respectively ; y is taken to be positive to the right, the semi-span of the wing being s.

The equations to the surface of the wing are :

$$\left.\begin{aligned}z' &= \frac{t_0}{c_0}\left(\frac{s-y'}{s}\right)^2\left\{1-\left(\frac{sx'_t}{s-y'}\right)^2\right\} \text{ ahead of the maximum thickness}\\ z' &= \frac{t_0}{c_0}\left(\frac{s-y'}{s}\right)^2\left\{1-\left(\frac{sx'_t}{s-y'}\right)^2\right\} \text{ aft of the maximum thickness}\end{aligned}\right\}, \qquad \text{(II.1)}$$

where z' = half thickness at point (x', y')

t_0/c_0 = centre-line thickness/chord ratio

x'_l, x'_t = intercepts on the x axis of lines passing through (x', y') parallel to the wing mid-chord line.

The corresponding source strength per unit area to represent this wing is :

$$q' = -2V_0 \frac{\partial z'}{\partial x'}, \qquad \text{(II.2)}$$

i.e., $q' = 4V_0(t_0/c_0)x'_l$ ahead of maximum thickness (II.3)

and $4V_0(t_0/c_0)x'_t$ aft of maximum thickness, (II.4)

where V_0 is the free-stream velocity.

The wing can therefore be represented by a series of uniform kinked source filaments as in the case of an untapered swept-back wing of constant thickness/chord ratio.

Thus the result for the tapered swept-back wing with linear spanwise variation of thickness/chord ratio can be derived by subtracting the supervelocity contribution due to those sources representing the parts of an infinite swept-back wing which lie outside the plan area of the finite tapered wing†. In calculating the effect of this ' excess ' wing, the supervelocities can be determined at points on the chord plane of the tapered wing, since no source filaments cross the wing plan-form. The result for the complete infinite swept wing has already been considered in Refs. 1, 2, 3 and the correct linearised-theory answer obtained.

Referring to Fig. 48, and considering only the right-hand half of the wing, the elemental velocity δv_x induced at a point $(x_0 - y \tan \varphi_0, y)$ by an infinitesimal source element $q'\,dx'\,dy'$ at the point (x', y') is :

$$\delta v_x = -\frac{q'\,dx'\,dy'}{4\pi R^3}(x_0 - x' - y \tan \varphi_0), \qquad \text{(II.5)}$$

where $R^2 = (x_0 - x' - y \tan \varphi_0)^2 + (y' - y)^2$

$x' = x'_t - y' \tan \varphi_0$.

Then $$dv_x = -\frac{q'\,dx'_l}{4\pi}\int_{y_l}^{y'=\infty} \frac{\{x_0 - x'_l + (y' - y)\tan \varphi_0\}\,dy'}{[\{x_0 - x'_l + (y' - y)\tan \varphi_0\}^2 + (y' - y)^2]^{3/2}}$$

for that part of the filament extending from the wing leading edge to infinity.

This integration involves no difficulties, and it is found that :

$$dv_x = \frac{-q'\,dx'_l \cos \varphi_0}{4\pi}\left(\frac{1}{x_0 - x'_l} - \frac{y_l - y}{(x_0 - x'_l)[(x_0 - x'_l)^2 \cos^4 \varphi_0 + \{y_l - y + (x_0 - x'_l)\sin \varphi_0 \cos \varphi_0\}^2]^{1/2}}\right). \qquad \text{(II.6)}$$

Substituting from $y_l = (1 - x'_l)s$, the supervelocity due to the filament ahead of the maximum thickness is :

$$dv_{xF} = \frac{-q'\,dx'_l \cos \varphi_0}{4\pi}\left[\frac{1}{x_0 - x'_l} - \frac{r_3^{1/2} + s(x_0 - x'_l)}{(x_0 - x'_l)\{r_1(x_0 - x'_l)^2 + r_2(x_0 - x'_l) + r_3\}^{1/2}}\right], \qquad \text{(II.7)}$$

†This device is adopted, in preference to direct integration over the wing desired, for the reason given in section 5 of the main text.

where : $r_1 = (s + \sin\varphi_0 \cos\varphi_0)^2 + \cos^4\varphi_0$

$r_2 = 2(s + \sin\varphi_0 \cos\varphi_0)\{s(1 - x_0) - y\}$

$r_3 = \{s(1 - x_0) - y\}^2.$

Similarly, for filaments aft of the maximum-thickness line, where $y_t = (1 + x'_t)\, s$:

$$dv_{xR} = \frac{-q'\, dx'_t \cos\varphi_0}{4\pi}\left[\frac{1}{x_0 - x'_t} - \frac{r_6^{1/2} - s(x_0 - x'_t)}{(x_0 - x'_t)\{r_4(x_0 - x'_t)^2 + r_5(x_0 - x'_t) + r_6\}^{1/2}}\right], \qquad \text{(II.8)}$$

where : $r_4 = (s - \sin\varphi_0 \cos\varphi_0)^2 + \cos^4\varphi_0$

$r_5 = -2(s - \sin\varphi_0 \cos\varphi_0)\{s(1 + x_0) - y\}$

$r_6 = \{s(1 + x_0) - y\}^2.$

Substituting for the source strength q' from equations (II.3) and (II.4) the supervelocities v_{xF} and v_{xR} are given by :

$$\begin{aligned} -v_{xF} = \left(\frac{t_0}{c_0}\right)\frac{V_0 \cos\varphi_0}{\pi}\Bigg[& x_0 \int_0^1 \frac{dx'_l}{x_0 - x'_l} - \int_0^1 dx'_l \\ & - x_0 r_3^{1/2} \int_0^1 \frac{dx'_l}{(x_0 - x'_l)\{r_1(x_0 - x'_l)^2 + r_2(x_0 - x'_l) + r_3\}^{1/2}} \\ & + (r_3^{1/2} - sx_0) \int_0^1 \frac{dx'_l}{\{r_1(x_0 - x'_l)^2 + r_2(x_0 - x'_l) + r_3\}^{1/2}} \\ & + s \int_0^1 \frac{(x_0 - x'_l)\, dx'_l}{\{r_1(x_0 - x'_l)^2 + r_2(x_0 - x'_l) + r_3\}^{1/2}}\Bigg] \qquad \text{(II.9)} \end{aligned}$$

$$\begin{aligned} -v_{xR} = \left(\frac{t_0}{c_0}\right)\frac{V_0 \cos\varphi_0}{\pi}\Bigg[& x_0 \int_{-1}^0 \frac{dx'_t}{x_0 - x'_t} - \int_{-1}^0 dx'_t \\ & - x_0 r_6^{1/2} \int_{-1}^0 \frac{dx'_t}{(x_0 - x'_t)\{r_4(x_0 - x'_t)^2 + r_5(x_0 - x'_t) + r_6\}^{1/2}} \\ & + (r_6^{1/2} + sx_0) \int_{-1}^0 \frac{dx'_t}{\{r_4(x_0 - x_t')^2 + r_5(x_0 - x'_t) + r_6\}^{1/2}} \\ & - s \int_{-1}^0 \frac{(x_0 - x'_t)\, dx'_t}{\{r_4(x_0 - x'_t)^2 + r_5(x_0 - x'_t) + r_6\}^{1/2}}\Bigg]. \qquad \text{(I.10)} \end{aligned}$$

Then the chordwise supervelocity v_x induced at the point $(x_0 - y \tan\varphi_0, y)$ by the right-hand half of the wing is given by :

$$v_x = v_{xF} + v_{xR}. \qquad \text{(II.11)}$$

These integrals present no difficulties, being of standard form, and after some rearrangement, the supervelocity v_x is obtained as :

$$-\frac{\pi v_x}{V_0(t_0/c_0)\cos\varphi_0} = -2 - x_0 \ln\left\{\frac{R_1 - (1-x_0)\sin\varphi_0\cos\varphi_0 - y}{R_2 + (1+x_0)\sin\varphi_0\cos\varphi_0 - y}\right\}$$

$$+\frac{\cos\varphi_l}{\cos\varphi_0}\left\{x_0 - \left(1 - x_0 - \frac{y}{s}\right)\frac{\sin\varphi_l\cos\varphi_l}{s}\right\}\ln\left\{\frac{R_1 - (1-x_0)\sin\varphi_l\cos\varphi_0 - y\cos(\varphi_l-\varphi_0)}{R_3 + x_0\sin\varphi_l\cos\varphi_0 + (s-y)\cos(\varphi_l-\varphi_0)}\right\}$$

$$+\frac{\cos\varphi_t}{\cos\varphi_0}\left\{x_0 - \left(1 + x_0 - \frac{y}{s}\right)\frac{\sin\varphi_t\cos\varphi_t}{s}\right\}\ln\left\{\frac{R_3 + x_0\sin\varphi_t\cos\varphi_0 + (s-y)\cos(\varphi_0-\varphi_t)}{R_2 + (1+x_0)\sin\varphi_t\cos\varphi_0 - y\cos(\varphi_0-\varphi_t)}\right\}$$

$$-\frac{\cos^2\varphi_l}{s\cos^2\varphi_0}[R_1 - R_3] + \frac{\cos^2\varphi_t}{s\cos^2\varphi_0}[R_3 - R_2], \quad \ldots\ldots\ldots\ldots\ldots\ldots \text{(II.12)}$$

where
$$R_1^2 = (1-x_0)^2\cos^2\varphi_0 + 2y(1-x_0)\sin\varphi_0\cos\varphi_0 + y^2$$
$$R_2^2 = (1+x_0)^2\cos^2\varphi_0 - 2y(1+x_0)\sin\varphi_0\cos\varphi_0 + y^2$$
$$R_3^2 = x_0^2\cos^2\varphi_0 + 2(s-y)x_0\sin\varphi_0\cos\varphi_0 + (s-y^2).$$

This result must be subtracted from that for a semi-infinite sheared wing which is given in Ref. 3 (equation 3.13) as :

$$-\frac{\pi v_x}{V_0(t_0/c_0)\cos\varphi_0} = -2 - x_0\ln\left\{\frac{R_1 - (1-x_0)\sin\varphi_0\cos\varphi_0 - y}{R_2 + (1+x_0)\sin\varphi_0\cos\varphi_0 - y}\right\}$$

$$+\frac{y}{\cos\varphi_0}\ln\left\{\frac{R_1 - (1-x_0)\cos\varphi_0 - y\sin\varphi_0}{R_2 + (1+x_0)\cos\varphi_0 - y\sin\varphi_0}\right\}. \quad \ldots\ldots\ldots \text{(II.13)}$$

Hence the supervelocity v_x at the point $(x_0 - y\tan\varphi_0, y)$ due to the right-hand half of wing (2) is :

$$-\frac{\pi v_x}{V_0(t_0/c_0)} = y\ln\left\{\frac{R_1 - (1-x_0)\cos\varphi_0 - y\sin\varphi_0}{R_2 + (1+x_0)\cos\varphi_0 - y\sin\varphi_0}\right\}$$

$$-\cos\varphi_l\left\{x_0 - \left(1 - x_0 - \frac{y}{s}\right)\frac{\sin 2\varphi_l}{2s}\right\}\ln\left\{\frac{R_1 - (1-x_0)\sin\varphi_l\cos\varphi_0 - y\cos(\varphi_l-\varphi_0)}{R_3 + x_0\sin\varphi_l\cos\varphi_0 + (s-y)\cos(\varphi_l-\varphi_0)}\right\}$$

$$-\cos\varphi_t\left\{x_0 - \left(1 + x_0 - \frac{y}{s}\right)\frac{\sin 2\varphi_t}{2s}\right\}\ln\left\{\frac{R_3 + x_0\sin\varphi_t\cos\varphi_0 + (s-y)\cos(\varphi_0-\varphi_t)}{R_2 + (1+x_0)\sin\varphi_t\cos\varphi_0 - y\cos(\varphi_0-\varphi_t)}\right\}$$

$$+\frac{\cos^2\varphi_l}{s\cos\varphi_0}R_1 + \frac{\cos^2\varphi_t}{s\cos\varphi_0}R_2 - \frac{(\cos^2\varphi_l + \cos^2\varphi_t)}{s\cos\varphi_0}R_3. \quad \ldots\ldots\ldots \text{(II.14)}$$

In order to make the chordwise ordinate in terms of the local chord independent of the spanwise position, new variables may conveniently be introduced, i.e., $y = \eta s$; $x_0 = (1-\eta)x$.

Then $$-\frac{\pi v_x}{V_0(t_0/c_0)} = \eta s \ln\left\{\frac{(R_5^2+\eta^2 s^2)^{1/2}-R_5}{(R_6^2+\eta^2 s^2)^{1/2}+R_6}\right\}$$

$$-(1-\eta)R_8\cos\varphi_l \ln\left[\frac{(R_5^2+\eta^2 s^2)^{1/2}-R_5\sin\varphi_l-\eta s\cos\varphi_l}{s(1-\eta)\{1+\cos(\varphi_l-\varphi)\}\sec\varphi}\right]$$

$$-(1-\eta)R_7\cos\varphi_t \ln\left[\frac{s(1-\eta)\{1+\cos(\varphi-\varphi_t)\}\sec\varphi}{R_6^2+\eta^2 s^2)^{1/2}+R_6\sin\varphi_t-\eta s\cos\varphi_t}\right]$$

$$+\frac{\cos\varphi_l}{s}(R_5^2+\eta^2 s^2)^{1/2}+\frac{\cos^2\varphi_t}{s}(R_6^2+\eta^2 s^2)^{1/2}$$

$$-\frac{(1-\eta)}{\cos\varphi}(\cos^2\varphi_l+\cos^2\varphi_t), \quad \ldots\ldots\ldots\ldots\ldots\ldots \quad \text{(II.15)}$$

where $$R_5 = 1-x+\eta s\tan\varphi \qquad R_8 = x-\frac{(1-x)}{2s}\sin 2\varphi_l$$

$$R_6 = 1+x-\eta s\tan\varphi \qquad R_9 = x-\frac{(1+x)}{2s}\sin 2\varphi_t.$$

It is now necessary to determine the contribution of the left-hand half of the wing to the supervelocity at the point $(x_0 - y\tan\varphi_0, y)$. This is equal to the supervelocity at the point P_1 (Fig. 48) due to the right-hand half of the wing. It is not sufficient however to put $(-y)$ for y in equation (II.14), as this would give the supervelocity at the point P_2 (Fig. 48), $2y\tan\varphi_0$ ahead of P_1. It is clearly necessary therefore to put $(x_0 + 2y\tan\varphi_0)$ for x_0 before substituting $(-y)$ for y in order to obtain the supervelocity at P_1.

Thus the contribution of the left-hand half of the wing to the supervelocity at the point $(x_0 - y\tan\varphi_0, y)$ is :

$$\frac{\pi v_x}{V_0(t_0/c_0)} = +y\ln\left\{\frac{R_1-(1-x_0)\cos\varphi_0-y\sin\varphi_0}{R_2+(1+x_0)\cos\varphi_0-y\sin\varphi_0}\right\}$$

$$+\cos\varphi_l\left\{x_0-\left(1-x_0-\frac{y}{s}\right)\frac{\sin 2\varphi_l}{2s}-\frac{y}{s}\left(2s\tan\varphi_0+\sin 2\varphi_l\tan\varphi_0+\frac{\sin 2\varphi_l}{s}\right)\right\}$$

$$\times\ln\left\{\frac{R_1-(1-x_0)\sin\varphi_l\cos\varphi_0+y\cos(\varphi_l-\varphi_0)}{R_4+x_0\sin\varphi_l\cos\varphi_0+(s-y)\cos(\varphi_l-\varphi_0)+2y\cos\varphi_l\cos\varphi_0}\right\}$$

$$+\cos\varphi_t\left\{x_0-\left(1+x_0-\frac{y}{s}\right)\frac{\sin 2\varphi_t}{2s}-\frac{y}{s}\left(2s\tan\varphi_0-\sin 2\varphi_t\tan\varphi_0+\frac{\sin 2\varphi_t}{s}\right)\right\}$$

$$\times\ln\left\{\frac{R_4+x_0\sin\varphi_t\cos\varphi_0+(s-y)\cos(\varphi_0-\varphi_t)+2y\cos\varphi_t\cos\varphi_0}{R_2+(1+x)\sin\varphi_t\cos\varphi_0+y\cos(\varphi_0+\varphi_t)}\right\}$$

$$-\frac{\cos^2\varphi_l}{s\cos\varphi_0}R_1-\frac{\cos^2\varphi_t}{s\cos\varphi_0}R_2+\frac{(\cos^2\varphi_l+\cos^2\varphi_t)}{s\cos\varphi_0}R_4. \quad \ldots\ldots\ldots \quad \text{(II.16)}$$

where $$R_4^2 = R_3^2 + 4sy\cos^2\varphi_0 .$$

Putting equation (II.16) in terms of x and η, and adding to equation (II.15) gives the supervelocity v_x at any point (x, η) due to the whole of the tapered wing :

$$\frac{\pi v_x}{4V_0(t_0/c_0)} = \frac{(\cos^2\varphi_l + \cos^2\varphi_t)(1 - \eta + R_7)}{4\cos\varphi}$$

$$- \frac{\cos^2\varphi_l}{2s}(R_5^2 + \eta^2 s^2)^{1/2} - \frac{\cos^2\varphi_t}{2s}(R_6^2 + \eta^2 s^2)^{1/2}$$

$$+ \frac{R_8}{4}(1 - \eta)\cos\varphi_l \ln\left[\frac{(R_5^2 + \eta^2 s^2)^{1/2} - R_5 \sin\varphi_l - \eta s\cos\varphi_l}{s(1 - \eta)\{1 + \cos(\varphi_l - \varphi)\}\sec\varphi}\right]$$

$$- \frac{R_9}{4}(1 - \eta)\cos\varphi_t \ln\left[\frac{(R_6^2 + \eta^2 s^2)^{1/2} + R_6 \sin\varphi_t - \eta s\cos\varphi_t}{s(1 - \eta)\{1 + \cos(\varphi - \varphi_t)\}\sec\varphi}\right]$$

$$+ \frac{(R_8 - R_{10})}{4}(1 - \eta)\cos\varphi_l \ln\left[\frac{(R_5^2 + \eta^2 s^2)^{1/2} - R_5 \sin\varphi_l + \eta s\cos\varphi_l}{s\{R_7 + (1 - \eta)\cos(\varphi_l - \varphi) + 2\eta\cos\varphi_l\cos\varphi\}\sec\varphi}\right]$$

$$- \frac{(R_9 - R_{11})}{4}(1 - \eta)\cos\varphi_t \ln\left[\frac{(R_6^2 + \eta^2 s^2)^{1/2} + R_6 \sin\varphi_t + \eta s\cos\varphi_t}{s\{R_7 + (1 - \eta)\cos(\varphi - \varphi_t) + 2\eta\cos\varphi_t\cos\varphi\}\sec\varphi}\right], \qquad \text{(II.17)}$$

where :

$$R_5 = 1 - x + \eta s\tan\varphi$$

$$R_6 = 1 + x - \eta s\tan\varphi$$

$$R_7^2 = (1 - \eta)^2 + 4\eta\cos^2\varphi$$

$$R_8 = x - \sin^2\varphi_l(1 - \cot\varphi_l\tan\varphi)$$

$$R_9 = x + \sin^2\varphi_t(1 - \cot\varphi_t\tan\varphi)$$

$$R_{10} = \frac{2\eta}{(1 - \eta)}(s\tan\varphi_l - \cos^2\varphi_l)$$

$$R_{11} = \frac{2\eta}{(1 - \eta)}(s\tan\varphi_t + \cos^2\varphi_t)\,.$$

If the semi-span s is now increased to infinity, $\eta s \to y$, and φ, and φ_l, $\varphi_t \to \varphi_0$.

Then :

$$\frac{\pi v_x}{4V_0(t_0/c_0)\cos\varphi_0} =$$

It $s \to \infty$

$$1 + \frac{x}{4}\ln\left\{\frac{R_1 - (1 - x)\sin\varphi_0\cos\varphi_0 - y}{R_2 + (1 + x)\sin\varphi_0\cos\varphi_0 - y}\right\}\left\{\frac{R_1 - (1 - x)\sin\varphi_0\cos\varphi_0 + y\cos 2\varphi_0}{R_2 + (1 + x)\sin\varphi_0\cos\varphi_0 + y\cos 2\varphi_0}\right\}$$

$$- \frac{y}{2}\tan\varphi_0 \ln\left\{\frac{R_1 - (1 - x)\sin\varphi_0\cos\varphi_0 + y\cos 2\varphi_0}{R_2 + (1 + x)\sin\varphi_0\cos\varphi_0 + y\cos 2\varphi_0}\right\} =$$

$$= 1 - \frac{x}{2} \ln \left\{ \frac{1 + x + (R_2 - y) \tan \varphi_0}{1 - x - (R_1 - y) \tan \varphi_0} \right\}$$

$$+ \frac{y}{2} \tan \varphi_0 \ln \left\{ \frac{R_2 + (1 + x) \sin \varphi_0 \cos \varphi_0 + y \cos 2\varphi_0}{R_1 - (1 - x) \sin \varphi_0 \cos \varphi_0 + y \cos 2\varphi_0} \right\}, \quad .. \quad .. \quad \text{(II.20)}$$

which is the formula given in Ref. 3 for the velocity at any point of an infinite swept-back wing of parabolic-arc aerofoil section (equation (4.15) of Ref. 3).

APPENDIX III

The Supervelocity at the Centre-line of a Tapered Swept Wing Having Constant Spanwise Thickness, and a Symmetrical Parabolic-Arc Aerofoil Section (Wing 3)

The wing is taken to have the centre-line chord along the x axis, the mid-chord point being at the origin, and the leading and trailing edges at $x = + 1$ and $x = - 1$ respectively (Figs. 1 and 49).

The equation to the surface of the right-hand half of the wings is :

$$z' = \left(\frac{t_0}{c_0}\right) \left\{ 1 - \frac{s^2 (x' + y' \tan \varphi_0)^2}{\{s - (1 - \lambda) y'\}^2} \right\}, \quad .. \quad .. \quad .. \quad .. \quad .. \quad \text{(III.1)}$$

where :

z' is the half thickness at the point (x', y')

(t_0/c_0) is the centre-line thickness/chord ratio

s is the semi-span of the wing

$\frac{s}{1 - \lambda}$ is the spanwise position at which the extended leading and trailing edges intersect

λ is the taper ratio $\frac{\text{tip chord}}{\text{centre-line chord}}$

φ_0 is the sweep of the mid-chord line.

Then

$$\frac{\partial z'}{\partial x'} = - 2 \left(\frac{t_0}{c_0}\right) \left(\frac{s}{s - (1 - \lambda) y'}\right)^2 (x' + y' \tan \varphi_0) \; .. \quad .. \quad .. \quad \text{(III.2)}$$

and the source strength per unit area to represent this wing is :

$$q' = - 2 V_0 \frac{\partial z'}{\partial x'} = 4 V_0 \left(\frac{t_0}{c_0}\right) \left(\frac{s}{s - (1 - \lambda) y'}\right)^2 (x' + y' \tan \varphi_0) \; .. \quad .. \quad \text{(III.3)}$$

where V_0 is the free-stream velocity.

Thus the actual source strength over an element $(dx'\, dy')$ is :

$$q'\, dx'\, dy' = 4 V_0 \left(\frac{t_0}{c_0}\right) \left(\frac{s}{s - (1 - \lambda) y'}\right)^2 (x' + y' \tan \varphi_0)\, dx'\, dy' \; . \quad .. \quad .. \quad \text{(III.4)}$$

Putting $$x' = x_0 - y' \tan \varphi'$$

$$= x_0\left(\frac{s - (1 - \lambda)y'}{s}\right) - y' \tan \varphi_0$$

where φ' is the sweepback of the constant-percentage chord-line passing through the point (x', y'), and x_0 is the intercept of this line on the x axis.

Then $$dx' = \left(\frac{s - (1 - \lambda)y'}{s}\right) dx_0$$

and $$q'\, dx'\, dy' = 4V_0\left(\frac{t_0}{c_0}\right) x_0\, dx_0\, dy'. \qquad \text{(III.5)}$$

Referring to Fig. 49, the elemental chordwise supervelocity δv_x at the point P due to the source element at the point (x', y') :

$$\delta v_x = -\left(\frac{t_0}{c_0}\right)\frac{V_0\, x_0\, dx_0\, dy'}{\pi R^2}\,(\cos\gamma\cos\varphi' + \sin\gamma\sin\varphi'), \qquad \text{(III.6)}$$

where R is the distance between P and the point (x', y')

γ is the angle between the line joining the points P and (x', y'), and the line passing through P normal to the constant-percentage chord line (x', y').

If n is the length of the perpendicular from P on to the constant-percentage chord-line through (x', y'), then :

$$R = n \sec\gamma$$

$$y' = y + R\sin(\gamma - \varphi)$$

$$= y + n(\tan\gamma\cos\varphi' - \sin\varphi')$$

and $$dy' = n\sec^2\gamma\cos\varphi'\, d\gamma\,.$$

Then the supervelocity (dv_x) at the point P due to the source filament $x_0 - y'\tan\varphi'$ extending from the centre-line to $y' = s$ is given by :

$$\frac{\pi\, dv_x}{V_0(t_0/c_0)} = -\int_{y'=0}^{y'=s}\frac{x_0\, dx_0\,(\cos\gamma\cos\varphi' + \sin\gamma\sin\varphi')\cos\varphi'\, d\gamma}{n}$$

$$= -\frac{x_0 dx_0}{n}\cos\varphi'\,\{\sin(\beta' - \varphi') + \sin(\varphi' - \alpha)\}, \qquad \text{(III.7)}$$

where $$\beta' = \gamma_{y'=s}$$

$$\alpha = \gamma_{y'=0}$$

Substituting $$y = \frac{\eta s}{(1 - \lambda)}\;;\; n = (1 - \eta)(x - x_0)\cos\varphi',$$

the supervelocity at the point P due to the right-hand half of the wing is given by :

$$\frac{\pi v_x}{V_0(t_0/c_0)} = -\int_{-1}^{+1}\left(\frac{x_0}{x-x_0}\right)\left(\frac{s}{1-\eta}\right)\left(\frac{1-\lambda-\eta}{[\{\lambda(1-\lambda)(x-x_0)+s(1-\lambda-\eta)\tan\varphi\}^2+s^2(1-\lambda-\eta)^2]^{1/2}}\right.$$

$$\left.+\frac{\eta}{[\{(1-\lambda)(x-x_0)-\eta s\tan\varphi\}^2+\eta^2s^2]^{1/2}}\right)dx_0$$

$$=-\left(\frac{s}{1-\eta}\right)\{x(1-\lambda-\eta)I_1-(1-\lambda-\eta)I_2+x\eta I_3-\eta I_4\}$$

where :

$$I_1=\int_{-1}^{+1}\frac{dx_0}{(x-x_0)\{\lambda^2(1-\lambda)^2(x-x_0)^2+2\lambda s(1-\lambda)(1-\lambda-\eta)(x-x_0)\tan\varphi+s^2(1-\lambda-\eta)^2\sec^2\varphi\}^{1/2}}$$

$$I_2=\int_{-1}^{+1}\frac{dx_0}{\{\lambda^2(1-\lambda)^2(x-x_0)^2+2\lambda s(1-\lambda)(1-\lambda-\eta)(x-x_0)\tan\varphi+s^2(1-\lambda-\eta)^2\sec^2\varphi\}^{1/2}}$$

$$I_3=\int_{-1}^{+1}\frac{dx_0}{(x-x_0)\{(1-\lambda)^2(x-x_0)^2-2\eta s(1-\lambda)(x-x_0)\tan\varphi+\eta^2s^2\sec^2\varphi\}^{1/2}}$$

$$I_4=\int_{-1}^{+1}\frac{dx_0}{\{(1-\lambda)^2(x-x_0)^2-2\eta s(1-\lambda)(x-x_0)\tan\varphi+\eta^2s^2\sec^2\varphi\}^{1/2}}.$$

All these integrals are of standard form, and after some rearrangement, the supervelocity at the point (x, o) due to the right-hand half of the wing is obtained as :

$$\frac{\pi v_x}{V_0(t_0/c_0)} = -x\cos\varphi\ln\frac{R_{12}+s-\lambda(1-x)\sin\varphi\cos\varphi}{R_{13}+s+\lambda(1+x)\sin\varphi\cos\varphi}$$

$$-\frac{s}{\lambda}\ln\frac{R_{12}+s\sin\varphi-\lambda(1-x)\cos\varphi}{R_{13}+s\sin\varphi+\lambda(1+x)\cos\varphi}$$

$$-x\cos\varphi\ln\left(\frac{1+x}{1-x}\right)\left(\frac{1+\sin\varphi}{1-\sin\varphi}\right) \qquad \text{(III.9)}$$

where :
$$R_{12}^2=\lambda^2(1-x)^2\cos^2\varphi-2\lambda s(1-x)\sin\varphi\cos\varphi+s^2$$
$$R_{13}^2=\lambda^2(1+x)^2\cos^2\varphi+2\lambda s(1+x)\sin\varphi\cos\varphi+s^2.$$

The contribution to v_x due to the left-hand half of the wing is, by symmetry, equal to that due to the right-hand half of the wing. Hence the supervelocity at the centre-line due to the complete wing is given by :

$$\frac{\pi v_x}{4V_0(t_0/c_0)}=\frac{s}{2\lambda}\ln\frac{R_{13}+s\sin\varphi+\lambda(1+x)\cos\varphi}{R_{12}+s\sin\varphi-\lambda(1-x)\cos\varphi}$$

$$+\frac{x}{2}\ln\frac{R_{13}+s+\lambda(1+x)\sin\varphi\cos\varphi}{R_{12}+s-\lambda(1-x)\sin\varphi\cos\varphi}$$

$$-\frac{x}{2}\cos\varphi\ln\left(\frac{1+x}{1-x}\right)\left(\frac{1+\sin\varphi}{1-\sin\varphi}\right). \qquad \text{(III.10)}$$

When $\lambda = 1$, $\varphi = \varphi_0$, and this equation reduces to :

$$\frac{\pi v_x}{4V_0(t_0/c_0)} = \frac{s}{2} \ln \frac{\{(1+x)^2\cos^2\varphi_0 + 2s(1+x)\sin\varphi_0\cos\varphi_0 + s^2\}^{1/2} + s\sin\varphi_0 + (1+x)\cos\varphi_0}{\{(1-x)^2\cos^2\varphi_0 - 2s(1-x)\sin\varphi_0\cos\varphi_0 + s^2\}^{1/2} + s\sin\varphi_0 - (1-x)\cos\varphi_0}$$

$$+ \frac{x}{2}\cos\varphi_0 \ln \frac{\{(1+x)^2\cos^2\varphi_0 + 2s(1+x)\sin\varphi_0\cos\varphi_0 + s^2\}^{1/2} + s + (1+x)\sin\varphi_0\cos\varphi_0}{\{(1-x)^2\cos^2\varphi_0 - 2s(1-x)\sin\varphi_0\cos\varphi_0 + s^2\}^{1/2} + s - (1-x)\sin\varphi_0\cos\varphi_0}$$

$$- \frac{x}{2}\cos\varphi_0 \ln\left(\frac{1+x}{1-x}\right)\left(\frac{1+\sin\varphi_0}{1-\sin\varphi_0}\right), \qquad \text{(III.11)}$$

which, since $s = A$ for an untapered wing, is in agreement with equation (4.13) of Ref. 3 for the supervelocity at the centre of a finite aspect-ratio, untapered, swept wing.

For $s = \infty$, the first term of equation (III.11) becomes $\cos\varphi_0$, and hence for an infinite swept wing, the supervelocity at the centre-line is given by :

$$\frac{\pi v_x}{4V_0(t_0/c_0)} = \cos\varphi_0 \left\{1 - \frac{x}{2}\ln\left(\frac{1+x}{1-x}\right) - \frac{x}{2}\ln\left(\frac{1+\sin\varphi_0}{1-\sin\varphi_0}\right)\right\}. \qquad \text{(III.12)}$$

To obtain the expression for the supervelocity at the centre-line of a fully tapered wing having constant spanwise thickness, it is necessary to put $\lambda = 0$. This is not strictly permissible, because the thickness/chord ratio at the tips of such a wing is infinite, and linearised theory cannot be applied under these conditions. A similar case occurs near the leading edges of round-nosed aerofoil sections, however, and it has been shown elsewhere that in this case, the results given by linearised theory are invalid only near the leading edge. Since, for the case of the fully tapered wing considered, only the velocities at the centre-line are required, it has been assumed, without formal proof, that the expression obtained from equation (III.10) for $\lambda = 0$ gives the correct value of the supervelocity at the centre-line chord. Some justification for this assumption is provided by the fact that for a given rate of planform taper, v_x/V_0 at the centre-line does not vary greatly with λ as $\lambda \to 0$: for $\lambda \neq 0$, the thickness/chord ratio at the tip is not infinite and can indeed be very small, thus complying with the requirements of linearised theory. Furthermore, the excellent agreement between the supervelocities at the centre of wing (6) which include the supervelocities due to wing (3), $\lambda = 0$, and those at the centre of the constant thickness/chord ratio wing considered in Ref. 7, shows that any errors involved in this assumption are small and of a negligible order.

As $\lambda \to 0$, the first term of equation (III.10) becomes $\cos\varphi$, and hence the expression for the supervelocity at the centre of a fully tapered wing, having constant spanwise thickness is :

$$\frac{\pi v_x}{4V_0(t_0/c_0)} = \cos\varphi \left\{1 - \frac{x}{2}\ln\left(\frac{1+x}{1-x}\right) - \frac{x}{2}\ln\left(\frac{1+\sin\varphi}{1-\sin\varphi}\right)\right\}. \qquad \text{(III.13)}$$

Equation (III.13) shows that the supervelocity at a point on the centre-line chord of such a wing is the same as that at the corresponding point of an infinite swept wing, having the same sweep as the constant-percentage chord-line of the tapered wing which passes through that point.

APPENDIX IV

The Supervelocity at the Centre-line of a Tapered Unswept Wing Having a Cubic Spanwise Variation of Thickness, and a Symmetrical Parabolic-Arc Aerofoil Section (Wing 4)

The wing is taken to have the centre-line chord along the x axis, the midpoint of the chord being at the origin, and the leading and trailing edges at $x = +1$ and $x = -1$ respectively.

The equation to the surface of the right-hand half of the wing is :

$$z' = \left(\frac{t_0}{c_0}\right)\left(1 + \frac{Ny'}{s}\right)\left\{1 - \frac{s^2x'^2}{(s-y')^2}\right\}\left(\frac{s-y'}{s}\right)^2, \quad .. \quad .. \quad .. \quad \text{(IV.1)}$$

where z' = is the half thickness of the wing at the point (x, y')

t_0/c_0 = is the centre-line thickness/chord ratio

s = is the semi-span of the wing

$\frac{t_0}{c_0}\left(1 + \frac{Ny'}{s}\right)\left(\frac{s-y'}{s}\right)$ is the thickness/chord ratio at spanwise position y', N being a coefficient varying from -1 to $+\infty$ for wings which have positive thickness through-out the span.

$$\frac{\partial z'}{\partial x'} = -2\left(\frac{t_0}{c_0}\right)\left(1 + \frac{Ny'}{s}\right)x'. \quad .. \quad .. \quad .. \quad .. \quad .. \quad .. \quad \text{(IV.2)}$$

Therefore q' (the source strength per unit area) required to represent this wing is :

$$q' = -2V_0\frac{\partial z'}{\partial x'} = 4V_0\left(\frac{t_0}{c_0}\right)\left(1 + \frac{Ny'}{s}\right)x', \quad .. \quad .. \quad .. \quad .. \quad \text{(IV.3)}$$

where V_0 is the free-stream velocity, i.e., q varies linearly along lines parallel to the maximum-thickness line. Thus, referring to Fig. 49, the supervelocity δv_x at the point P (x, y) due to the elemental source at the point (x', y') is given by :

$$\delta v_x = -\frac{q'\,dx'\,dy'}{4\pi R^2}\cos\gamma$$

$$= -\frac{V_0}{\pi}\left(\frac{t_0}{c_0}\right)\frac{x'}{R^2}\left(1 + \frac{Ny'}{s}\right)\cos\gamma\,dx'\,dy', \quad .. \quad .. \quad .. \quad .. \quad \text{(IV.4)}$$

where : R is the distance between P and the point (x', y')

γ is the angle between the line joining P with (x', y'), and the perpendicular from P on to the source filament $x = x'$.

Thus the supervelocity dv_x at P due to the source filament $x = x'$ is given by :

$$\frac{\pi\,dv_x}{V_0(t_0/c_0)} = -x'\,dx'\int_{y'=0}^{y'=y_l}\left(1 + \frac{Ny'}{s}\right)\frac{\cos\gamma}{R^2}\,dy' =$$

$$= \left(\frac{x'}{x-x'}\right)\left\{\left(1+\frac{Ny}{s}\right)\left[\frac{y-y_l}{\{(x-x')^2+(y-y_l)^2\}^{1/2}}-\frac{y}{\{(x-x')^2+y^2\}^{1/2}}\right]\right.$$

$$\left.+\frac{N(x-x')^2}{s}\left[\frac{1}{\{(x-x')^2+(y-y_l)^2\}^{1/2}}-\frac{1}{\{(x-x')^2+y^2\}^{1/2}}\right]\right\}dx'. \quad .. \quad \text{(IV.5)}$$

For the front half of the wing, $y_l = s(1-x')$; putting $x' = x-(x-x')$ and integrating from $x'=0$ to $x'=1$, we obtain for $y=0$:

$$\frac{\pi v_x}{V_0(t_0/c_0)} = x\ln\frac{x}{\sqrt{(x^2+s^2)}-s}$$

$$+\frac{s}{\sqrt{(1+s^2)}}\left\{1-2x-\frac{s(1-x)}{(1+s)^2}\left(s+\frac{xN}{s}\right)-\frac{N}{2}\frac{(2s^2-1)(1-x)^2}{(1+s^2)^2}\right\}\ln\frac{\sqrt{(1+s^2)}\sqrt{(x^2+s^2)}+x+s^2}{(1-x)(\sqrt{(1+s^2)}-1)}$$

$$-\frac{1}{(1+s^2)}\left\{s+\frac{xN}{s}+\frac{2Ns(1-x)}{(1+s^2)}\{1-x-\sqrt{(x^2+s^2)}\}-\frac{N(x+s^2)\sqrt{(x^2+s^2)}}{2s(1+s^2)^2}\right.$$

$$\left.+\frac{N(1-x^2)}{2s}\left\{1-\frac{1}{(1+s^2)^2}\right\}+\frac{xN}{s}(1-2x)+\frac{Nx^2}{2s}\right. \quad .. \quad .. \quad .. \quad .. \quad .. \quad \text{(IV.6)}$$

The supervelocity at the point (x, o) due to the rear half of the right-hand wing can be obtained from equation (IV.6) by putting $-x$ for x. Adding the result obtained to equation (IV.6), and doubling to give the supervelocity due to the left- and right-hand halves of the wing, gives the supervelocity at the centre-line of the whole wing as :

$$\frac{\pi v_x}{4V_0(t_0/c_0)} = \frac{N}{4s}\left\{1-\frac{1}{(1+s^2)^2}\right\}\left\{(1-x)^2+(1+x)^2\right\}-\frac{3x^2N}{2s}-\frac{Ns}{2(1+s^2)^2}\sqrt{(x^2+s^2)}$$

$$-\frac{1}{2(1+s)^2}\left\{\frac{2Ns(1-x)}{(1+s^2)}+s+\frac{Nx}{s}\right\}\{1-x-\sqrt{x^2+s^2})\}$$

$$-\frac{1}{2(1+s^2)}\left\{\frac{2Ns(1+x)}{(1+s^2)}+s-\frac{Nx}{s}\right\}\{1+x-\sqrt{(x^2+s^2)}\}$$

$$+\frac{s}{2\sqrt{(1+s^2)}}\left\{1-2x-\frac{s(1+x)}{(1+s^2)}\left(s+\frac{Nx}{s}\right)\right.$$

$$\left.-\frac{N(2s^2-1)(1-x)^2}{2(1+s^2)^2}\right\}\ln\frac{\sqrt{(1+s^2)}\sqrt{(x^2+s^2)}+x+s^2}{(1-x)\{\sqrt{(1+s^2)}-1\}}$$

$$+\frac{s}{2\sqrt{(1+s^2)}}\left\{1-2x-\frac{s(1+x)}{1(+s^2)}\left(s-\frac{Nx}{s}\right)\right.$$

$$\left.-\frac{N(2s^2-1)(1-x)^2}{2(1+s^2)^2}\right\}\ln\frac{\sqrt{(1+s^2)}\sqrt{(x^2+s^2)}-x+s^2}{(1+x)\{\sqrt{(1+s^2)}-1\}}$$

TABLE 1—*continued*

x/c	(1) $S^{(1)}(x,\eta)$ All η	(2) $S^{(2)}(x,o)$	(3) φ	(4) $\cos\varphi$	(5) $\sin\varphi$	(6) $f(\varphi)\cos\varphi$	(7) $S^{(2)}(x,o)$ x (6)	(8) $S^{(1)}(x,\eta)$ $x\cos\varphi$
0·05	0·151	+0·255	51° 0′	0·629	0·777	0·415	+0·106	0·095
0·10	0·158	0·146	49° 29′	0·650	0·760	0·412	0·060	0·103
0·20	0·153	+0·049	46° 7′	0·693	0·721	0·401	+0·020	0·106
0·30	0·133	0	42° 18′	0·740	0·673	0·384	0	0·098
0·40	0·112	−0·030	37° 57′	0·789	0·615	0·361	−0·011	0·088
0·50	0·091	−0·051	33° 2′	0·838	0·531	0·319	−0·016	0·076
0·60	0·067	−0·067	27° 29′	0·887	0·462	0·284	−0·019	0·059
0·70	0·046	−0·080	21° 18′	0·932	0·363	0·226	−0·018	0·043
0·80	0·020	−0·093	14° 34′	0·968	0·252	0·159	−0·015	0·019

x/c	(9) $\eta=0$	(10) $\eta=0{\cdot}165$	(11) $\eta=0{\cdot}366$	(12) $\eta=0{\cdot}584$	(13) $\eta=0{\cdot}733$	(14) $\eta=0$	(15) $\eta=0{\cdot}165$	(16) $\eta=0{\cdot}366$	(17) $\eta=0{\cdot}584$	(18) $\eta=0{\cdot}733$
	← $1+K_1(x,\eta)$ →					← $\{1+K_1(x,\eta)\}S^{(1)}(x,\eta)\cos\varphi$ →				
0·05	1·000	1·167	1·152	1·079	1·050	0·095	0·111	0·110	0·102	0·100
0·10	1·000	1·152	1·145	1·077	1·050	0·103	0·119	0·118	0·111	0·108
0·20	1·000	1·123	1·128	1·072	1·047	0·106	0·119	0·119	0·114	0·111
0·30	1·000	1·097	1·099	1·061	1·040	0·098	0·108	0·108	0·104	0·102
0·40	1·000	1·068	1·073	1·048	1·033	0·088	0·094	0·094	0·092	0·091
0·50	1·000	1·044	1·049	1·034	1·026	0·076	0·079	0·080	0·079	0·078
0·60	1·000	1·027	1·030	1·023	1·017	0·059	0·061	0·061	0·060	0·060
0·70	1·000	1·018	1·019	1·013	1·009	0·043	0·044	0·044	0·044	0·043
0·80	1·000	1·008	1·008	1·006	1·005	0·019	0·019	0·019	0·019	0·019

x/c	(19) $\eta=0$ $K_2=1{\cdot}00$	(20) $\eta=0{\cdot}165$ $K_2=0{\cdot}02$	(21) $\eta=0{\cdot}366$ $K_2=-0{\cdot}19$	(22) $\eta=0{\cdot}584$ $K_2=-0{\cdot}22$	(23) $\eta=0{\cdot}733$ $K_2=-0{\cdot}20$	(24) $\eta=0$	(25) $\eta=0{\cdot}165$	(26) $\eta=0{\cdot}366$	(27) $\eta=0{\cdot}584$	(28) $\eta=0{\cdot}733$
	← $K_2S^{(2)}(x,o)f(\varphi)\cos\varphi$ →					← $[\{1+K_1(x,\eta)\}S^{(1)}(x,\eta)-K_2S^{(2)}(x,\eta)f(\varphi)]\cos\varphi$ →				
0·05	+0·106	0·003	−0·020	−0·023	−0·021	−0·011	0·108	0·130	0·125	0·121
0·10	0·060	0·001	−0·011	−0·013	−0·012	−0·043	0·118	0·129	0·124	0·120
0·20	+0·020	0	−0·004	−0·004	−0·004	+0·086	0·119	0·123	0·118	0·115
0·30	0	0	0	0	0	0·098	0·108	0·108	0·104	0·102
0·40	−0·011	0	+0·002	+0·002	+0·002	0·099	0·094	0·092	0·090	0·089
0·50	−0·016	0	0·003	0·004	0·003	0·092	0·079	0·077	0·075	0·075
0·60	−0·019	0	0·004	0·004	0·004	0·078	0·061	0·057	0·056	0·056
0·70	−0·018	0	0·003	0·004	0·004	0·061	0·044	0·041	0·040	0·039
0·80	−0·015	0	+0·003	+0·003	+0·003	+0·034	0·019	0·016	0·016	0·016

η	(29) $S^{(1)}(k,\eta)$	(30) $\frac{\Delta v_x(k,\eta)_{\varphi=0}}{V_0}$	(31) $\frac{\{\Delta v_x(k,o)_s\}_{\varphi=0}}{V_0}$	(32) $\frac{\{\Delta v_x(k,o)_\lambda\}_{\varphi=0}}{V_0}$	(33) $\frac{\{\Delta v_x(k,o)_t\}_{\varphi=0}}{V_0}$	(34) $\frac{\{v_x(k,\eta)\}_{\varphi=0}}{V_0}$	(35) $S^{(1)}(k,o)$ $x(1-\cos\varphi_k)$	(36) $\frac{\Delta v_x(k,o)_{s,\varphi}}{V_0}$	(37) $\frac{\Delta v_x(k,o)_{\lambda,\varphi}}{V_0}$	(38) $\frac{\Delta v_x(k,o)_{t,\varphi}}{V_0}$	(39) $\frac{\Delta v_x(k,o)_\varphi}{V_0}$	(40) $K_1(k,o)x$ $S^{(1)}(k,\eta)\cos\varphi_k$	(41) $\frac{v_x(k,\eta)}{V_0}$	(42) τ
0	0·133	—	0·008	0·008	0·025	0·108	0·035	0·010	0·010	0·014	0·021	0	0·087	0·888
0·165	0·133	+0·019	—	—	—	0·114	0·035	0·010	0·010	0·014	0·021	0·009	0·102	0·945
0·366	0·133	0·011	—	—	—	0·122	0·035	0·010	0·010	0·014	0·021	0·010	0·111	1·029
0·584	0·133	+0·003	—	—	—	0·130	0·035	0·010	0·010	0·014	0·021	0·006	0·115	1·106
0·733	0·133	−0·003	—	—	—	0·136n	0·035	0·010	0·010	0·014	0·021	0·004	0·119	1·167

x/c	(43) $\eta=0$	(44) $\eta=0{\cdot}165$	(45) $\frac{v_x(x,\eta)}{V_0}$ $\eta=0{\cdot}366$	(46) $\eta=0{\cdot}584$	(47) $\eta=0{\cdot}733$	(48) $\eta=0$	(49) $\eta=0{\cdot}165$	(50) $-C_p$ $\eta=0{\cdot}366$	(51) $\eta=0{\cdot}584$	(52) $\eta=0{\cdot}733$	(53) $\frac{1}{1+(S^{(2)}(x))^2}$	(54) $\eta=0$	(55) $\eta=0{\cdot}165$	(56) $\eta=0{\cdot}366$	(57) $\eta=0{\cdot}584$	(58) $\eta=0{\cdot}733$
	←			→		←			→		←		$-C_p$ (with thickness correction)		→	
0·05	−0·010	0·102	0·134	0·138	0·141	−0·020	0·214	0·286	0·295	0·302	0·943	−0·076	0·145	0·213	0·221	0·228
0·10	+0·038	0·112	0·133	0·137	0·140	+0·078	0·236	0·284	0·293	0·300	0·980	+0·056	0·212	0·258	0·266	0·274
0·20	0·076	0·113	0·127	0·131	0·134	0·158	0·238	0·270	0·280	0·286	0·997	0·154	0·234	0·265	0·275	0·281
0·30	0·087	0·102	0·111	0·115	0·119	0·182	0·214	0·234	0·242	0·252	1·000	0·182	0·214	0·234	0·242	0·252
0·40	0·088	0·089	0·095	0·100	0·104	0·184	3·187	0·200	0·210	0·218	0·999	0·182	0·185	0·199	0·209	0·216
0·50	0·082	0·075	0·079	0·083	0·088	0·170	0·156	0·165	0·173	0·184	0·997	0·166	0·152	0·161	0·169	0·180
0·60	0·069	0·058	0·059	0·062	0·065	0·142	0·120	0·122	0·129	0·135	0·995	0·136	0·115	0·116	0·124	0·129
0·70	0·054	0·042	0·042	0·044	0·046	0·110	0·087	0·087	0·090	0·094	0·993	0·092	0·080	0·080	0·083	0·086
0·80	+0·030	0·018	0·016	0·018	0·019	+0·060	0·036	0·032	0·036	0·039	0·991	+0·050	0·026	0·023	0·026	0·030

TABLE 1

Calculation of the Chordwise Pressure Distributions on a Delta Wing :
$A = 3{\cdot}08$ *; Aerofoil Section NACA* 0010 *Throughout the Span*

From equation (20) :

$$\frac{v_x(x, \eta)}{V_0} = \tau[\{1 + K_1(x, \eta)\}\, S^{(1)}\,(x, \eta) - K_2 S^{(2)}(x, o)\, f\,(\varphi)\,]\cos\varphi\,.$$

From equation (21) :

$$\tau = \frac{v_x(k, \eta)}{V_0\{1 + K_1(k, \eta)\}\, S^{(1)}(k, \eta)\, \cos\varphi_k}\,.$$

From equation (22) :

$$\frac{v_x(k, \eta)}{V_0} = \left\{\frac{v_x(k, \eta)}{V_0}\right\}_{\varphi=0} - \frac{\Delta v_x(k, o)_\varphi}{V_0} + K_1(k, \eta)\, S^{(1)}(k, \eta)\cos\varphi_k\,.$$

From equation (23) :

$$\left\{\frac{v_x(k, o)}{V_x}\right\}_{\varphi=0} = S^{(1)}(k, o) - \left\{\frac{\Delta v_x(k, o)_s}{V_0}\right\}_{\varphi=0} + \left\{\frac{\Delta v_x(k, o)_\lambda}{V_0}\right\}_{\varphi=0} - \left\{\frac{\Delta v_x(k, o)_t}{V_0}\right\}_{\varphi=0},$$

$\left\{\dfrac{\Delta v_0(k, o)_{s,\,\lambda \text{ and } t}}{V_0}\right\}_{\varphi=0}$ being obtained from Fig. 25,

and from equation (24) :

$$\left\{\frac{v_x(k, \eta)}{V_0}\right\}_{\varphi=0} = S^{(1)}(k, \eta) - \left\{\frac{\Delta v_x(k, \eta)}{V_0}\right\}_{\varphi=0}$$

$\left\{\dfrac{\Delta v_x(k, \eta)}{V_0}\right\}_{\varphi=0}$ being obtained from Fig. 10b or the results of Ref. 7.

From equation (27) :

$$\frac{\Delta v_x(k, o)_\varphi}{V_0} = S^{(1)}(k, o)\{1 - \cos\varphi_k -\}\, \frac{\Delta v_x(k, o)_{s,\varphi}}{V_0} + \frac{\Delta v_x(k, o)_{\lambda,\varphi}}{V_0} - \frac{\Delta v_x(k, o)_{t,\varphi}}{V_0},$$

$\dfrac{\Delta v_x(k, o)_{s,\,\varphi;\,\lambda,\,\varphi \text{ and } t,\,\varphi}}{V_0}$ being obtained from Fig. 47.

Then $$C_p = 1 - \left\{1 + \frac{v_x(x, \eta)}{V_0}\right\}^2,$$

or allowing for the effects of aerofoil thickness :

$$C_p = 1 - \frac{\left\{1 + \dfrac{v_x(x, \eta)}{V_0}\right\}^2}{1 + \{S^{(2)}(x, \eta)\}^2}\,.$$

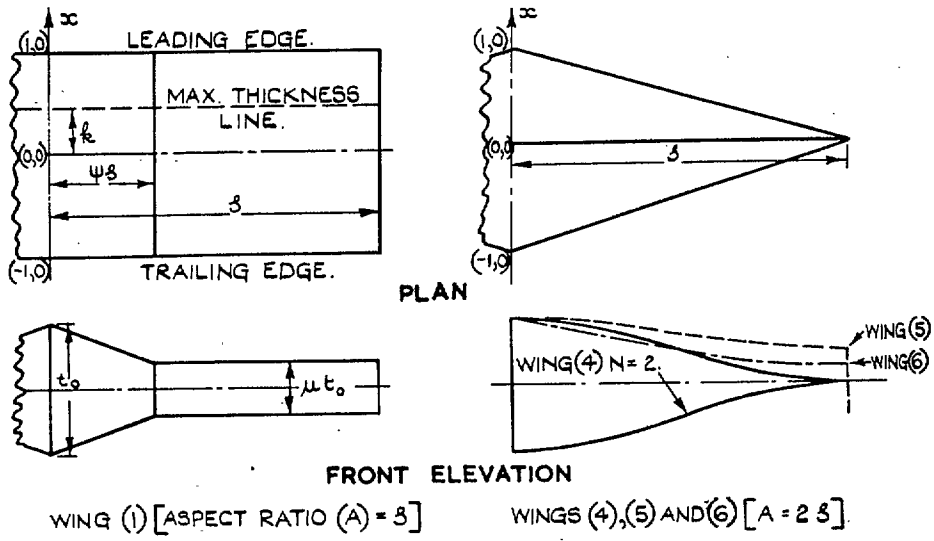

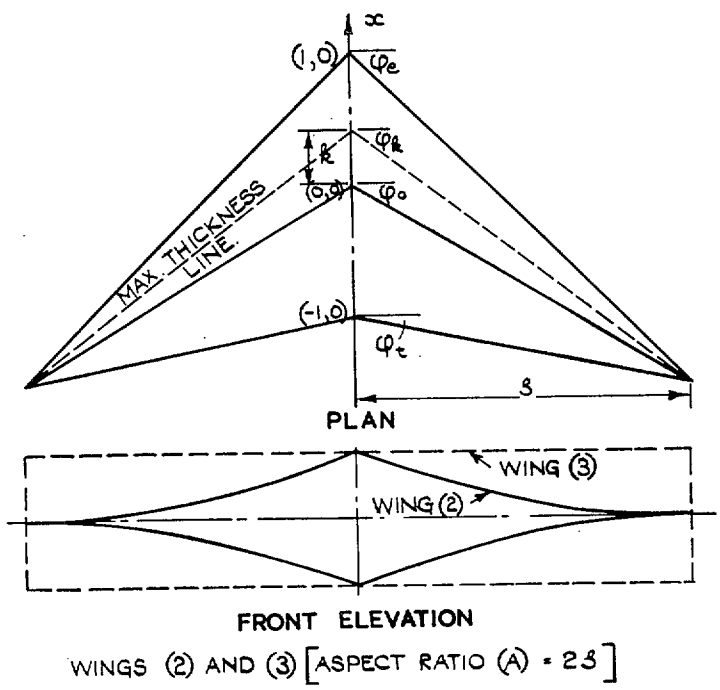

FIG. 1. Types of wing considered.

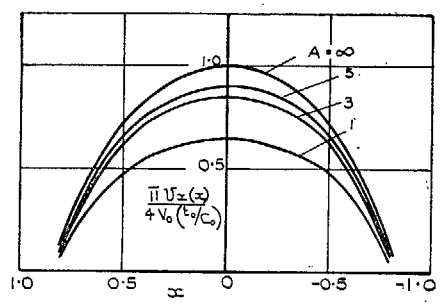

(a) EFFECT OF ASPECT RATIO.

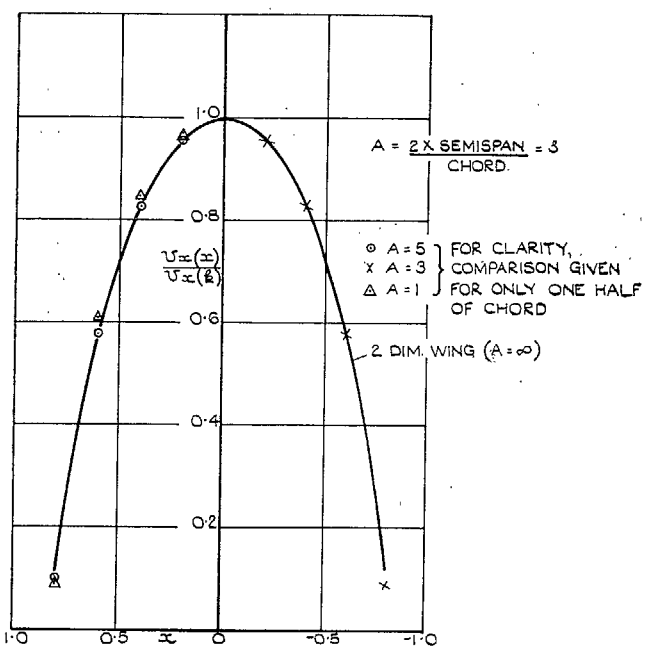

(b) COMPARISON WITH TWO-DIMENSIONAL DISTRIBUTION.

FIGS. 2a and 2b. Centre-line supervelocity distributions.
Wing (1). $k = 0$. $\psi = 1{\cdot}0$. $\mu = 0$.

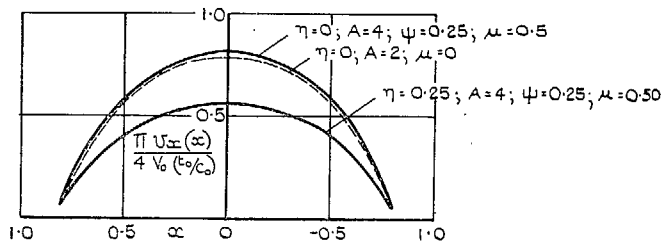

(a) EFFECT OF SPANWISE POSITION AND SPANWISE THICKNESS DISTRIBUTION.

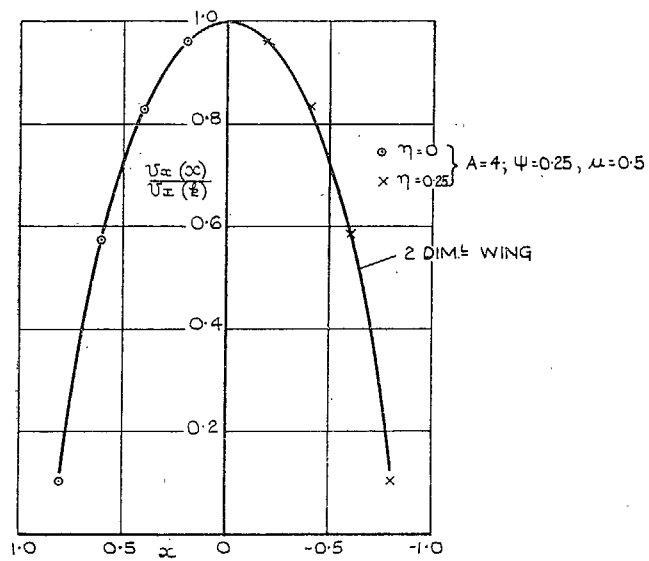

(b) COMPARISON WITH TWO-DIMENSIONAL DISTRIBUTION.

FIGS. 3a and 3b. Chordwise supervelocity distributions.
Wing (1). $k = 0$. $s' = C_0$.

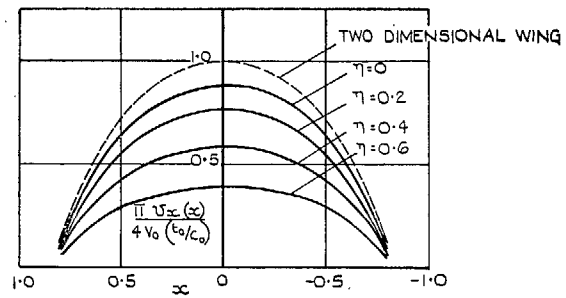

(a) EFFECT OF SPANWISE POSITION.

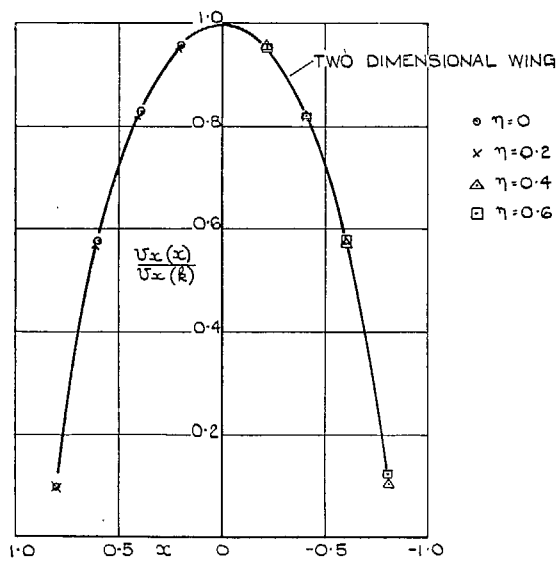

(b) COMPARISON WITH TWO-DIMENSIONAL DISTRIBUTION.

FIGS. 4a and 4b. Chordwise supervelocity distributions. Wing (1). $k = 0$. $A = 4$. $\psi = 1{\cdot}0$. $\mu = 0$.

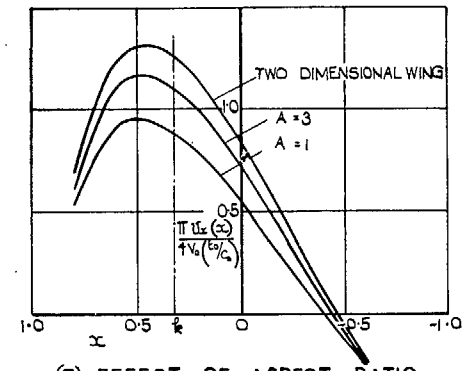

(a) EFFECT OF ASPECT RATIO.

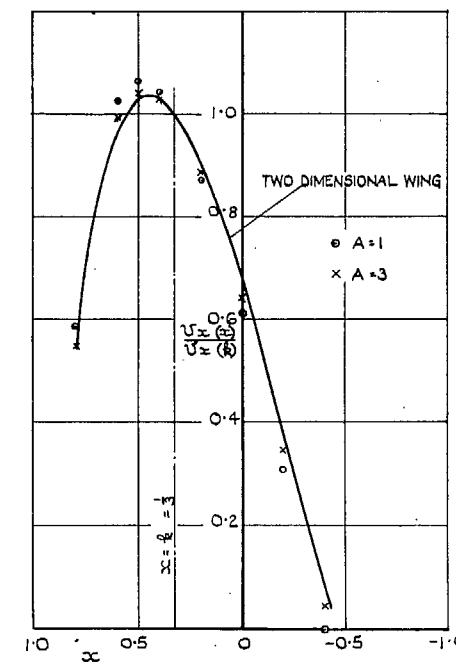

(b) COMPARISON WITH TWO-DIMENSIONAL DISTRIBUTION.

FIGS. 5a and 5b. Centre-line supervelocity distributions. Wing (1). $k = 1/3$. $\psi = 1{\cdot}0$. $\mu = 0$.

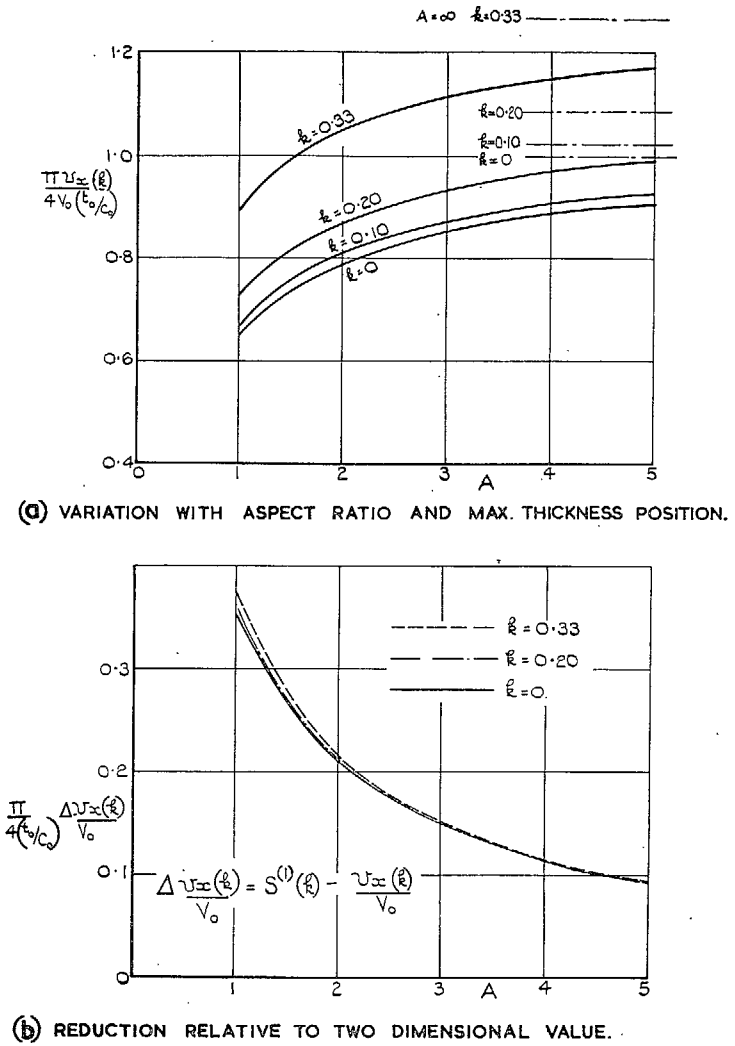

FIGS. 6a and 6b. Supervelocity at maximum thickness of centre-line chord. Wing (1). $\psi = 1{\cdot}0$. $\mu = 0$.

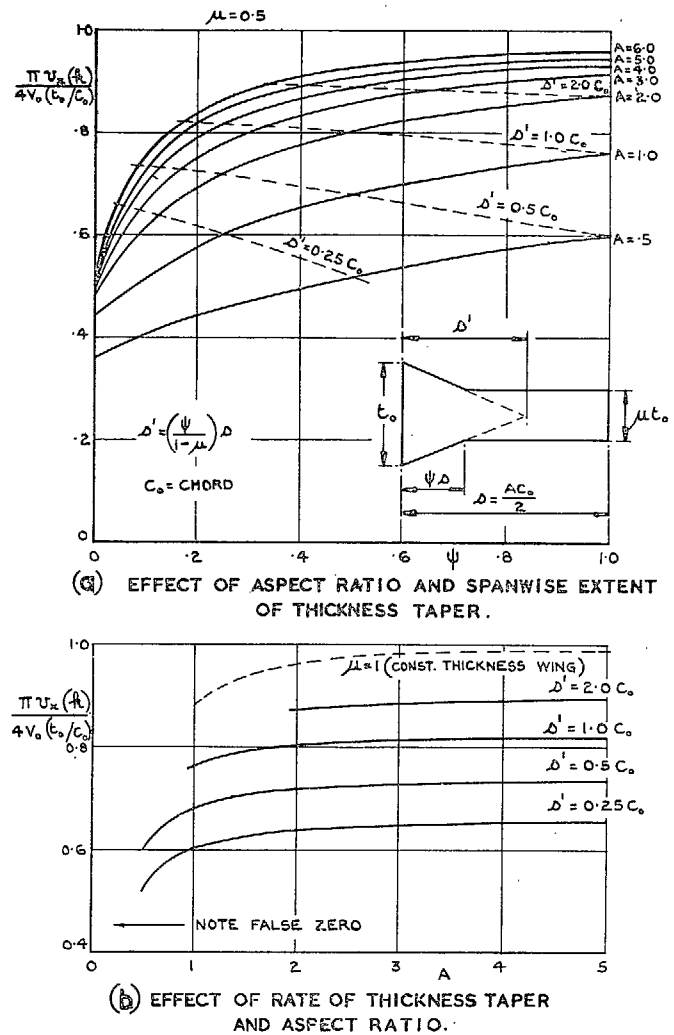

FIGS. 7a and 7b. Supervelocity at maximum thickness of centre-line chord. Wing (1). $k = 0$. $\mu = 0{\cdot}5$.

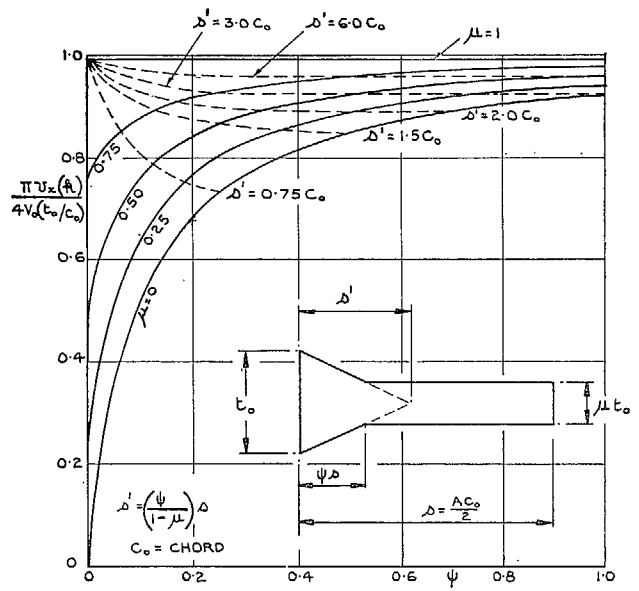

(a) VARIATION WITH TIP THICKNESS AND SPANWISE EXTENT OF THICKNESS TAPER.

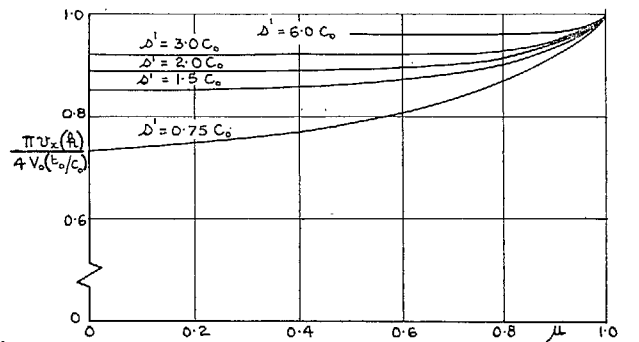

(b) EFFECT OF RATE OF THICKNESS TAPER AND TIP THICKNESS.

FIGS. 8a and 8b. Supervelocity at maximum thickness of centre-line chord. Wing (1). $k = 0$. $A = 6$.

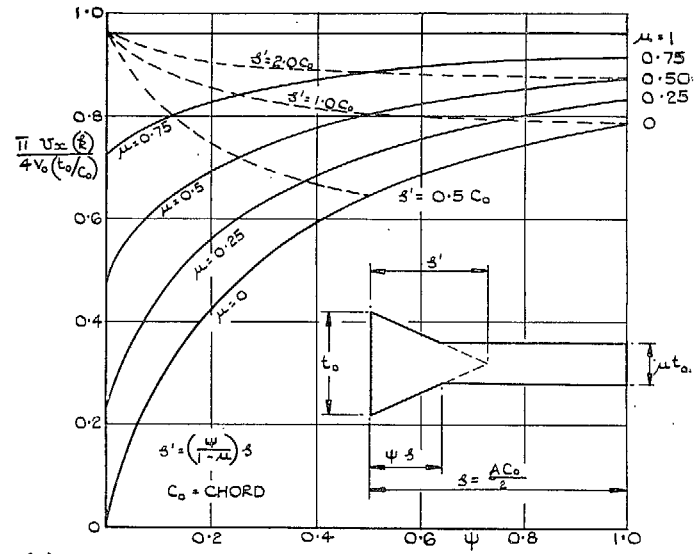

(a) VARIATION WITH TIP THICKNESS AND SPANWISE EXTENT OF THICKNESS TAPER.

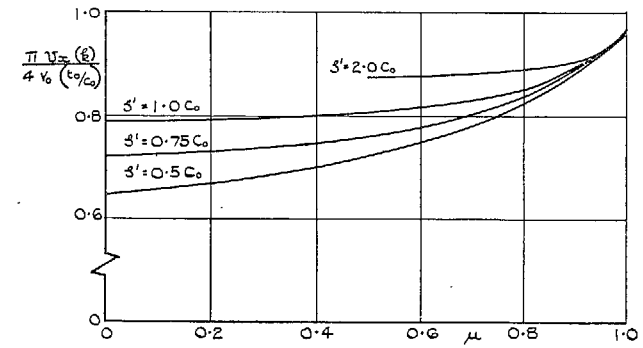

(b) EFFECT OF RATE OF THICKNESS TAPER AND TIP THICKNESS.

FIGS. 9a and 9b. Supervelocity at maximum thickness of centre-line chord. Wing (1). $k = 0$. $A = 2$.

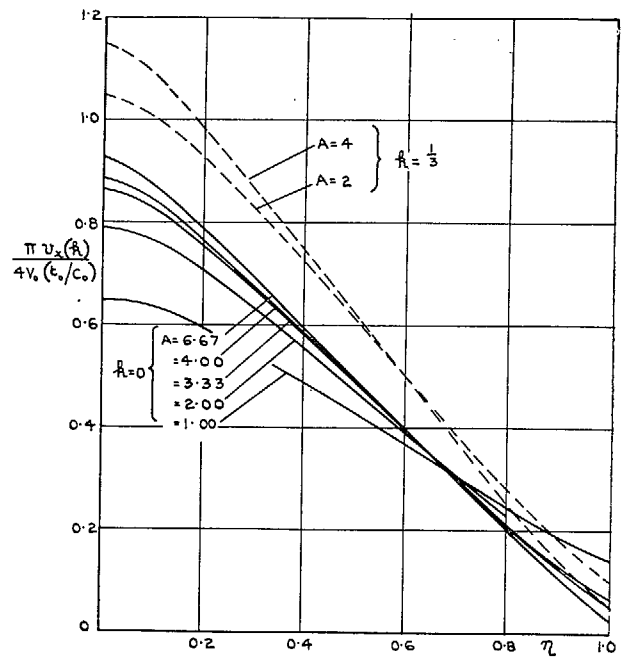

(a) EFFECT OF ASPECT RATIO AND MAX THICKNESS POSITION.

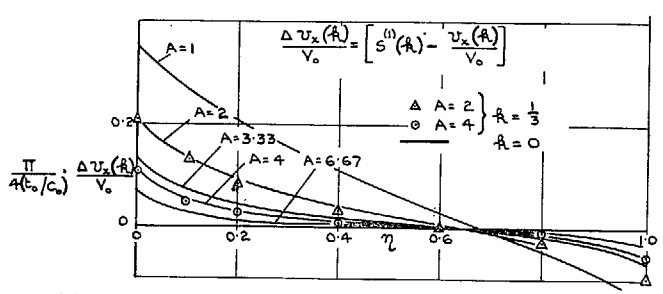

(b) REDUCTION OF v_x RELATIVE TO TWO-DIMENSIONAL VALUE FOR LOCAL THICKNESS / CHORD RATIO.

FIGS. 10a and 10b. Spanwise variation of supervelocity at maximum thickness. Wing (1). $\psi = 1$. $\mu = 0$.

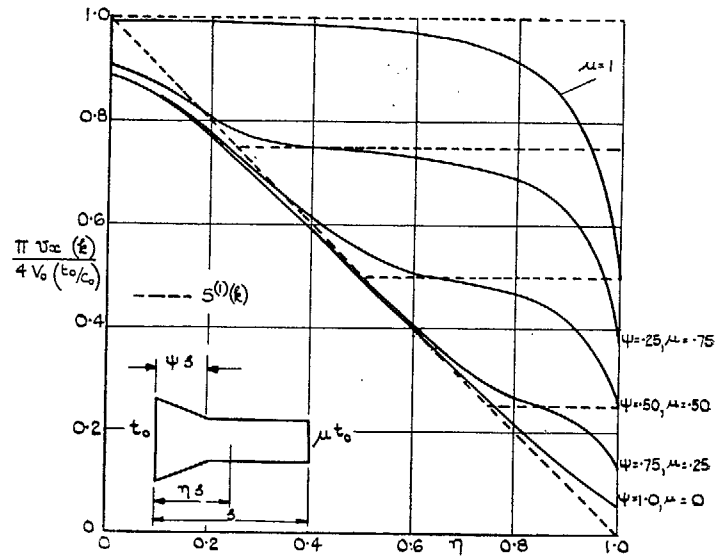

(a) EFFECT OF SPANWISE EXTENT OF TAPER.

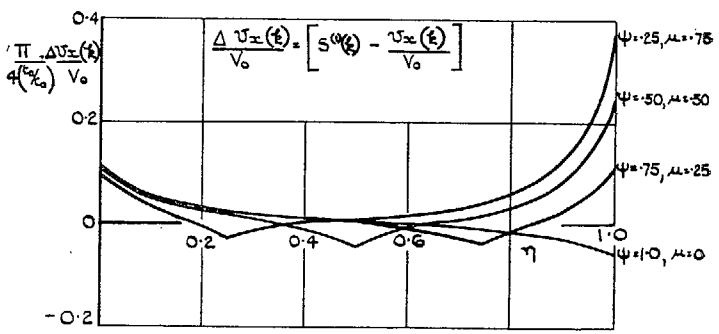

(b) REDUCTION OF v_x RELATIVE TO TWO-DIMENSIONAL VALUE.

FIGS. 11a and 11b. Spanwise variation of supervelocity at maximum thickness. Wing (1). $k = 0$. $A = 4$. $s' = 2\,C_0$.

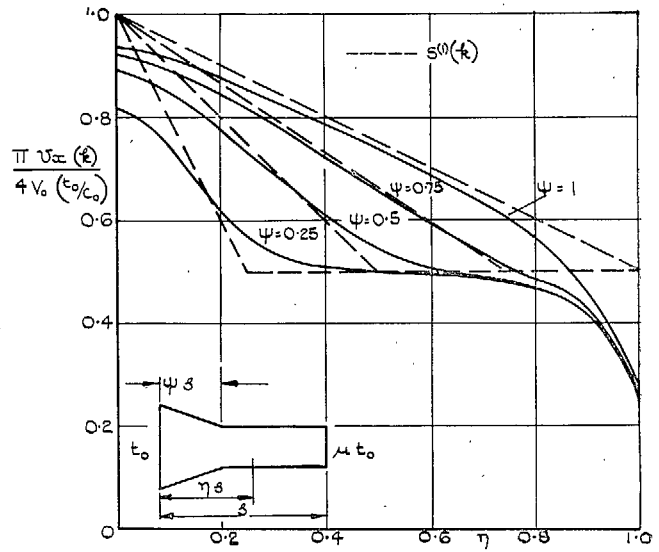

(a) EFFECT OF SPANWISE EXTENT OF TAPER.

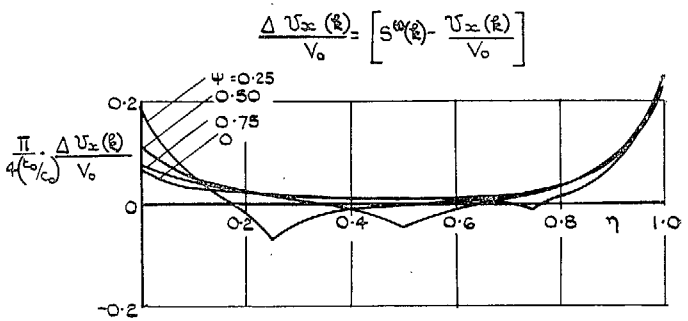

(b) REDUCTION OF v_∞ RELATIVE TO TWO-DIMENSIONAL VALUE.

FIGS. 12a and 12b. Spanwise variation of supervelocity at maximum thickness. Wing (1). $k = 0$. $A = 4$. $\mu = 0{\cdot}50$.

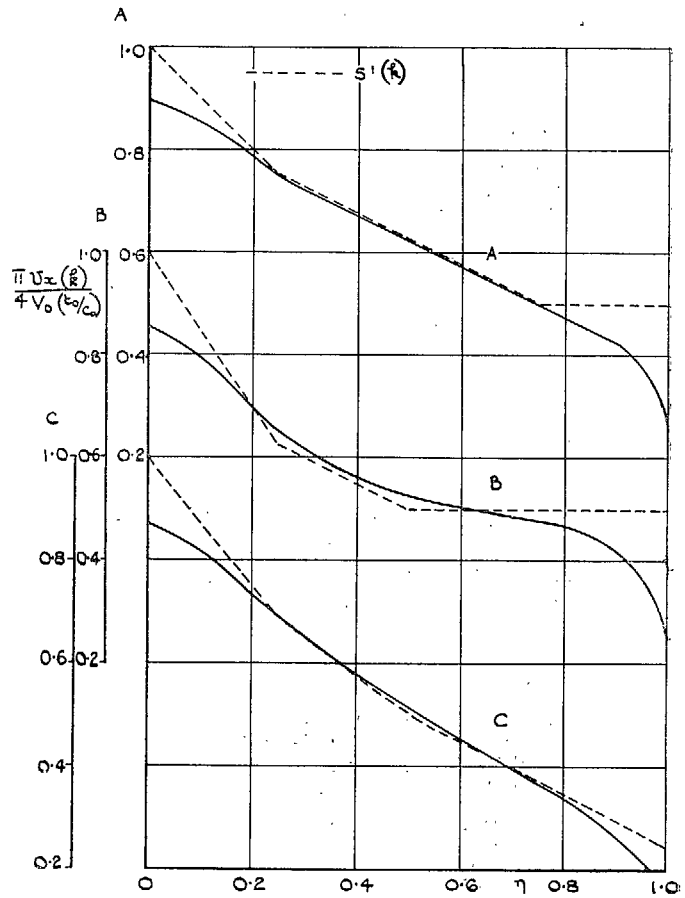

FIG. 13. Effect of spanwise thickness distribution on supervelocity at maximum thickness of a rectangular wing. Wing (1). $A = 4$.

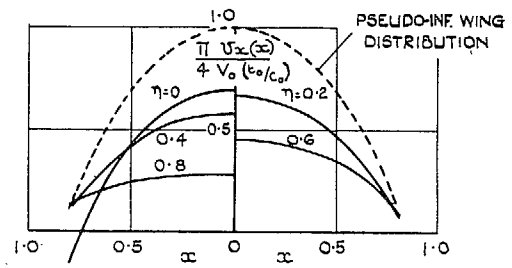

(a) EFFECT OF SPANWISE POSITION.

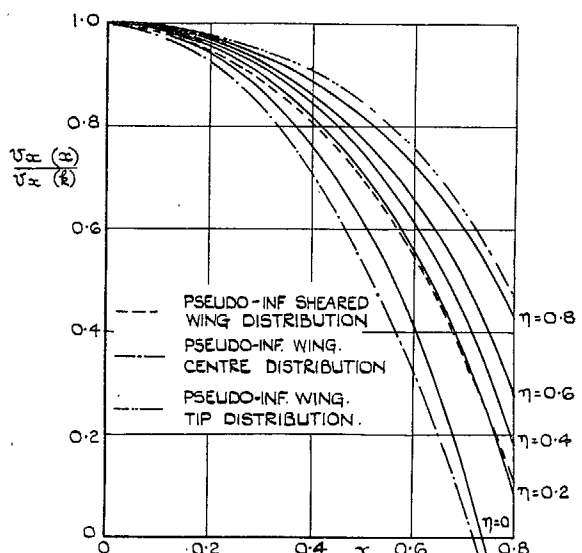

(b) COMPARISON WITH PSEUDO INFINITE WING DISTRIBUTIONS.

FIGS. 14a and 14b. Chordwise supervelocity distributions. Wing (2). $k = 0$. $A = 3$. $\varphi_k = 0$ deg.

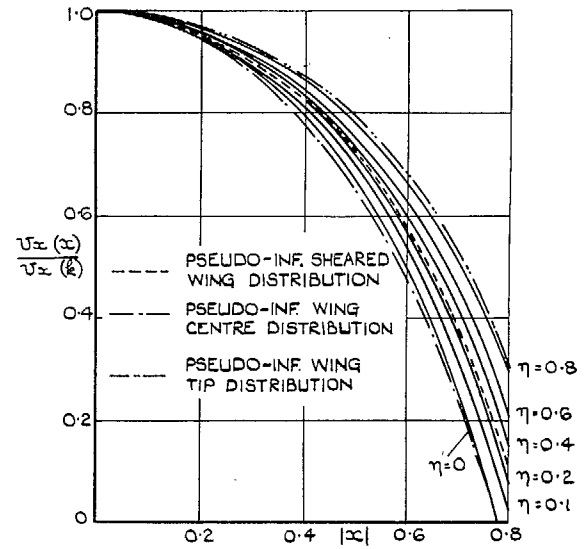

(a) WING (2).

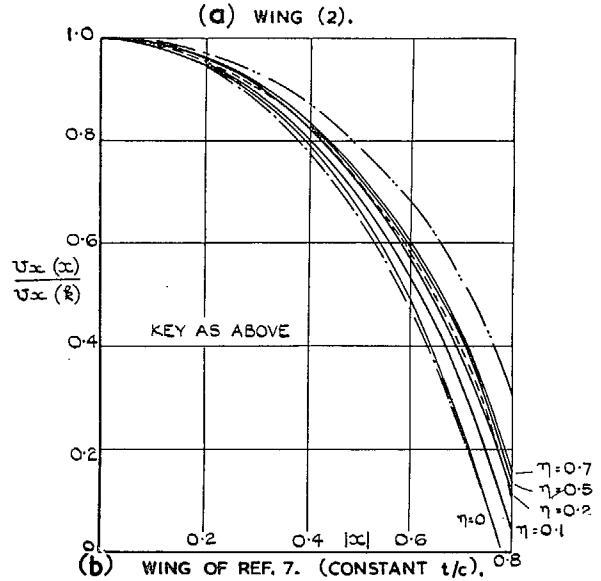

(b) WING OF REF. 7. (CONSTANT t/c).

FIGS. 15a snd 15b. Chordwise supervelocity distributions. $k = 0$. $A = 6{\cdot}67$. $\varphi_k = 0$ deg.

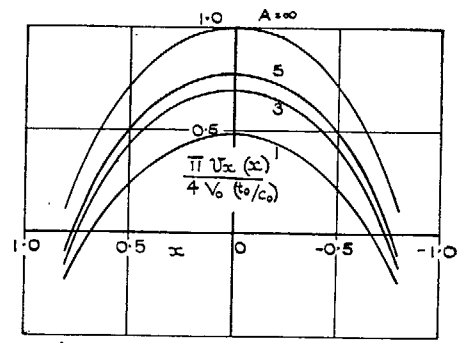

(a) EFFECT OF ASPECT RATIO.

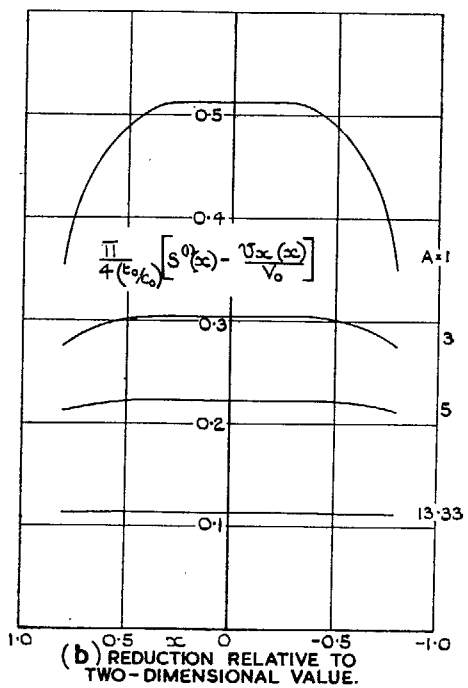

(b) REDUCTION RELATIVE TO TWO-DIMENSIONAL VALUE.

FIGS. 18a and 18b. Centre-line supervelocity distribution. Wing (2). $k = 0$. $\varphi_k = 0$ deg.

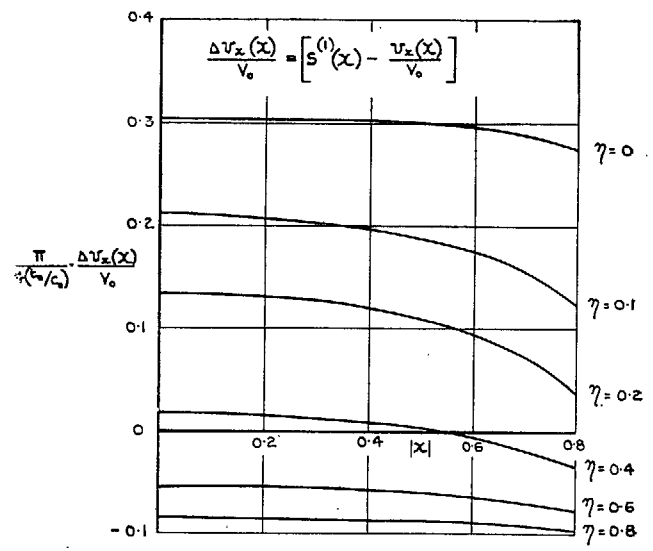

(a) WING (2), A = 3, $\varphi_R = 0°$.

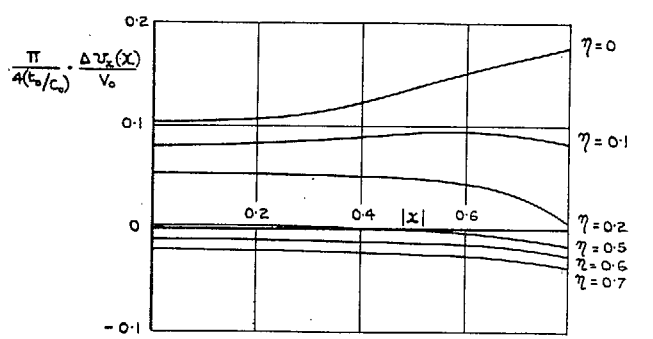

(b) WING OF REF. 7, A = 6·67, $\varphi_R = 0°$.

FIGS. 19a and 19b. Reduction of supervelocity relative to two-dimensional value.

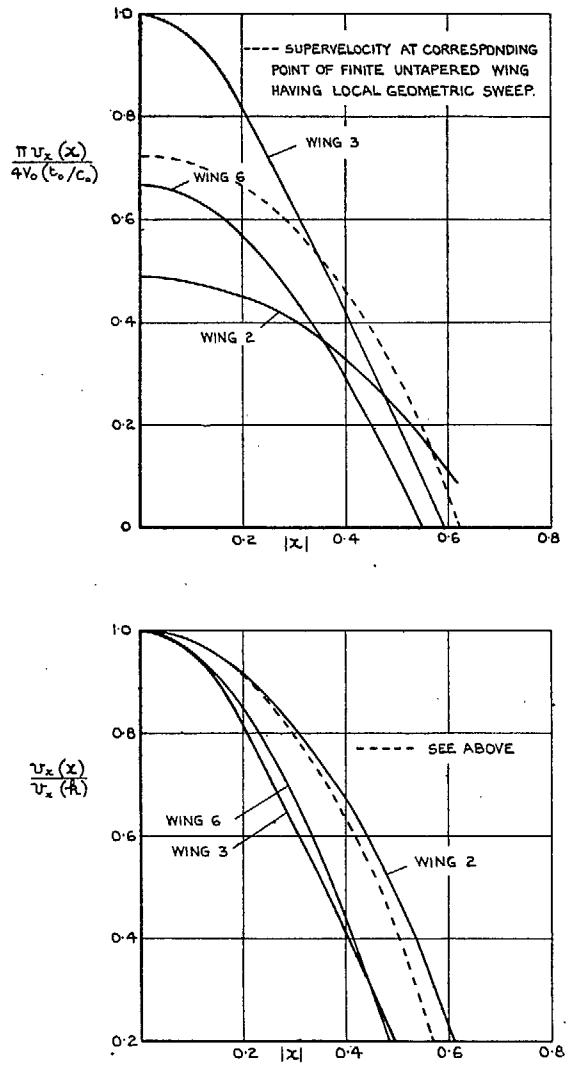

FIG. 20. Centre-line supervelocity distributions. Wings 2, 3 and 6. $A = 1$. $\varphi_k = 0$ deg.

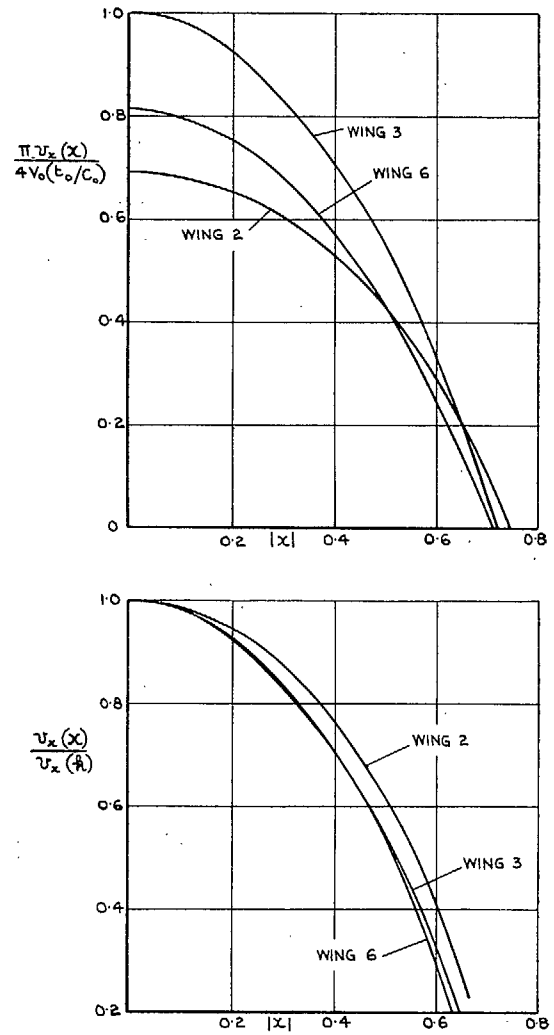

FIG. 21. Centre-line supervelocity distributions. Wings 2, 3 and 6. $A = 3$. $\varphi_k = 0$ deg.

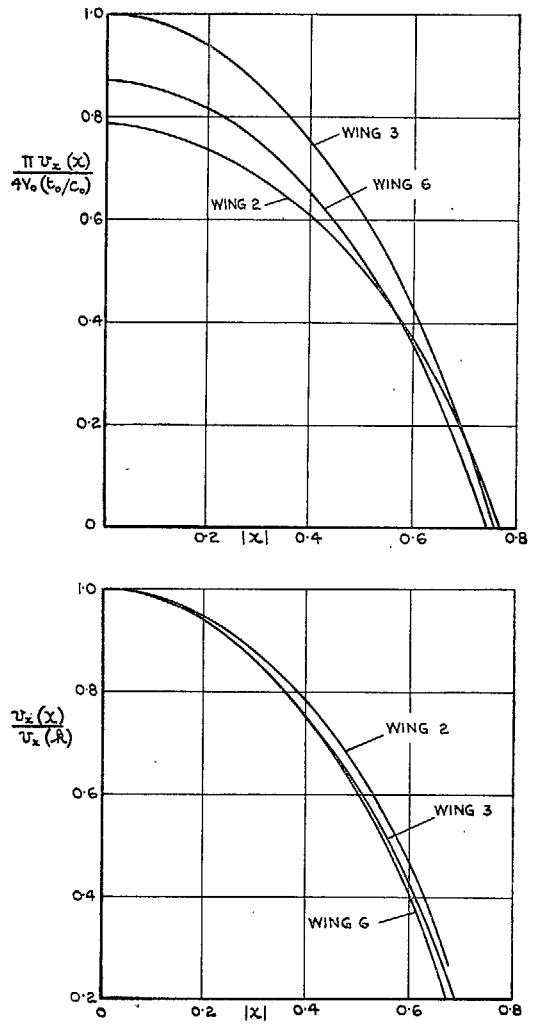

FIG. 22. Centre-line supervelocity distributions. Wings 2, 3 and 6. $A = 5$. $\varphi_k = 0$ deg.

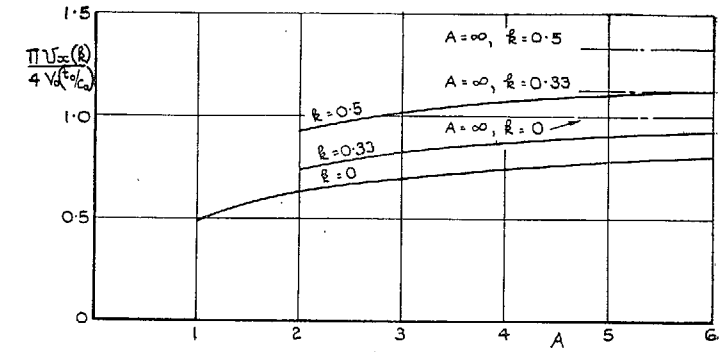

(a) VARIATION WITH ASPECT RATIO AND MAX. THICKNESS POSITION.

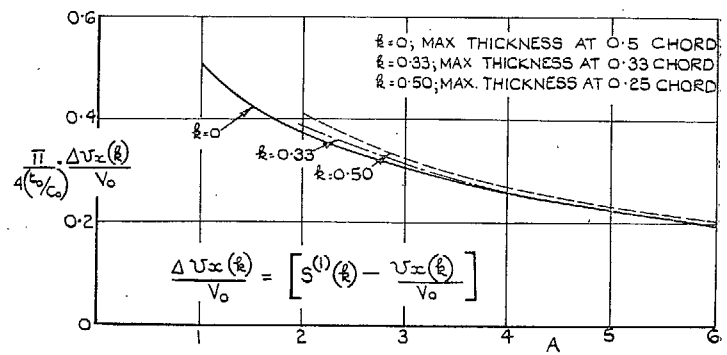

(b) REDUCTION OF v_x RELATIVE TO TWO-DIMENSIONAL VALUE.

FIGS. 23a and 23b. Supervelocity at maximum thickness of centre-line chord. Wing (2). $\varphi_k = 0$ deg.

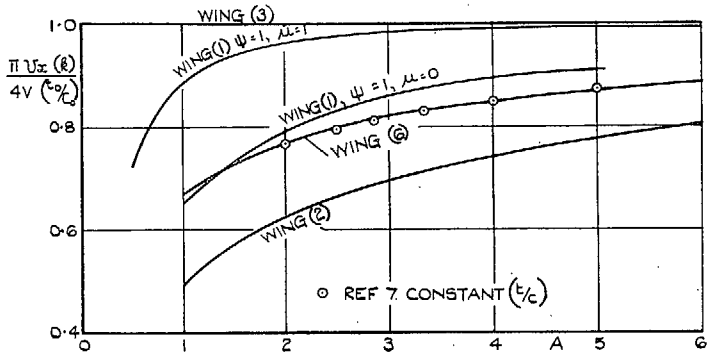

(a) VARIATION OF SUPERVELOCITY AT MAX. THICKNESS OF CENTRE LINE CHORD WITH ASPECT RATIO.

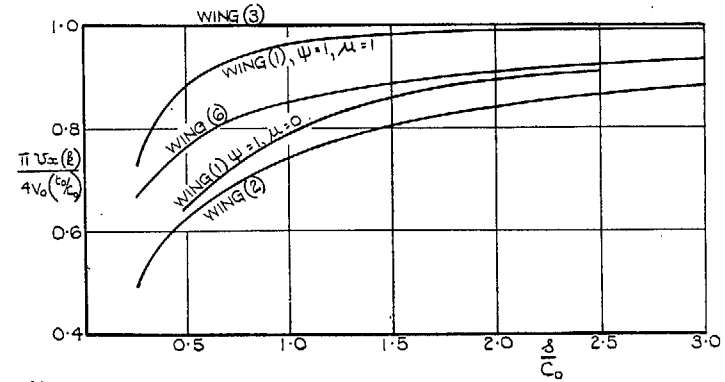

(b) VARIATION OF SUPERVELOCITY AT MAX. THICKNESS OF CENTRE LINE CHORD WITH SPAN.

FIGS. 24 and 24b. Effect of wing geometry on supervelocity at maximum thickness of centre-line chord. $\varphi_k = 0$ deg.

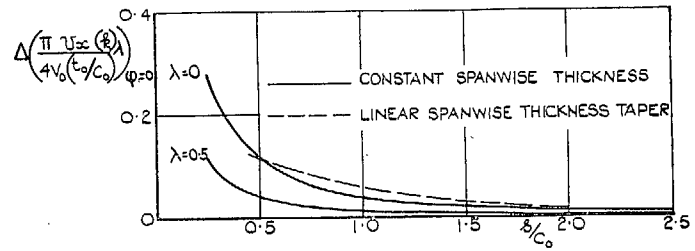

(a) INCREASE OF SUPERVELOCITY DUE TO PLANFORM TAPER.

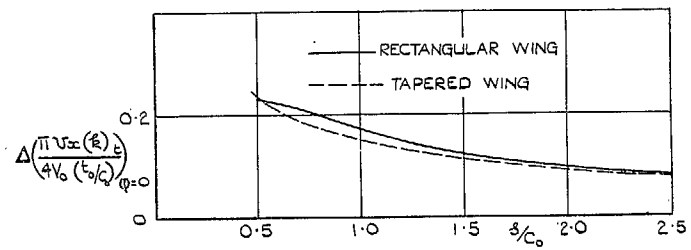

(b) REDUCTION OF SUPERVELOCITY DUE TO THICKNESS TAPER.

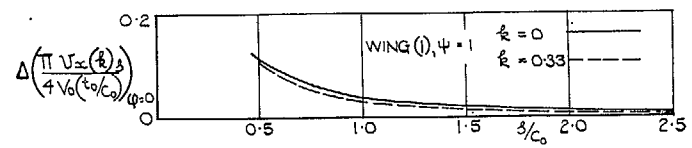

(c) REDUCTION OF SUPERVELOCITY DUE TO FINITE SPAN.

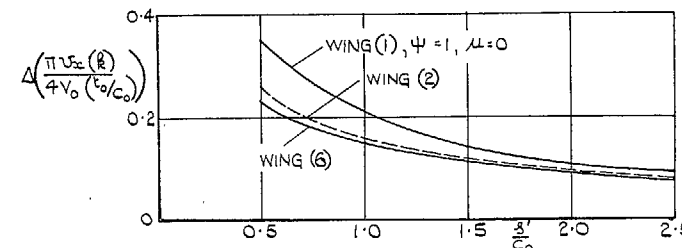

(d) EFFECT OF SPANWISE THICKNESS TAPER & PLANFORM ON REDUCTION OF SUPERVELOCITIES, RELATIVE TO TWO-DIMENSIONAL VALUE.

FIGS. 25a to 25d. Effect of aspect ratio, plan-form and thickness taper on supervelocity at maximum thickness of centre-line chord. $\varphi_k = 0$ deg.

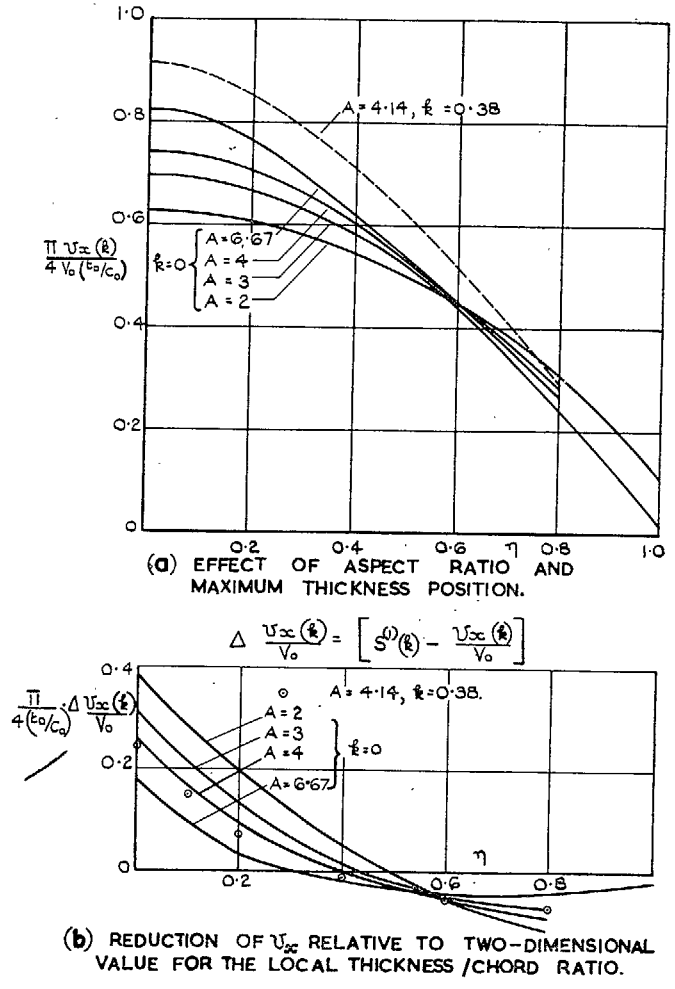

FIGS. 26a and 26b. Spanwise variation of supervelocity at maximum thickness. Wing (2). $\varphi_k = 0$ deg.

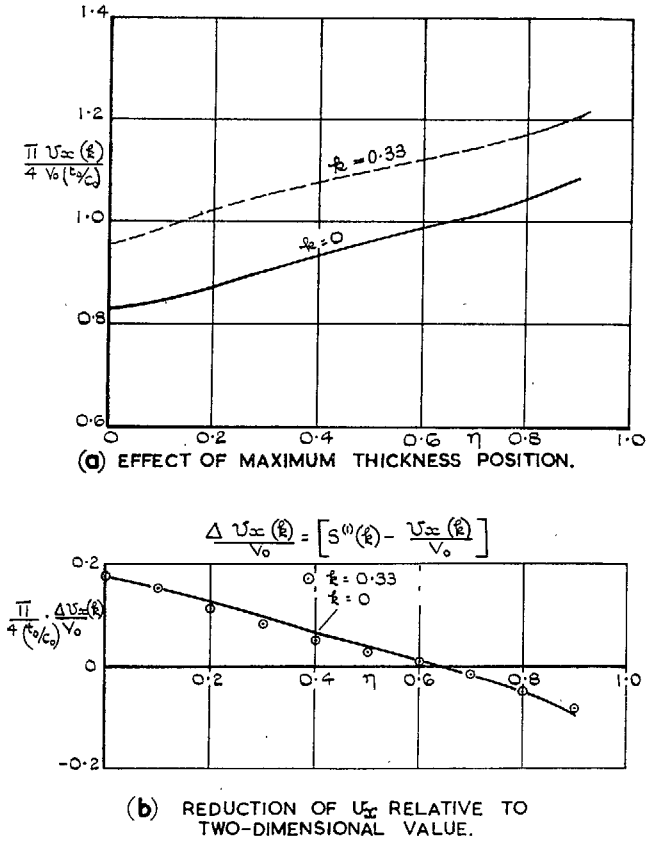

FIGS. 27a and 27b. Spanwise variation of supervelocity at maximum thickness. Wing of Ref. 7. $\varphi_k = 0$ deg. $A = 3{\cdot}33$.

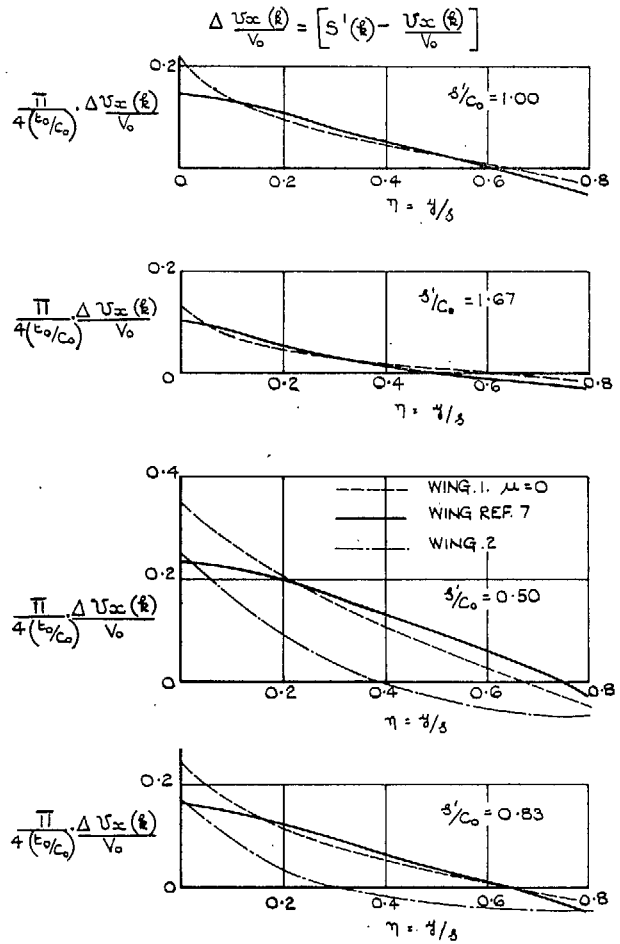

FIG. 28. Effect of plan-form and thickness distribution on spanwise variation of V_x at maximum thickness. Wings 1, 2 and wing of Ref. 7. $\varphi_k = 0$ deg.

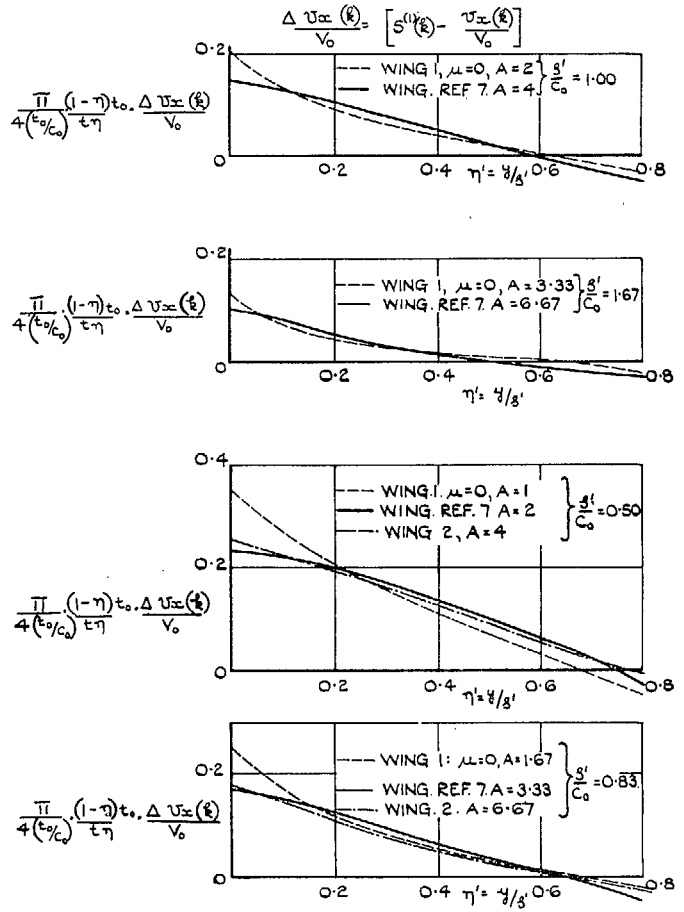

FIG. 29. Comparison between spanwise variations of V_x at maximum thickness. Wings 1 and 2, and wing of Ref. 7. $\varphi_k = 0$ deg.

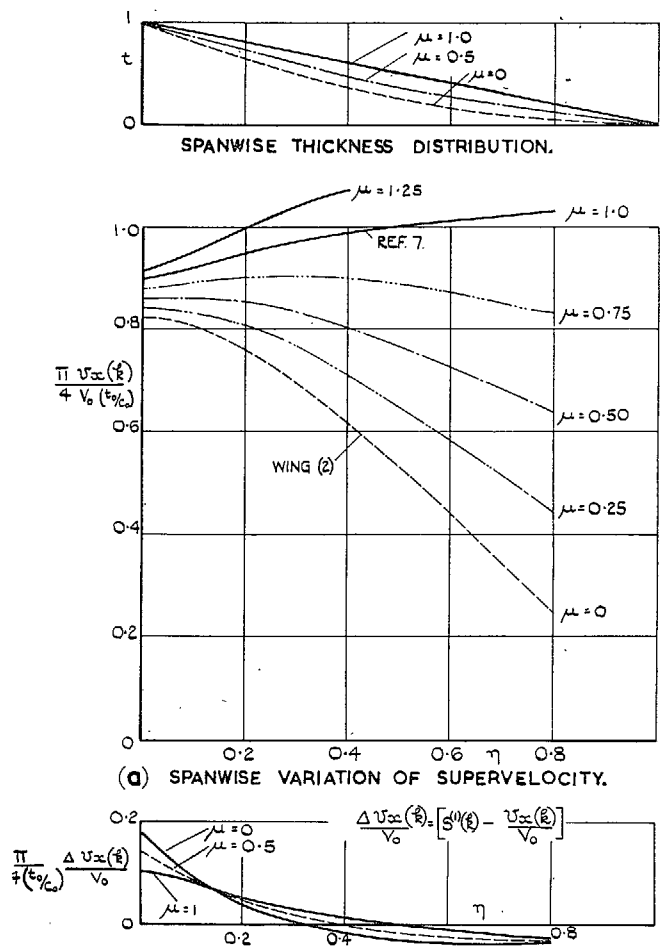

FIGS. 30a and 30b. Effect of spanwise thickness distribution on supervelocity at maximum-thickness position (Wings having linear spanwise variation of thickness/chord ratio). $\varphi_k = 0$ deg. $A = 6{\cdot}67$.

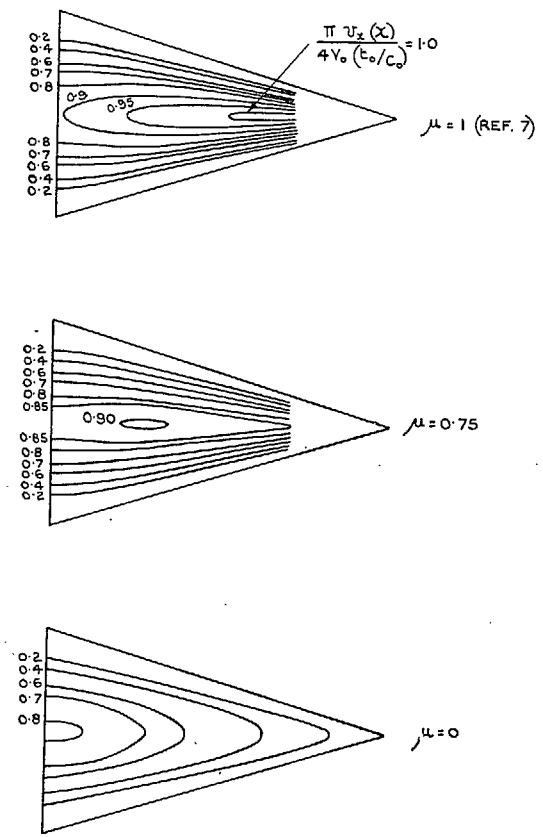

FIG. 31. Effect of spanwise thickness distribution on isobar patterns (Linear spanwise variation of thickness/chord ratio). $\varphi_k = 0$ deg. $A = 6{\cdot}67$.

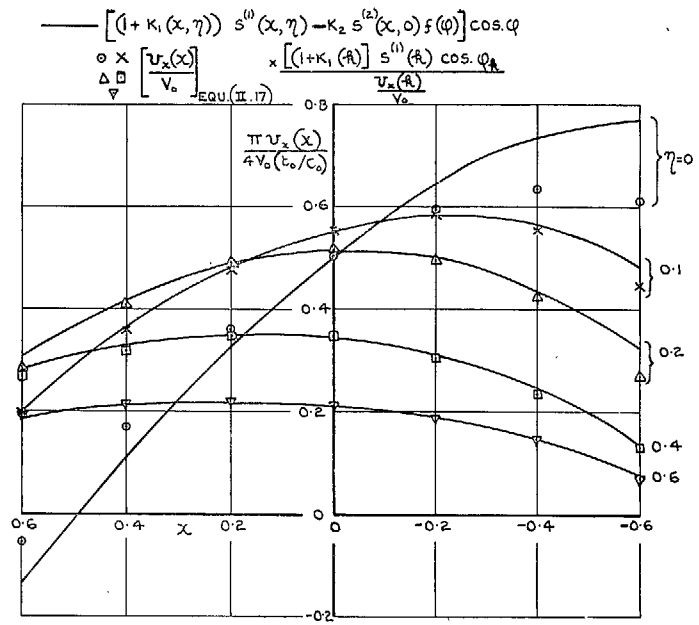

(a) EFFECT OF SPANWISE POSITION ON SHAPE OF SUPERVELOCITY DISTRIBUTION.

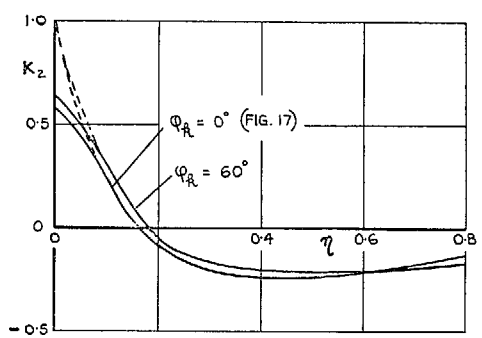

(b) SPANWISE VARIATION OF KINK TERM REDUCTION FACTOR.

FIGS. 32a and 32b. Supervelocity distributions on 60-deg swept wing. Wing (2). $A = 3$.

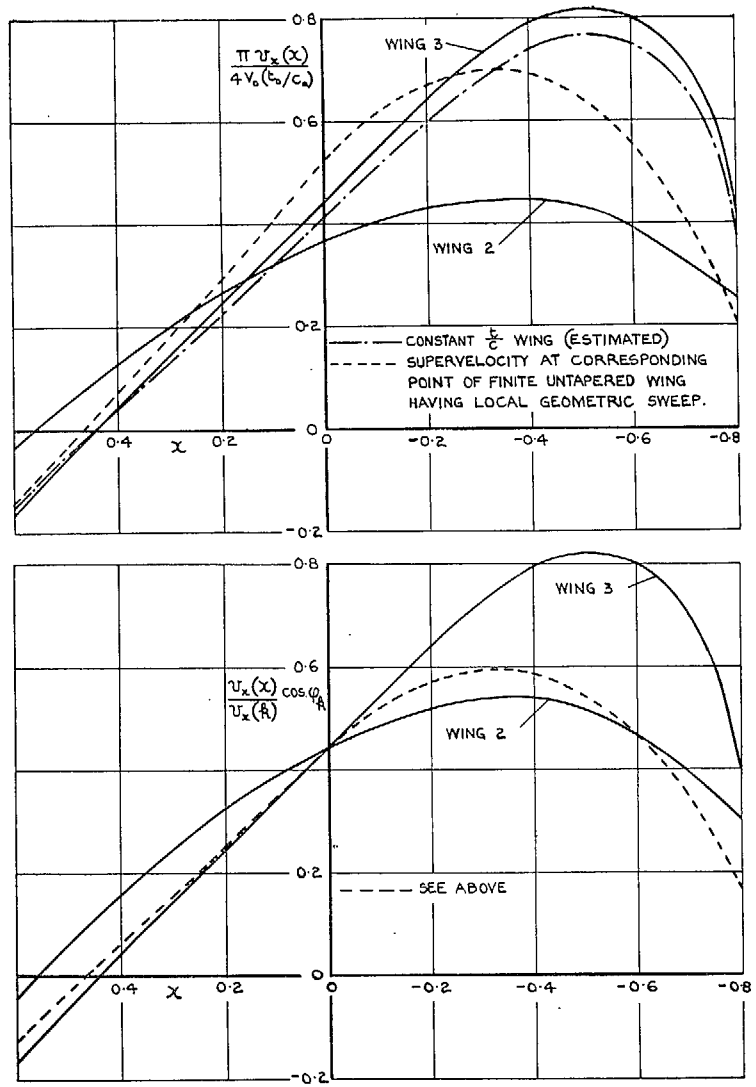

FIG. 33. Centre-line supervelocity distributions. Wings 2 and 3. $A = 1$. Delta.

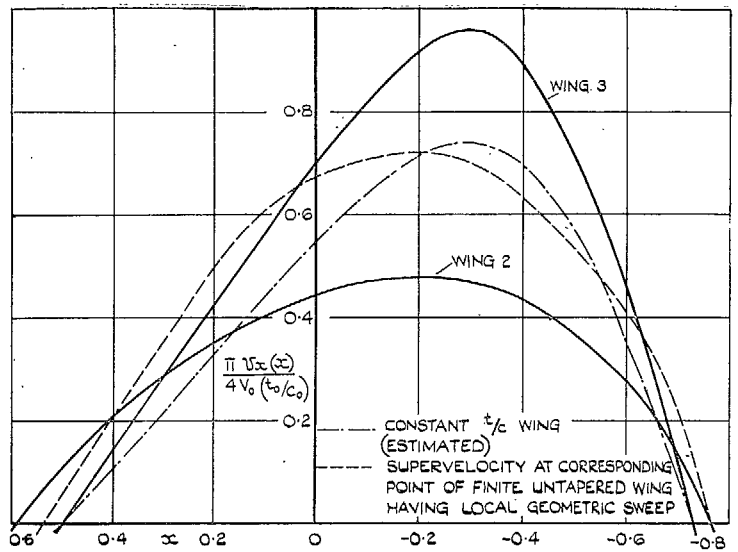

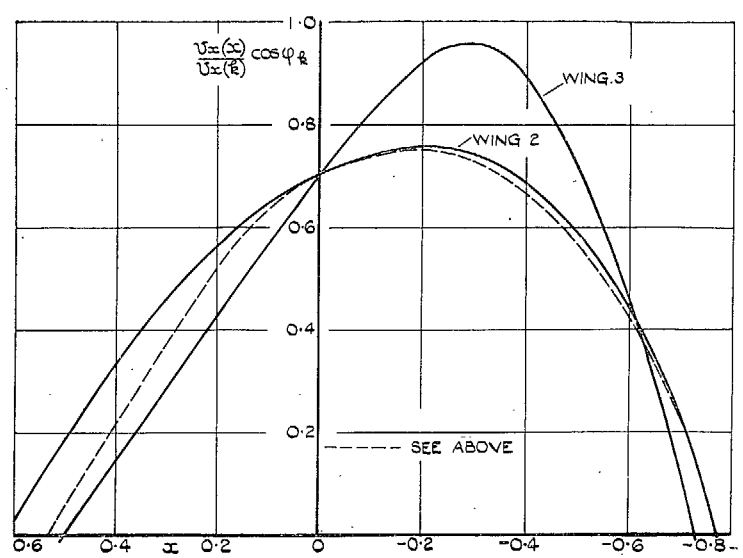

FIG. 34. Centre-line supervelocity distributions.
Wings 2 and 3. $A = 1$. $\varphi_k = 45$ deg.

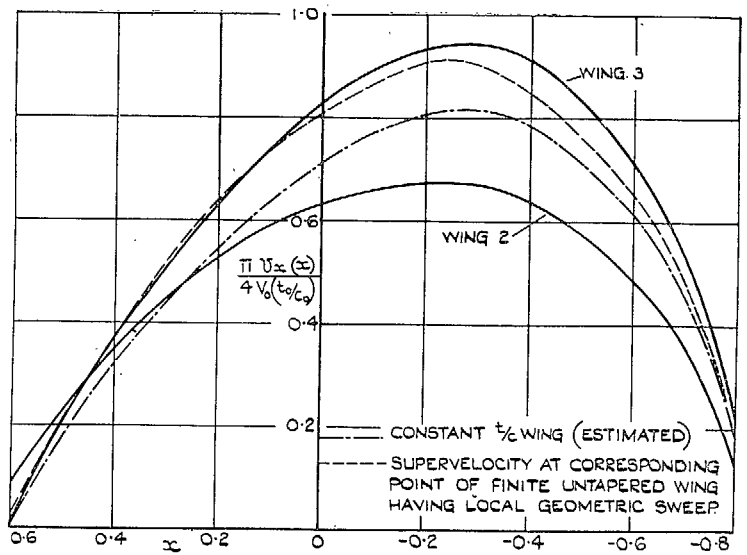

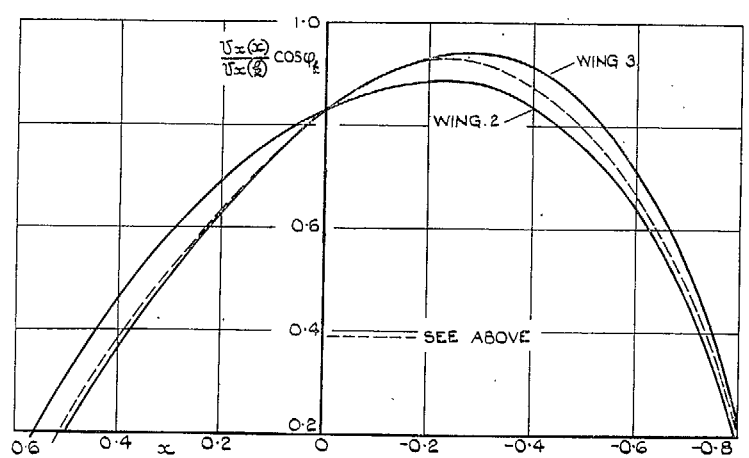

FIG. 35. Centre-line supervelocity distributions.
Wings 2 and 3. $A = 3$. Delta.

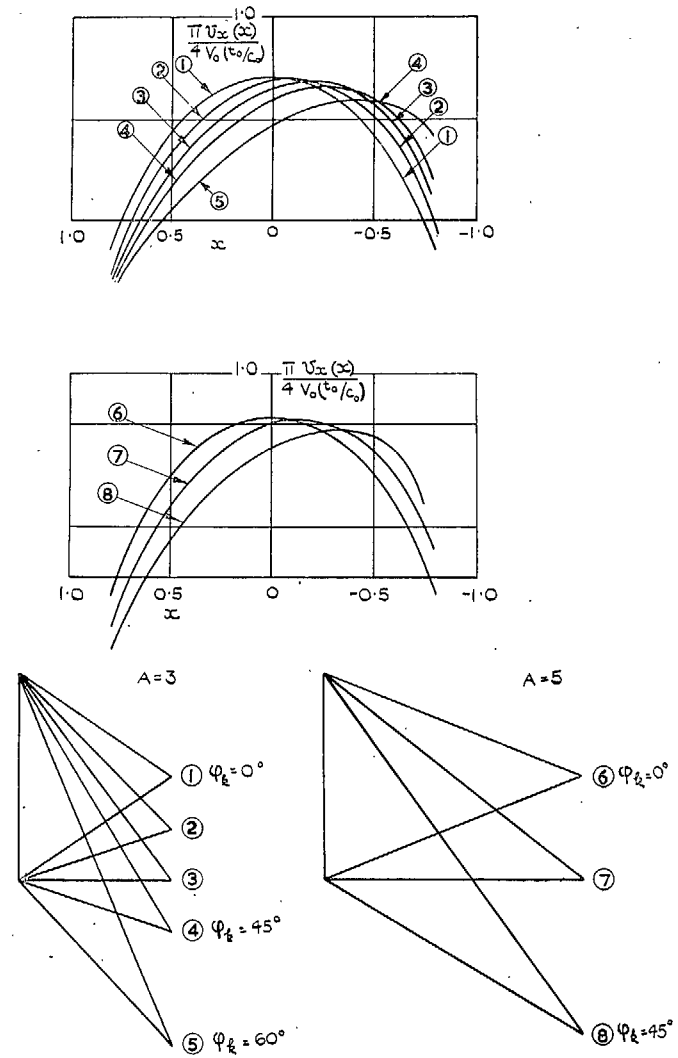

FIG. 36. Effect of sweepback on supervelocity distribution at centre of wing (2). $k = 0$.

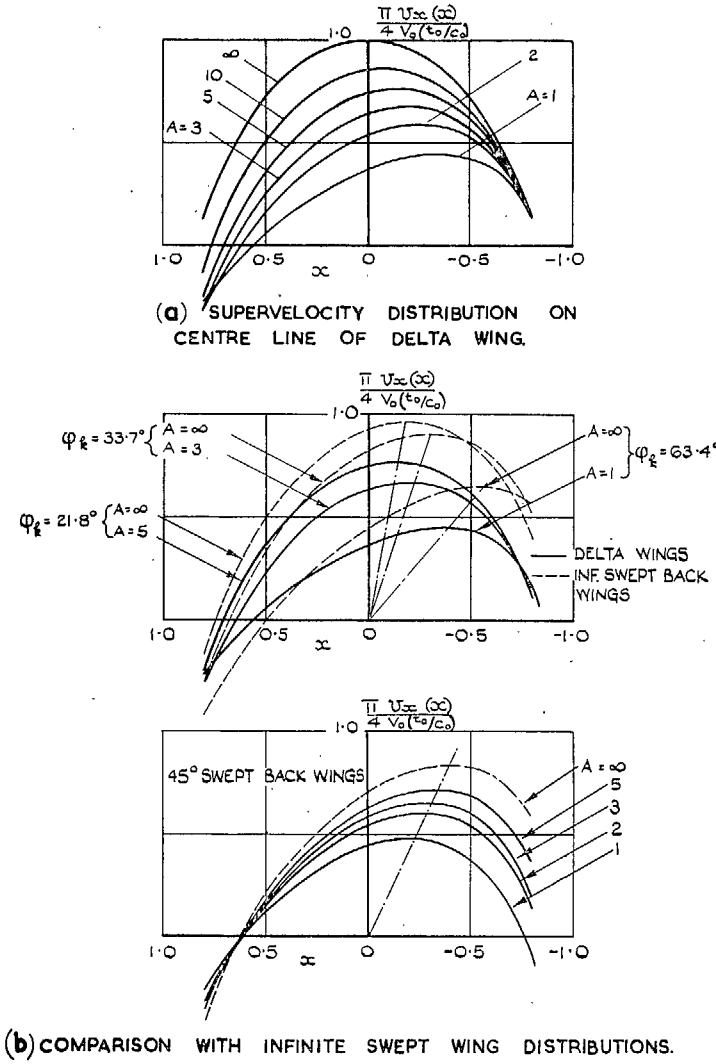

(a) SUPERVELOCITY DISTRIBUTION ON CENTRE LINE OF DELTA WING.

(b) COMPARISON WITH INFINITE SWEPT WING DISTRIBUTIONS.

FIGS. 37a and 37b. Effect of aspect ratio on centre-line supervelocity distributions of wing (2). $k = 0$.

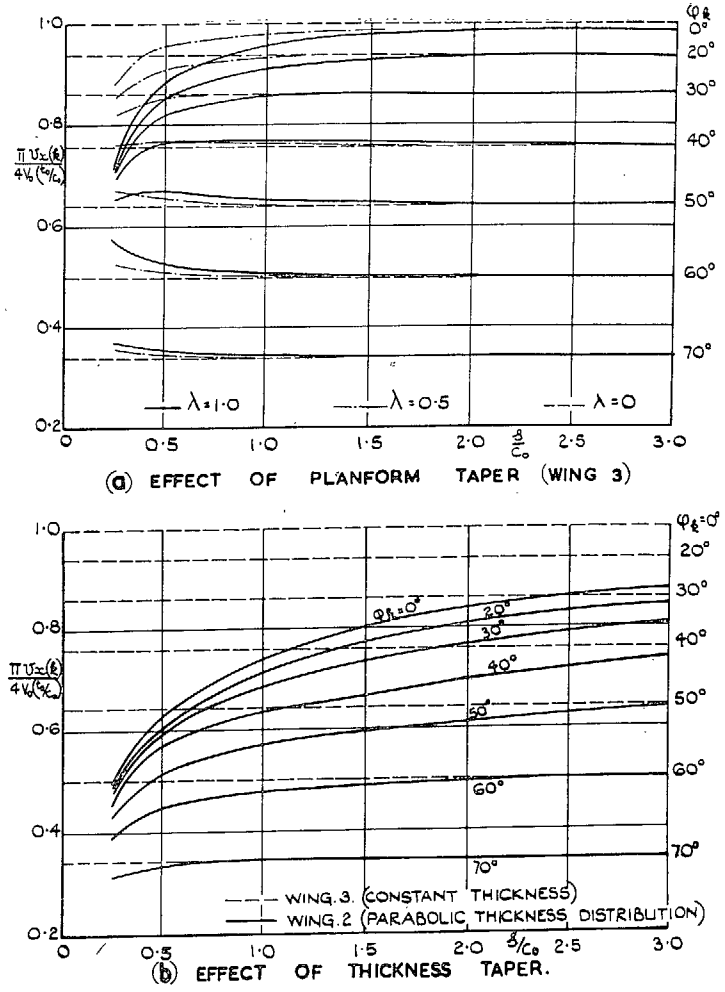

FIGS. 38a and 38b. Effects of plan-form and thickness taper on supervelocity at maximum thickness of centre-line chord.

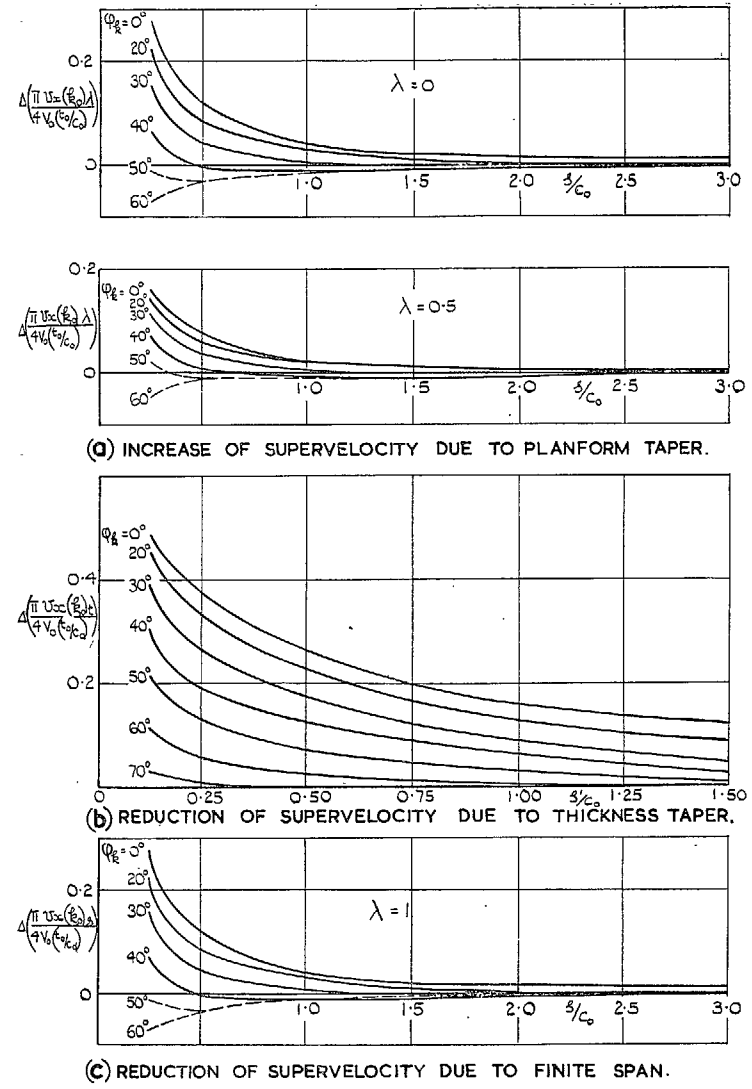

FIGS. 39a to 39c. Effect of aspect ratio, plan-form and thickness taper on supervelocity at maximum thickness of centre-line chord.

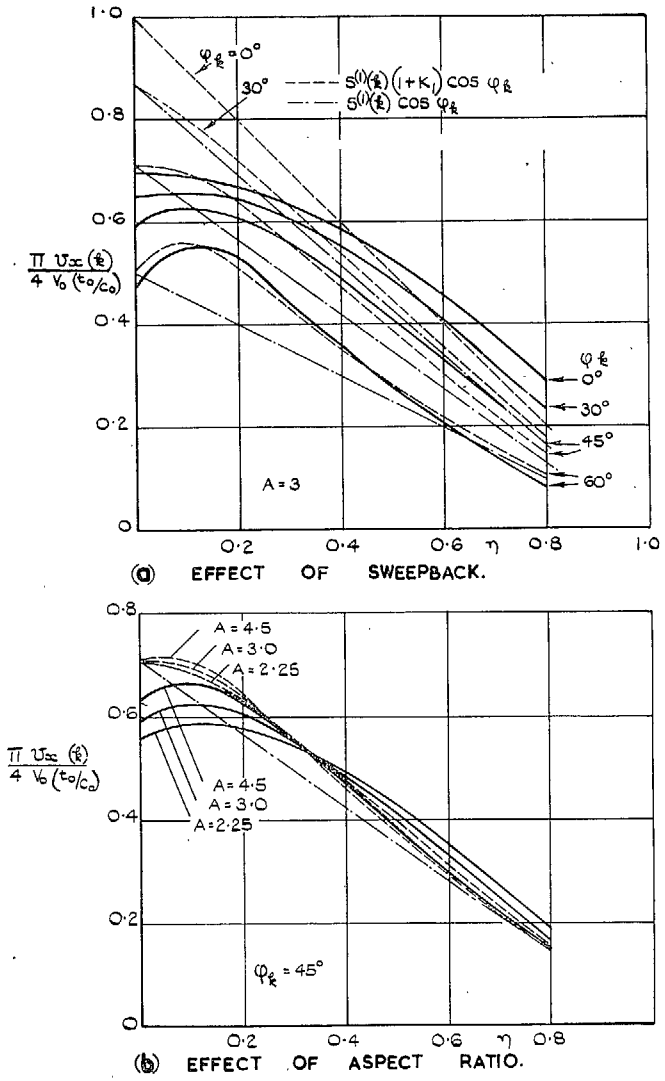

FIGS. 40a and 40b. Spanwise variation of supervelocity at maximum thickness. Wing (2).

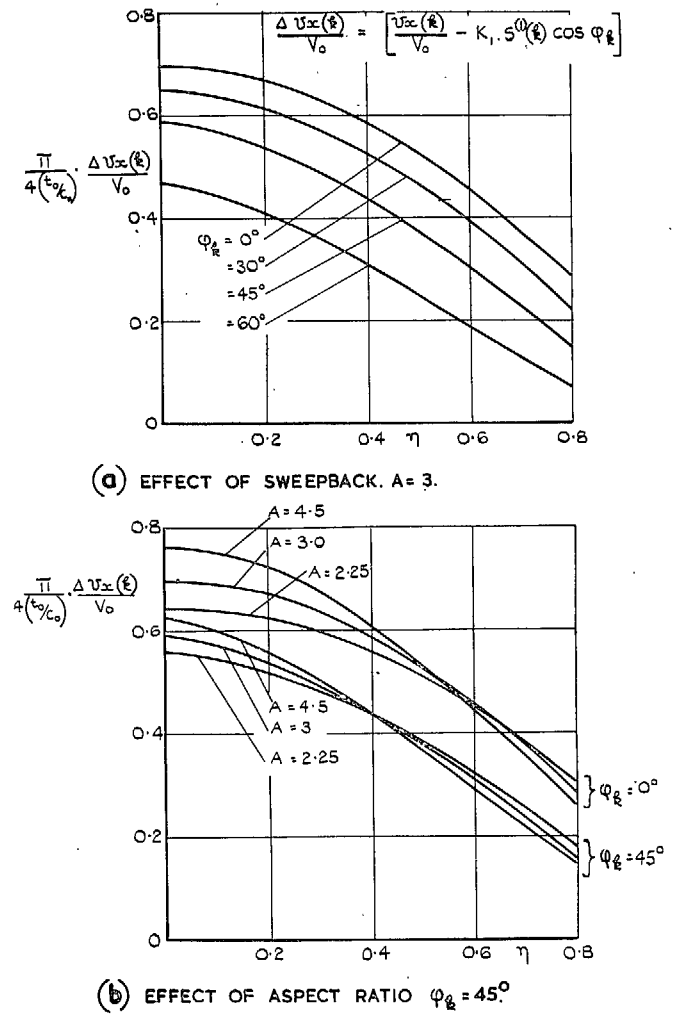

FIGS. 41a and 41b. Effect of sweepback and aspect ratio on quasi-spanwise variation of V_x at maximum thickness. Wing (2).

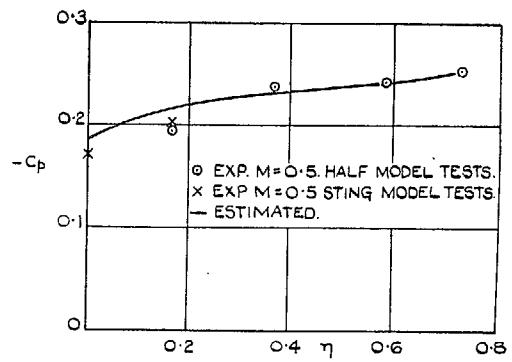

(a) DELTA WING ASPECT RATIO 3·08 NACA 0010 SECTION.

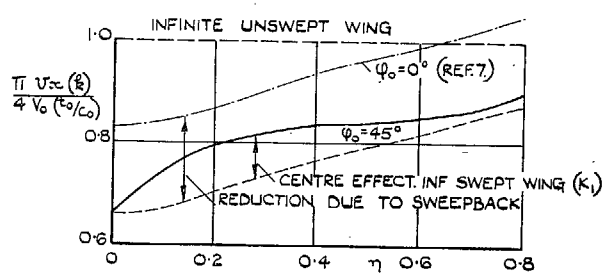

(b) 45° SWEPT BACK WING ASPECT RATIO 3·33 SYMMETRICAL PARABOLIC ARC SECTION.

FIGS. 42a and 42b. Estimated spanwise variation of supervelocity at maximum thickness of wings having constant spanwise thickness/chord ratio.

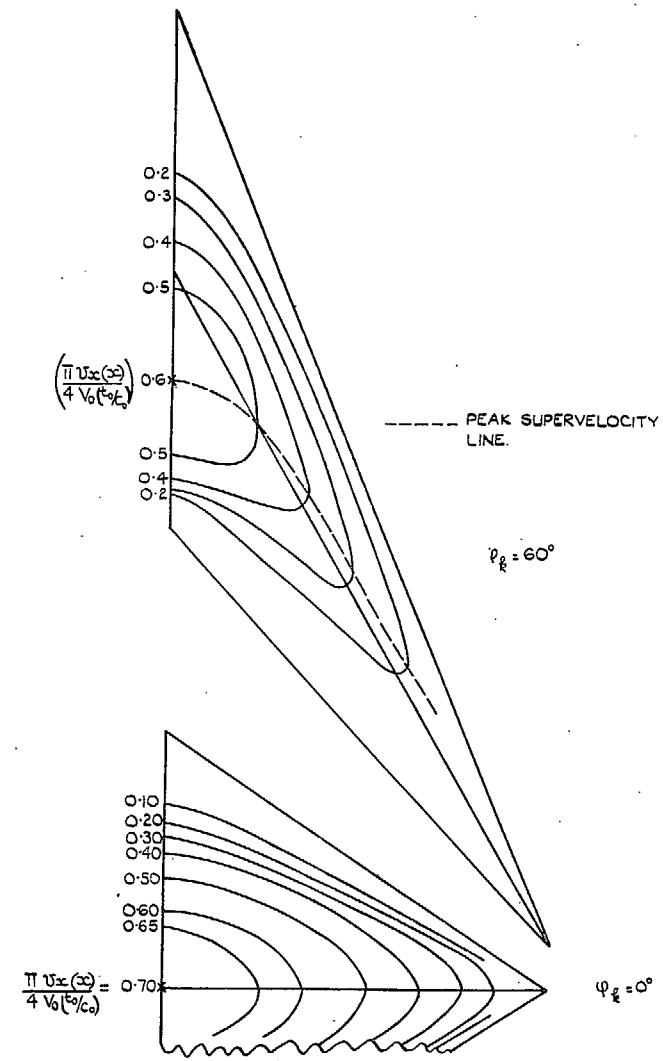

FIG. 43. Effect of sweepback on isobar patterns. Wing (2). $A = 3$.

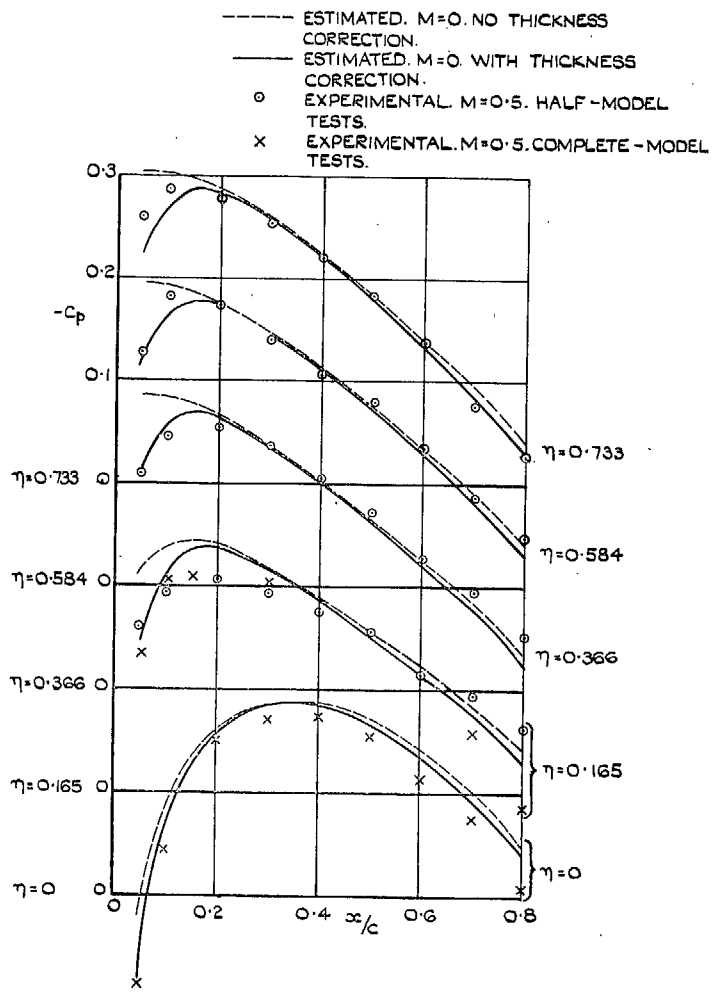

FIG. 44. Comparison of estimated and experimental pressure distributions. Delta wing. $A = 3{\cdot}08$. NACA 0010 section.

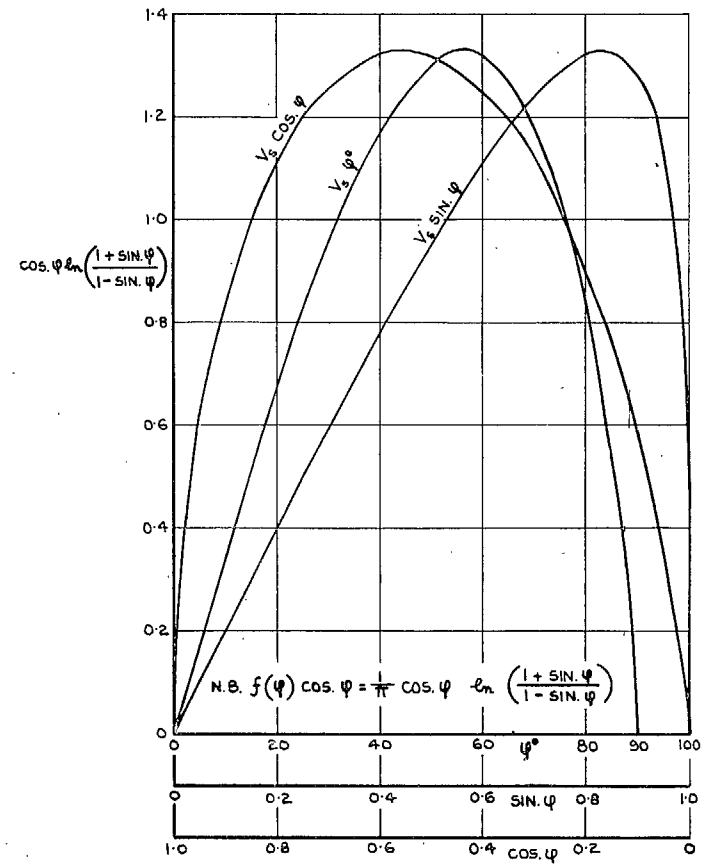

FIG. 45. Variation of $\cos\varphi\, l_n\left(\dfrac{1+\sin\varphi}{1-\sin\varphi}\right)$ with φ.

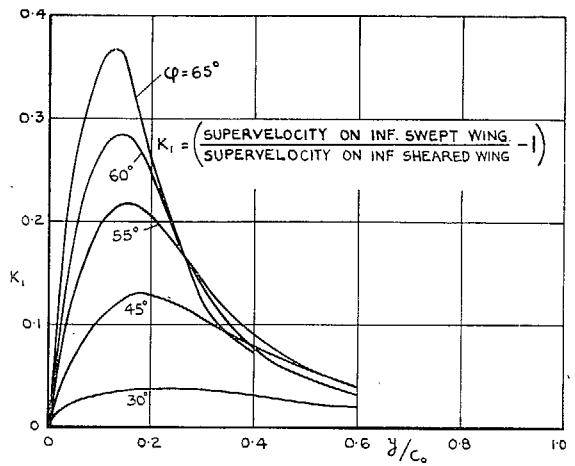

(a). EFFECT OF SWEEPBACK ON INCREASE OF SUPERVELOCITIES AT MAX. THICKNESS OF AEROFOIL DUE TO CENTRE EFFECT.

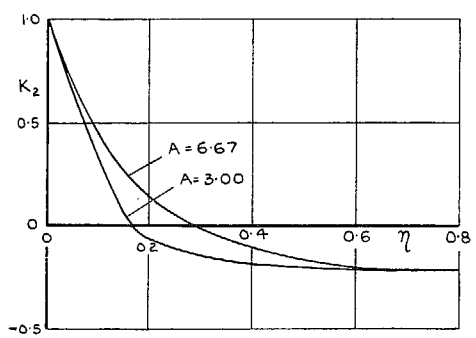

(b) APPROXIMATE EFFECT OF PLANFORM TAPER ON "KINK" TERM REDUCTION FACTOR

FIGS. 46a and 46b. Centre-effect factors for wing having parabolic-arc aerofoil section.

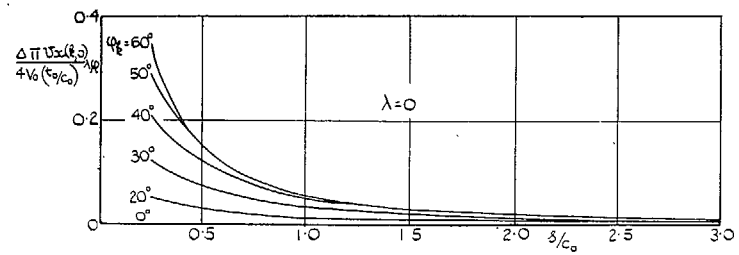

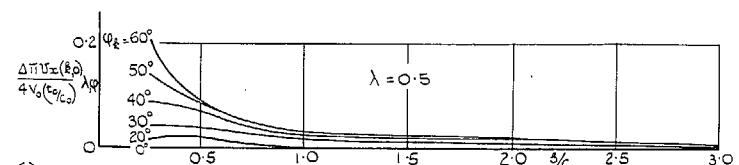

(a) REDUCTION WITH SWEEPBACK OF THE INCREASE OF SUPERVELOCITY DUE TO PLANFORM TAPER.

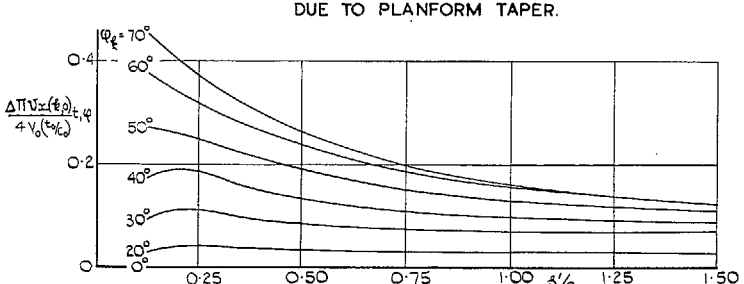

(b) REDUCTION WITH SWEEPBACK OF THE DECREASE OF SUPERVELOCITY DUE TO THICKNESS TAPER.

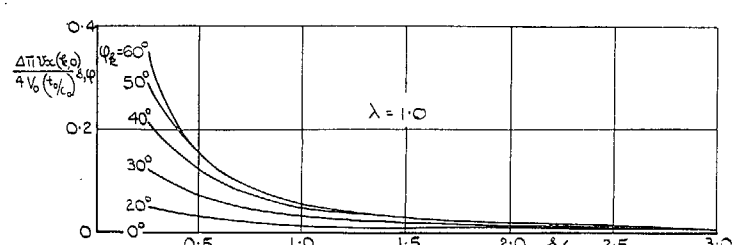

(c) REDUCTION WITH SWEEPBACK OF THE DECREASE OF SUPERVELOCITY DUE TO FINITE SPAN.

FIGS. 47a and 47b. Reduction with sweepback of the effects of aspect ratio, plan-form and thickness taper on the supervelocity at the maximum thickness of centre-line chord.

J4380 Wt.20/9036 K7 12/56 D&Co. 34/263

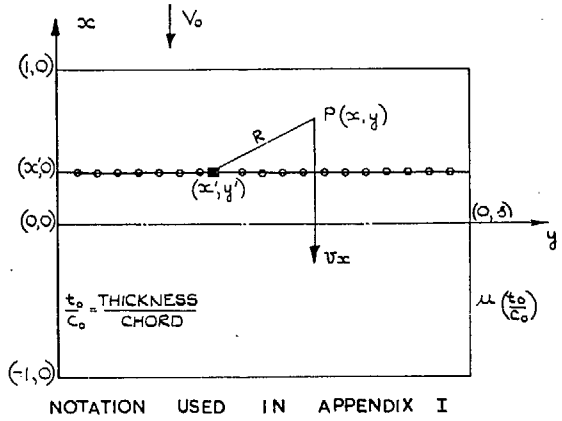

NOTATION USED IN APPENDIX I

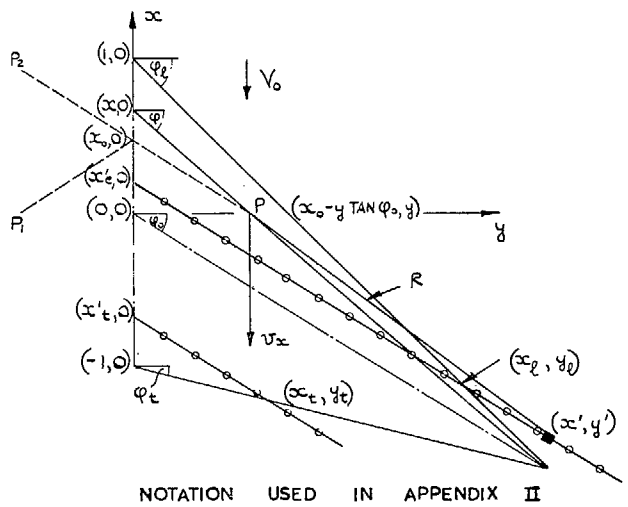

NOTATION USED IN APPENDIX II

FIG. 48. Notation used in Appendices I and II.

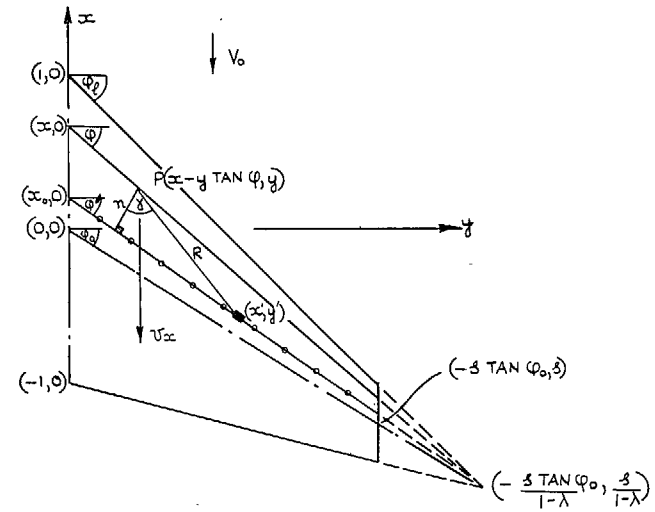

NOTATION USED IN APPENDIX III.

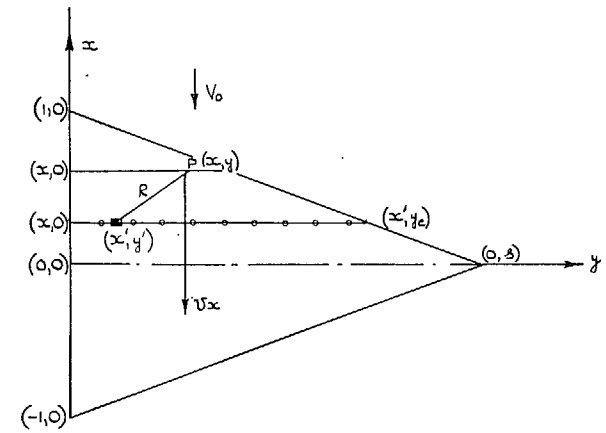

NOTATION USED IN APPENDIX IV.

FIG. 49. Notation used in Appendices III and IV.

PRINTED IN GREAT BRITAIN

Publications of the Aeronautical Research Council

ANNUAL TECHNICAL REPORTS OF THE AERONAUTICAL RESEARCH COUNCIL (BOUND VOLUMES)

1939 Vol. I. Aerodynamics General, Performance, Airscrews, Engines. 50*s*. (51*s*. 9*d*.)
Vol. II. Stability and Control, Flutter and Vibration, Instruments, Structures, Seaplanes, etc. 63*s*. (64*s*. 9*d*.)

1940 Aero and Hydrodynamics, Aerofoils, Airscrews, Engines, Flutter, Icing, Stability and Control, Structures, and a miscellaneous section. 50*s*. (51*s*. 9*d*.)

1941 Aero and Hydrodynamics, Aerofoils, Airscrews, Engines, Flutter, Stability and Control, Structures. 63*s*. (64*s*. 9*d*.)

1942 Vol. I. Aero and Hydrodynamics, Aerofoils, Airscrews, Engines. 75*s*. (76*s*. 9*d*.)
Vol. II. Noise, Parachutes, Stability and Control, Structures, Vibration, Wind Tunnels. 47*s*. 6*d*. (49*s*. 3*d*.)

1943 Vol. I. Aerodynamics, Aerofoils, Airscrews. 80*s*. (81*s*. 9*d*.)
Vol. II. Engines, Flutter, Materials, Parachutes, Performance, Stability and Control, Structures. 90*s*. (92*s*. 6*d*.)

1944 Vol. I. Aero and Hydrodynamics, Aerofoils, Aircraft, Airscrews, Controls. 84*s*. (86*s*. 3*d*.)
Vol. II. Flutter and Vibration, Materials, Miscellaneous, Navigation, Parachutes, Performance, Plates and Panels, Stability, Structures, Test Equipment, Wind Tunnels. 84*s*. (86*s*. 3*d*.)

1945 Vol. I. Aero and Hydrodynamics, Aerofoils. 130*s*. (132*s*. 6*d*.)
Vol. II. Aircraft, Airscrews, Controls. 130*s*. (132*s*. 6*d*.)
Vol. III. Flutter and Vibration, Instruments, Miscellaneous, Parachutes, Plates and Panels, Propulsion. 130*s* (132*s*. 3*d*.)
Vol. IV. Stability, Structures, Wind tunnels, Wind Tunnel Technique. 130*s*. (132*s*. 3*d*.)

ANNUAL REPORTS OF THE AERONAUTICAL RESEARCH COUNCIL—

1937 2*s*. (2*s*. 2*d*.) 1938 1*s*. 6*d*. (1*s*. 8*d*.) 1939–48 3*s*. (3*s*. 3*d*.)

INDEX TO ALL REPORTS AND MEMORANDA PUBLISHED IN THE ANNUAL TECHNICAL REPORTS, AND SEPARATELY—

April, 1950 – – – – – R. & M. No. 2600. 2*s*. 6*d*. (2*s*. 8*d*.)

AUTHOR INDEX TO ALL REPORTS AND MEMORANDA OF THE AERONAUTICAL RESEARCH COUNCIL—

1909–January, 1954 – – – R. & M. No. 2570. 15*s*. (15*s*. 6*d*.)

INDEXES TO THE TECHNICAL REPORTS OF THE AERONAUTICAL RESEARCH COUNCIL—

December 1, 1936 — June 30, 1939. R. & M. No. 1850. 1*s*. 3*d*. (1*s*. 5*d*.)
July 1, 1939 — June 30, 1945. – R. & M. No. 1950. 1*s*. (1*s*. 2*d*.)
July 1, 1945 — June 30, 1946. – R. & M. No. 2050. 1*s*. (1*s*. 2*d*.)
July 1, 1946 — December 31, 1946. R. & M. No. 2150. 1*s*. 3*d*. (1*s*. 5*d*.)
January 1, 1947 — June 30, 1947. – R. & M. No. 2250. 1*s*. 3*d*. (1*s*. 5*d*.)

PUBLISHED REPORTS AND MEMORANDA OF THE AERONAUTICAL RESEARCH COUNCIL—

Between Nos. 2251–2349. – – R. & M. No. 2350. 1*s*. 9*d*. (1*s*. 11*d*.)
Between Nos. 2351–2449. – – R. & M. No. 2450. 2*s*. (2*s*. 2*d*.)
Between Nos. 2451–2549. – – R. & M. No. 2550. 2*s*. 6*d*. (2*s*. 8*d*.)
Between Nos. 2551–2649. – – R. & M. No. 2650. 2*s*. 6*d*. (2*s*. 8*d*.)

Prices in brackets include postage

HER MAJESTY'S STATIONERY OFFICE

York House, Kingsway, London W.C.2; 423 Oxford Street, London W.1;
13a Castle Street, Edinburgh 2; 39 King Street, Manchester 2; 2 Edmund Street, Birmingham 3; 109 St. Mary Street, Cardiff; Tower Lane, Bristol 1; 80 Chichester Street, Belfast, *or through any bookseller*

S.O. Code No. 23-3032